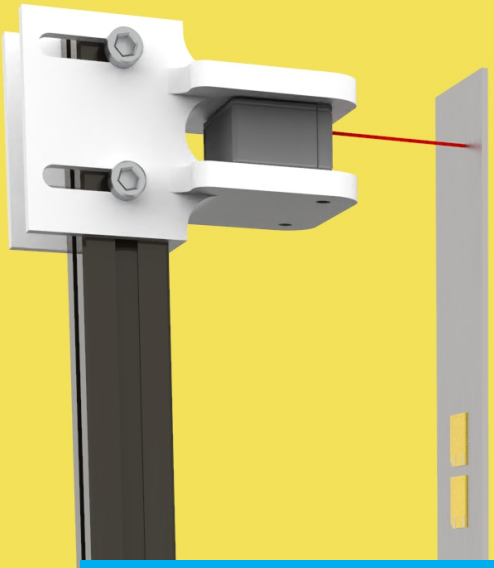

Department of Precision and Microsystems Engineering

A comparative study on distributed active damping of flexible systems

Madhan Gopal Muruganandam Mallur

Report no	: 2020.040
Coach	: Dr.Niranjan Saikumar
Professor	: Dr.Hassan HossienNia
Specialisation	: Mechatronics System Design
Type of report	: MSc Thesis
Date	: 30 September 2020

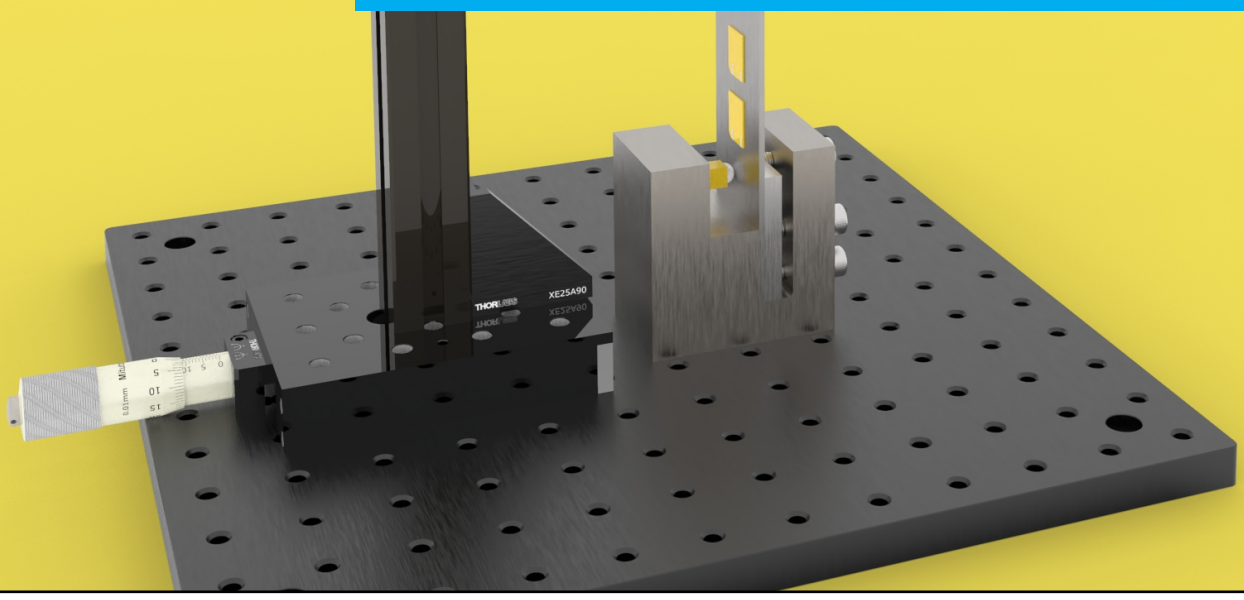

TU Delft Delft University of Technology

Challenge the future

A COMPARATIVE STUDY ON DISTRIBUTED ACTIVE DAMPING OF FLEXIBLE SYSTEMS

A thesis submitted to the Delft University of Technology in partial fulfilment of the requirements for the degree of

Master of Science in Mechanical Engineering

by

Madhan Gopal Muruganandam Mallur
[4804430]

September 2020

Supervisors:	Dr. Hassan HossienNia
	Dr. Niranjan Saikumar
Thesis committee:	Dr. Riccardo Ferrari
	Dr. Andres Hunt

ABSTRACT

As systems become more lightweight, to satisfy inertia and size requirements, vibration becomes a prominent factor in their dynamics. This vibration is undesirable and various suppression methods exist such as passive, semi-active, and active. In this thesis, active control methods are explored for this purpose. The present technology utilizes under-actuation for suppression of multiple modes, which has a sub-optimal performance. This work provides a comparative study on the different vibration suppression algorithms, which would aid in developing a distributed placement of actuators (over-actuation) and sensors. The main aim is to achieve multi-mode suppression systems and improve collocation for higher-order modes which facilitates accurate control of the end-effector of a system. A comparison is drawn between point actuation and over-actuation in terms of energy consumption, amount of damping, and precision. Also, a new control strategy is developed to circumvent the limitations posed by the present control strategies such as low-frequency spillover and steady-state error. The benefits in terms of damping and shortcomings are presented based on the conclusion drawn.

keywords: Piezoelectric actuators, Flexible system, Over-actuation, Active damping, Distributed control, Positive Position Feedback, Band pass filters, Co-located system,Modal decomposition, Finite element method and MIMO control.

ACKNOWLEDGEMENTS

I would like to acknowledge my indebtedness and render my warmest thanks to Professor Hassan HossienNia, Dr.Niranjan Saikumar, and Dr.Andres Hunt.

Dr. Hassan HossienNia made this research possible for me and was supportive right from the first meeting. The freedom and the advice that he provided me with were valuable throughout all stages of my work.

Dr.Niranjan Saikumar supervised me every week and was providing me with valuable suggestions that have contributed greatly to the improvement of the thesis. He was a great help with the implementation of my experiments and also for forming the structure of this thesis as well.

Dr. Andres Hunt was influential during the setting up of the thesis. His expertise with piezoelectric actuators helped me immensely. He was also very helpful in ordering components immediately and gave good insights for measurements and also looked after my safety for the duration of the project.

I would also like to thank the experts and lab support who helped me immensely during the project validation and experiment phase: Ali Ahmadi Dastjerdi, Gideon Emmanuel, Bradley Butt, Rob Luttjeboer, and Patrick van Holst. Without their participation and input, the experiments could not have been successfully conducted.

This thesis would not possible to complete within a short duration, considering the lock-downs, without the quick and sensible decisions taken by TU Delft. I would also like to thank the Department of Precision and Microsystem Engineering (PME) for fostering a good environment and creating a strong connection. I have had good and healthy discussions in the form of Monday meetings, coffee talks, Taylor Board meetings, etc. which helped me to get cross-functional advice.

Finally, I must express my very profound gratitude to my parents, relatives, and my friends for providing me with unfailing support and continuous encouragement throughout my years of study and through the process of researching and writing this thesis. This accomplishment would not have been possible without them.

CONTENTS

LIST OF FIGURES

LIST OF TABLES

ACRONYMS

SISO Single-Input Single-Output v
PPF Positive Position Feedback v
1-BPF 1st order Band Pass Filter v
2-BPF 2nd order Band Pass Filter viii
LPF Low Pass Filter viii
FRF Frequency Response Function v
TMD Tuned Mass Damper 1
AVC Active Vibration Control 2
DVF Direct Velocity Feedback 2
IRC Integral Resonance Control 2
LQR Linear Quadratic Regulator 2
LQG Linear Quadratic Gaussian 2
DOF Degree of Freedom 2
LHP Left Half Plane 10
RC Resonance Control 13
MIMO Multi-Input Multi-Output 40
BP Band pass 31
FEA Finite Element Analysis 54

1 INTRODUCTION

1.1 INTRODUCTION

Recent developments have facilitated systems with high support stiffness and low mass, in a bid to shift the resonance beyond the band of excitation. Nevertheless, such a lightweight design has low damping, which is manifested as undesired vibrations. The traditional process of shifting to reduce vibrations is limited by the fact that increasing stiffness leads to an increase in mass. This is particularly an issue in certain applications of aerospace, medical technology (MRI and CT Scanners), electronics (pick and place robots, wafer steppers), automotive industry, printers, etc. where there are high demands on precision, energy consumption, and vibration are usually the limiting factor. Also, with the increasingly popular use of positioning systems with long flexures, they bring vibration problems due to the presence of multiple modes.

Positioning systems which employ piezo-motors also suffer from vibration problems due to structural resonances, particularly due to high resonant peaks (high Q-factor) and are limited in bandwidth due to its steep roll-off.

The amplitude of mechanical vibrations ranges from meters to nanometers. They have a detrimental effect in terms of :

- **Failure** - such as fatigue in mechanical structures and flutter in bridges, spacecraft.
- **Comfort** - examples include noise and vibrations in helicopters, flights, car-suspensions, windfarm etc.
- **Loss of Precision** - precision devices are subjected to tighter tolerances such as wafer steppers, telescopes, interferometers where the progression of micro-vibrations from different sub-assemblies have to be limited.

Damping is employed to dissipate vibrational energy, thereby aid in the reduction of resonance peaks. There are various damping techniques possible:

- Passive damping - systems which use simple mechanical devices such as Tuned Mass Damper (TMD), friction joints, viscous materials, etc,
- Semi-active damping - A variant of TMD with an electrical circuit connected to the structure. The energy is dissipated as heat through the electrical system.
- Active damping - This employs actuators and sensors to achieve damping and usually are tuned to affect only resonance modes.

Passive systems are not employed in high-tech systems due to the increase in mass for achieving the same performance compared to active damping and the fact that viscoelastic materials are subject to out-gassing, makes it not suitable for vacuum applications.TMD are also not suited for varying modes and can only damp one structural mode. Shunt damping is also of least importance because they are not suitable for damping multiple modes as the circuitry becomes complex. They are not suitable for systems with low resonant frequencies as the electric circuit would require a large inductance and capacitance. Active shunt control, employing op-amps, are also not preferred as they lead to substantial power consumption and complex electronic circuits [10].

Hence, Active Vibration Control (AVC) is employed in these high bandwidth systems for their superior performance in terms of higher damping, cost, size, and mass constraints, etc. Also, with the increased application of flexures in industries, AVC is employed to attain high bandwidth and precise systems. Smart materials (piezoelectric transducers) are often employed as sensors and actuators in AVC because of their advantages: low cost, ease of integration, high sensitivity, wide frequency range, and adaptability in vacuum environments. The present technologies focus on the use of fewer actuators to dampen multiple modes (under-actuation). However, there has been proof that over-actuation has better performance in terms of tracking and precision in motion control systems [5]. This paves way for the first objective of this thesis.

As flexible systems have a lot of inherent modes, the achievable bandwidth greatly depends on the amount of damping and is greatly influenced by the location of actuators. Collocated systems (systems with actuator and sensor attached to the same Degree of Freedom (DOF)) are particularly used for the control algorithm due to its inherent behavior of pole-zero interlacing, by which the phase always lies between $0^{\circ}$and 180°. Collocated systems ensure that the closed-loop is always stable for out of bandwidth modes [2].

There have been numerous control algorithms for collocated systems with respect to active damping such as PPF [11], Direct Velocity Feedback (DVF)[2], Integral Resonance Control (IRC) [12] etc., Traditionally AVC were also employed by state feedback such as Linear Quadratic Regulator (LQR) and Linear Quadratic Gaussian (LQG) [13] [14].However, system feedback is usually not preferred as it requires a perfect estimation of states and requires a lot of computational resources [15]. Also, high authority controllers such as H_2 & H_∞ controllers are not used as they appear to be very sensitive to model uncertainty and modeling errors caused by model truncation. On the other hand, using a high-order model for the synthesis of these controllers leads to higher-order controllers, which need a reduction for implementation which reduces performance and might cause an unstable closed-loop system [16][17].

DVF strategy is the easiest to implement but, they are obsolete as they suffer from spillover effects and need additional dynamics to roll-off at higher frequencies. DVF generally results in low performance and phase margin [18] [19]. They also require higher control effort at all frequencies and suffer from actuator saturation and reduced efficiency. IRC have some disadvantages such as the modes cannot be treated individually and the tuning requires the model of the plant but are similar to PPF otherwise. The well known, PPF which is touted for its unconditional stability and roll-off characteristics also suffers from some disadvantages:

- Low-frequency spillover, wherein the PPF tuned for higher-order modes changes the location of lower-order modes.
- PPF also amplifies the response in the quasi-static region
- Multi-mode PPF controller is limited by saturation

Various modifications to the PPF algorithms have been researched such as positive velocity feedback, positive acceleration feedback [20], Positive Position Feedback with Feed-through [21], etc. but they have been ineffective to overcome the limitations. The first objective of over-actuation is realized by the implementation of PPF, also with this, a new strategy of control is studied for overcoming the above-stated limitation. This paves way for the second objective of the research.

Thus, over-actuation with the use of PPF as the control algorithm is studied to improve the performance which otherwise is limited by actuator saturation in under-actuated systems. We would also achieve collocation of various modes and thus broadband damping by the use of over-actuation which translates to improved precision and bandwidth.

1.2 THESIS OUTLINE

Chapter 1 presents the motivation for the research. Chapter 2 provides the required preliminaries required for the context of the thesis and defines the problem statement based on the gap in the literature. It is then followed by the experimental setup and system identification in chapter 3. Chapter 4 proposes the methodology and the tuning of the controller. Chapter 5 provides the discussion of experimental results and the conclusion is given in chapter 6 along with some recommendations.

2 PRELIMINARIES

This chapter aims to introduce the concepts necessary to understand the thesis. A Bird's eye view is presented with references to detail it in depth.

2.1 PIEZOELECTRIC PHENOMENON

The term Piezo-electricity refers to the electricity generated from pressure, which occurs naturally in some mono-crystalline materials like quartz, topaz, Rochelle salt, etc. This phenomenon was first discovered by the Curie brothers. The production of electric charges by these materials when subjected to mechanical stress is termed as Direct Piezoelectric effort (sensing mode). Mechanical deformations due to the application of an electric field are called converse piezoelectric effect (Actuation mode).

Several ceramics or polymers like Lead zirconate Titanate (PZT), Polyvinylidene fluoride (PVDF), can also be made piezoelectric by the process of poling, where dipole pairs or domains are aligned by exposing the element to a strong DC electric field (below the curie temperature). This creates a permanent polarisation in the polymer.

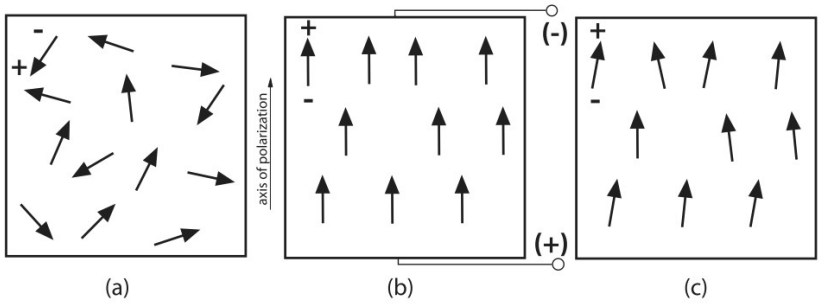

Figure 2.1: (a) Polar domains in Crystal before poling (b) Application of large DC Electric field (c) Removal of Electric field - Remnant Polarisation [1]

The Compression along the direction of Polarisation, leads to voltage as same as the poling voltage, while a tension creates a voltage of opposite polarity, which is the underlying principle of piezoelectric sensors.

Application of voltage similar to a poling voltage, in the direction of polarisation, results in a length increase. An opposite voltage results in a reduction of length, which is the actuation mode of piezoelectric actuators.

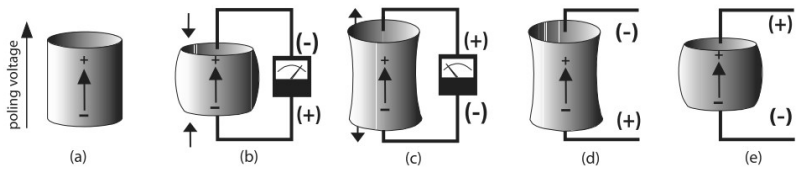

Figure 2.2: (a) Poling direction;(b) & (c) sensing mode; (d) & (e) actuation mode [1]

The constitutive equations that govern the piezoelectric material are,

$$S_{ij} = s^E_{ijkl} T_{kl} + d_{kij} E_k \tag{2.1}$$

$$D_i = d_{ikl} T_k l + \epsilon^T_{ik} E_k \tag{2.2}$$

where

T_{ij} = components of the stress tensor
S_{kl} = components of the strain tensor
s^E_{ijkl} = tensor of compliance under constant electric field
d_{ikl} = piezoelectric constants
E_k = Applied electric field
D_i = vector of electric displacements
ϵ^T_{ik} = dielectric constant under constant stress

Equation 2.1 & 2.2 assumes that the direction of polarisation is along the z-axis. Equation 2.1 describes the situation of actuator while 2.2 refers to the case when the transducer is used as a sensor.

2.1.1 Types of Piezo Transducers

The piezoelectric coefficient, d_{ij} signifies that a strain is developed along the i-axis when the Electric field is applied along the j-axis (external stresses are held constant). For an isotropic structure, there are three kinds of actuation modes possible.

Piezo Stack Actuators

Stack actuators work on the principle of piezoelectric effect (ceramics) using the d_{33} coefficient. Hence, an electric field applied parallel to the polarisation direction results in an extension in the same direction, accompanied by shrinkage in directions 1 and 2, perpendicular to E_3. The movement does not depend on the size of the piezo elements and hence piezo elements are stacked for its multiplicative property. Hence, multiple stacked actuators produce a higher displacement for the same voltage compared to a single layer actuator. These actuators can, therefore, generate a high force or strain for a small voltage. However, Due to the stacked nature of the ceramics, they are susceptible to tension, torsion, or bending stresses and hence are prestressed with an external spring with lesser axial stiffness than the piezo-actuator (Higher stiffness can affect the displacement range).

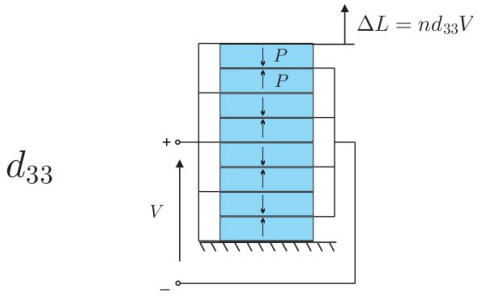

Figure 2.3: Piezostack actuator operation [2]

Piezo Bending Transducers

The purpose of these actuators is to generate bending and is generated by the d_{31} effect of the piezo transducer. These types of actuators are usually bonded to a

beam directly or with a substrate (unimorph or bimorph). A voltage applied in the polarization direction (Z-axis - E_3) generates an axial strain along the x-axis. However, since the actuator is bonded to the relatively stiff beam or substrate, piezo's movement is constrained. Usually, two piezo benders are used for good amplification as when they are driven 180° out of phase with each other, then the top bender extends while the bottom bender contracts which facilitates uniform distribution of strain.

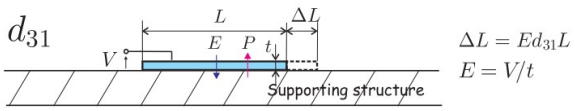

Figure 2.4: Piezo bending actuator operation [2]

The strain (ϵ_p)in the axial direction of the piezoelectric bender, when the Voltage (V) is applied in the polarisation direction is given by,

$$\epsilon_p = \frac{d_{31}V}{t_p} \tag{2.3}$$

where t_p is the thickness of the piezoelectric actuator. The strain distribution is assumed to be linear considering the perfect attachment of the actuator. The stress is discontinuous and the axial force acting on the center of mass of the beam creates a moment.

Since collocated systems have been employed for vibration control, a single piezoelectric bending actuator is usually employed with a piezoelectric bender acting in a sensor mode. The ability to employ a piezo bending actuator in both modes has made it a popular choice in the precision industry.

Actuation Mode

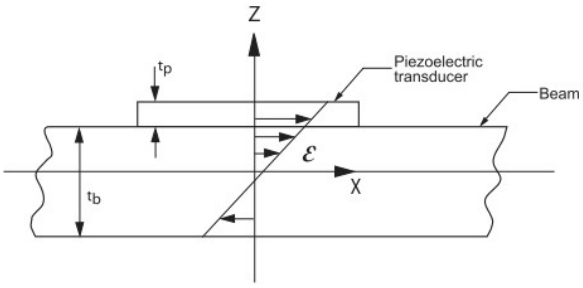

Figure 2.5: Beam with single Piezoelectric actuator [1]

The moment intensity and strain distribution is,

$$M = E_b I \alpha \tag{2.4}$$

$$\epsilon(z) = (\alpha z + \epsilon_0) \tag{2.5}$$

where

E_b = Elastic Modulus of the beam
I = beam's moment of inertia
αz = flexural component of strain
ϵ_0 = longitudinal component of strain

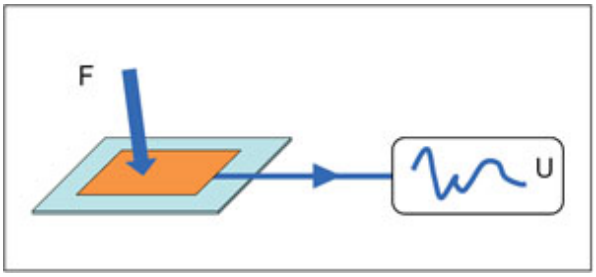

Figure 2.6: Piezoelectric sensor[2]

Sensor Mode

Sensing is based on the direct piezoelectric effect. When a PZT sensor is subjected to a stress, the resulting electric displacement vector is,

$$\begin{Bmatrix} D_1 \\ D_2 \\ D_3 \end{Bmatrix} = \begin{bmatrix} 0 & 0 & 0 & 0 & d_{15} & 0 \\ 0 & 0 & 0 & d_{15} & 0 & 0 \\ d_{31} & d_{31} & d_{33} & 0 & 0 & 0 \end{bmatrix} \begin{Bmatrix} \sigma_1 \\ \sigma_2 \\ \sigma_3 \\ \tau_{23} \\ \tau 31 \\ \tau_{12} \end{Bmatrix} \tag{2.6}$$

A charge is generated by the sensor which is proportional to the d_{31} mode which is collected by the electrodes in the polarisation direction. The generated voltage (V_p) is related to the charge as,

$$V_p = \frac{q}{C_p} \tag{2.7}$$

where C_p is the capacitance of the piezoelectric sensor.

$$V_s = \frac{d_{31} E_p w}{C_p} \int_l \epsilon_1 dx \tag{2.8}$$

where ϵ_1 is the strain in axial direction averaged over the sensor length.

2.2 COLLOCATED MODAL CONTROL

In this section, a brief discussion of Collocated systems is presented and some modal control methods such as Direct Velocity Feedback (DVF), Positive Position Feedback (PPF), Integral Resonance Control (IRC), Integral Force Feedback (IFF), Lead Controller are discussed.

2.2.1 Collocated systems

A collocated system is where actuator and sensor are attached to the same degree of freedom (DOF) and the pair of sensor and actuator are dual such that the product of the pair represents the energy exchange between the structure and control system, Examples of dual systems are a force actuator associated with a displacement sensor, systems with torque actuator with a rotational sensor. Thus, for a collocated system with sensor and actuator attached to DOF k, the transfer function can be written as,

$$G_{kk}(\omega) = \sum_{i=1}^{m} \frac{\phi_i^2(k)}{\mu_i(\omega_i^2 - \omega^2)} + R_{kk} \tag{2.9}$$

where,
ω_i is the resonance of the structure of mode i
ϕ_i is the participation factor of mode and is dependent on the position of actuator and sensor (DOF - k)
R_{kk} is the residue due to modal truncation and is positive (squared term)

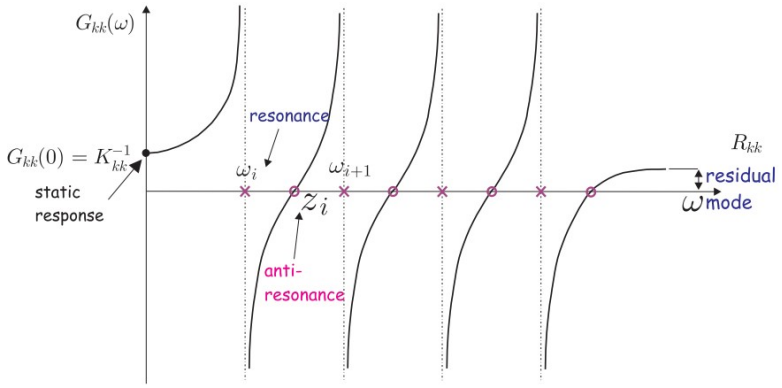

Figure 2.7: Open-loop FRF of an undamped structure with a collocated actuator/sensor pair [2]

Since, the transfer function is a monotonously increasing function (refer figure 2.7) and goes from $-\infty$ at ω_i to ∞ at ω_{i+1}. There must be a point where the transfer function is zero (z_i) between two adjacent resonance frequencies.

Thus a collocated undamped or lightly damped system always leads to a pole-zero combination. The Phase response is limited between 0°and -180°, thus facilitating robustness.

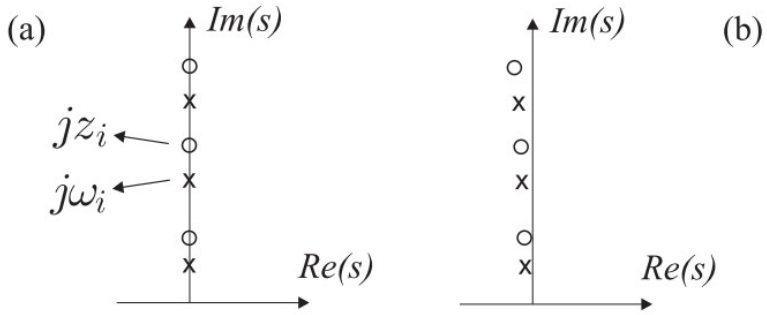

Figure 2.8: Pole/Zero pattern of a collocated actuator/sensor pair (a) undamped; (b) lightly damped [2]

This pole-zero combination can be effectively used for achieving damping by control action. The relation between the location of pole and damping coefficient is shown in figure 2.9,

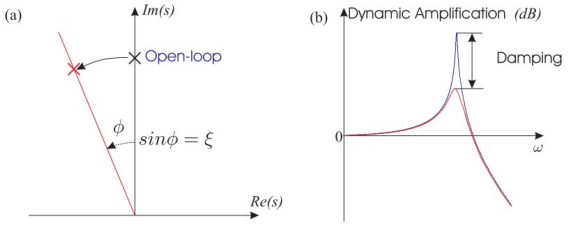

Figure 2.9: Role of damping [2]

The role of the active damping controller is to increase the negative real part of the system poles while maintaining the natural frequencies unchanged.

2.2.2 Direct Velocity Feedback (DVF)

DVF is an active method where the output signals from velocity sensors, multiplied by its gain, is fed back into collocated force actuators.

The DVF for a single DOF is defined as,

$$\ddot{x} + 2\zeta\omega\dot{x} + \omega^2 x = \omega^2 f \tag{2.10}$$

where,

x = Modal Coordinate of the structure
ω = natural frequency of the structure
ζ = Modal damping of the structure
f=g = Modal control force
g = feedback gain

It can be seen that the above equation can be rewritten as,

$$\ddot{x} + \left(2\zeta\omega + g\omega^2\right)\dot{x} + \omega^2 x = 0 \tag{2.11}$$

Thus the damping is achieved by the gain feedback of the velocity. DVF has unconditional closed-loop stability since collocated systems have a phase between 0° and -180° and along with the fixed 90 ° phase of the differentiator and negative feedback gain of -1, signifies that the transfer function will not encircle -1 point in the Nyquist plane. DVF has several limitations as they are subjected to spillover effect (though this does not contribute to loss of stability) [1], Additional dynamics are needed for the roll-off at high frequencies and this might cause instability[2][11]. DVF also requires high control effort at all frequencies as opposed to other methods that facilitate the use of control effort around the damping region. Hence, DVF may lead to actuator saturation and reduced efficiency. DVF cannot be adaptively used with all sensors as velocity measurement requires an additional differentiator for position sensors and an integrator for acceleration measurement. On account of these limitations, DVF is generally not preferred for vibration control.

2.2.3 Positive Position Feedback (PPF)

PPF is a popular collocated modal control method proposed by Goh and Caughey [11]. The idea of PPF is to create additional DOF which would join particular modes [22].PPF introduces a second-order filter, which is fed by the sensed position of the structure. The position response of the filter is then fed back to give the force input to the structure[23]. This is useful for systems that have a transfer function with the same order for numerator and denominator (pole-zero systems). For stability, the overall degree of the denominator of H(s)G(s) must not exceed the degree of the numerator. The controller H(s) must have more poles than zeros. The Positive Position Feedback controller was proposed to solve this problem. The second-order PPF is a second-order filter with the transfer function,

$$H(s) = \frac{K}{s^2 + 2\zeta_f\omega_f s + \omega_f^2} \tag{2.12}$$

where the damping coefficient ζ_f is usually high (0.5 to 0.7) and the corner frequency ω_f is tuned to target a specific mode of interest.

In modal domain, the two-equation for a single DOF system and PPF compensator are:
system:

$$\ddot{\xi} + 2\zeta\omega\dot{\xi} + \omega^2\xi = \omega^2 f \tag{2.13}$$

Compensator:

$$\ddot{\eta} + 2\zeta_f \omega_f \dot{\eta} + \omega_f^2 \eta = \omega_f^2 \xi \tag{2.14}$$

where

f=gη	= modal force for the PPF
ξ	= Modal coordinates
η	= Filter coordinates
ω & ω_f	= system and filter frequencies
ζ & ζ_f	= system and filter damping ratios

The fact that the modal coordinate of the system is positively fed to the compensator and vice versa, it is referred to as PPF.

PPF Tuning

The controller has three variables ω_f (corner frequency), ζ_f (damping ratio) and K (gain). For effective action, it is necessary to tune the corner frequency equal to the resonance frequency that needs to be damped. This facilitates that the damping force is applied at the corner frequency. Thus, the parameters for the tuning are damping ratio and gain.

A combined approach of open-loop and root-locus tuning is proposed. Open-loop is used to guarantee stability and prediction of spill-over effects in the low-frequency region while root-locus is used for maximizing modal damping.

Root-locus

The idea of PPF translates to the addition of a pole to attract translation of open-loop pole of the structure to the Left Half Plane (LHP) as much as possible to impart damping (as shown in figure 2.10).

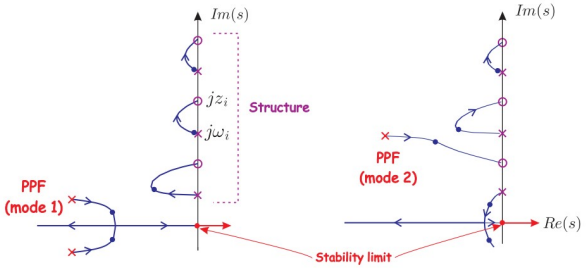

Figure 2.10: Left: PPF aimed at mode1; Right: PPF aimed at mode 2 [2]

The placement of a controller pole creates a loop of each mode which depends on the damping ratio of the controller. Closed-loop poles are tuned based on the gain to impart maximum damping as much as possible.

Thus, the tuning parameters are interconnected and the damping ratio decides the placement of the controller pole, which in turn decides the attraction of a particular mode of the plant and gain decides the placement of closed-loop pole and the optimal value varies for different damping ratio.

Figure 2.11 shows that damping of mode 1 for the same gain and different damping ratios of the controller. Thus, tuning is optimal for a particular combination of damping ratio and gain.

2.2.4 Open-loop: Stability and Performance of PPF

Open-loop tuning is valuable for stability analysis via the Nyquist stability criterion since it is directly based on measurement data (contains time delay and amplifier dynamics) and does not suffer from modeling errors like root-locus [3].

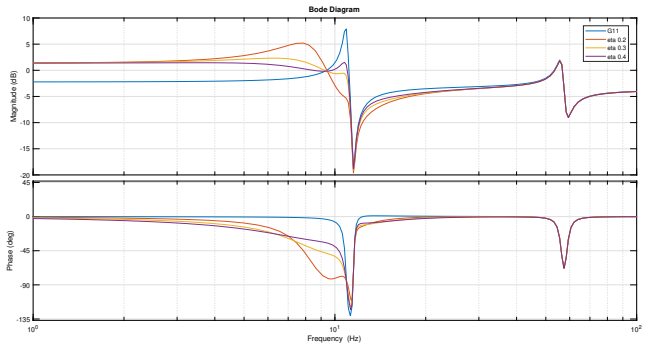

Figure 2.11: Bode plot for different damping ratios - same gain (2000)

The stiffness of the mechanical system appears at -180 ° because of positive position feedback and this low-frequency behavior becomes the limiting factor for stability, resulting in a nondynamic stability criterion according to Nyquist stability criterion [24]. The necessary condition for stability [25] is

$$|PC(\omega = 0)| < 1 \tag{2.15}$$

The closed-loop is always stable since the controller has roll-off characteristics at high frequency and operates on a collocated transfer function.

Performance :

Closing the control-loop creates a new dynamic behaviour, P_{cl}. The local closed

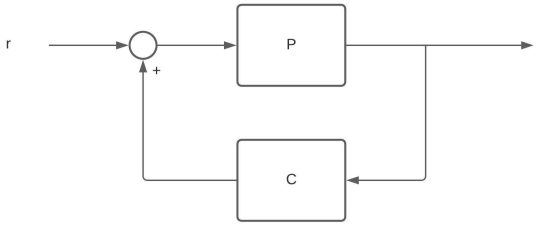

Figure 2.12: PPF

loop disturbance rejection with respect to uncontrolled plant is,

$$S(j\omega) = \frac{P_{cl}(j\omega)}{P(j\omega)} = \frac{1}{1 + PC} \tag{2.16}$$

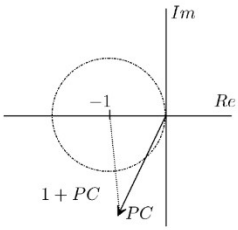

Figure 2.13: Sensitivity in root-locus [3]

The sensitivity can be interpreted as the inverse of PC(jω) to the point minus one in the Nyquist plot as shown in figure 2.13. An optimal performance requires

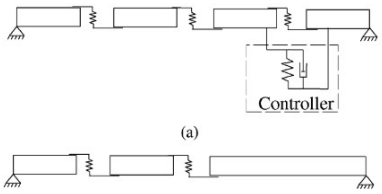

Figure 2.14: High feedback gain of (a) will result in undamped behaviour (b) [3]

$|S| < 1$. It is to be noted that high feedback gain, though leading to increased disturbance rejection might lead to a fixed controlled DOF as shown in figure 2.14. Thus, making it sensitive to disturbances acting on other DOF. Hence, the goal is to maximize energy dissipation from targeted modes.

The sensitivity function also shows the limit of performance according to the bode-sensitivity integral [26],

$$\int_0^\infty log|S(j\omega)|d\omega = 0 \tag{2.17}$$

Thus, combining equation 2.16 and equation A.1, we would get a constant value that would suggest the limits of damping achieved by feedback systems.

$$|P_{cl}| = 10^{\frac{\int_0^{f_u} log|P|d\omega}{f_u}} \tag{2.18}$$

where f_u is the frequency till which the transfer function can be manipulated.

In summary, controllers for active damping add +90 ° or -270 ° phase in open-loop. This can be translated to the control force and measured velocity to be 180° out of phase for energy dissipation. As dynamic controller properties change due to feedback of the plant, it is easier to tune using root-locus rather than open-loop for maximum energy dissipation.

As Seen above, the low pass characteristic of the controller provides active flexibility at low-frequency[27][28][29], active damping at corner frequency (ω_f) and attenuation after ω_f. Physically, the controller provides -90° of phase at the resonant frequency and the structure also provides -90° with respect to its input at the resonance frequency, thus providing a combined effect of -180° of phase at the control frequency. The signal is then positively fed back to the system thus providing the canceling effect [30].

Limitations

- Though PPF prevents the high-frequency spillover, low-frequency spillover causes a shift in resonance. Hence, it has been shown in various studies that multi-mode suppression requires tuning the PPF from higher modes to lower modes to achieve optimum performance [31][21].
- The disadvantage of PPF is that the control makes it more flexible which can lead to large steady-state errors and difficult control in multi-mode suppression [22].
- The PPF modes are limited as increasing the modes leads to lesser gain per mode (due to low-frequency stability criterion), which would lead to less damping and complicated higher-order controllers.
- Also, The tradeoff between the local and global performance is limited by the stiffness loss due to PPF controllers [29].

Various studies have shown the effectiveness of PPF to be a reliable and simple active damping system in applications like space structures [25],nano-positioners [32]. A study between negative and positive position feedback [33] shows that PPF performs better unless the higher structural resonances are located far away with lesser magnitudes. Also, variations of PPF such as Positive velocity position control (PVPF), Positive acceleration Position control (PAPF) were investigated[34] to place the pole at arbitrary locations by inducing additional DOFs for the controller.

2.2.5 Resonance Control (RC)

Resonance Control (RC) is also a second order filter, similar to PPF, but works with negative feedback. It has a second order transfer function with a s^2 term in the numerator [35] [36] [37].

$$H(s) = \frac{-Ks^2}{s^2 + 2\zeta_f \omega_f s + \omega_f^2} \tag{2.19}$$

The Bode plot of the filter is,

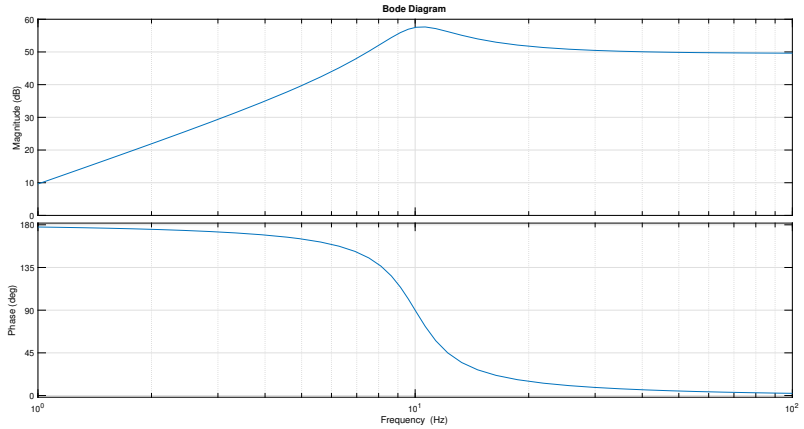

Figure 2.15: Resonance Control

The high pass characteristic causes amplification of sensor noise and may cause instability due to unmodeled dynamics.

2.2.6 Integral Resonance Control (IRC)

IRC is a simple, robust control which is generally employed for collocated sensor and actuators. IRC is a popular algorithm employed in most of the piezoelectric stages [12],[38],[39],[19] which generally uses a force sensor-displacement actuator pair (Pole-Zero interlacing starting with a zero). In principle, IRC uses an integrator to add damping to the system. However, this leads to the limitation of the bandwidth of the system due to the phase lag introduced by the integral action to the second-order system.(refer figure 2.16)

The inherent property of a collocated pair is the pole-zero interlacing in the root locus plot. IRC is used to modify the system into a zero-pole interlacing by the addition of the feed-through term.

As shown in fig 2.17, The controller in feedback can be

- Simple Integrator

$$C(s) = \frac{K}{s} \tag{2.20}$$

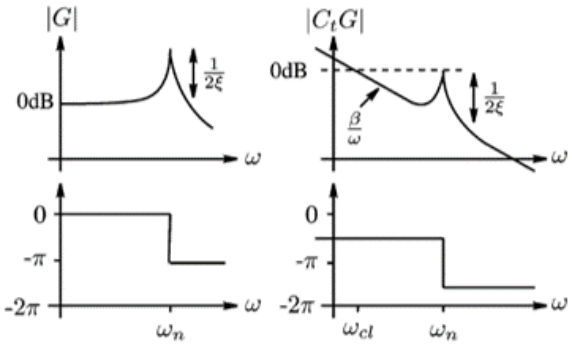

Figure 2.16: limitation of Integral action [4]

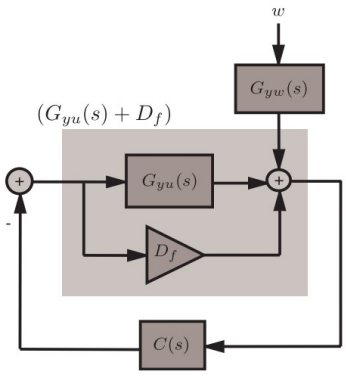

Figure 2.17: limitation of Integral action [4]

It has been well used in positioning systems, particularly in piezo electric stages which usually suffer from hysteresis [12]. But, it suffers from high sensitivity at low frequencies and high control input at low frequencies, which may lead to actuator saturation.

- Lossy Integrator

$$C(s) = \frac{K}{s + p_1} \tag{2.21}$$

A First low pass filter to reduce the gain at low frequencies. But, it is usually not preferred due to its low closed-loop phase margin.

- Band-pass filter

$$C(s) = \frac{Ks}{(s + p_1)(s + p_2)} \tag{2.22}$$

Band pass is an attempt to improve the phase margin by placing a zero at o rad/s and two poles with $p2 < p1$.

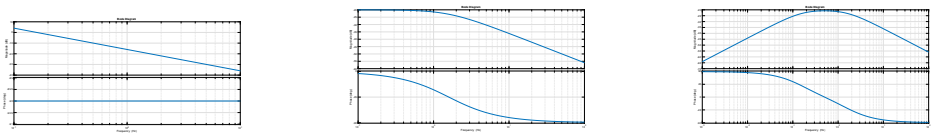

(a) Simple Integrator **(b)** Lossy Integrator **(c)** Bandpass

Figure 2.18: IRC Controller

2.2.7 Lead Control

Lead control has a transfer function of the form,

$$H(s) = g\frac{s+z}{s+p} \tag{2.23}$$

It produces a phase lead in the band between z and p, thus providing active damping for modes within the band. The fact that collocated systems have a phase between 0 ° to 180 ° facilitates the phase of 90 ° when the target mode of the structure lies in the band. The controller does not have a roll-off and is limited by the roll-off of the structure.

The root-locus of a Lead filter applied to a collocated system with two poles in excess of zeros is shown below,

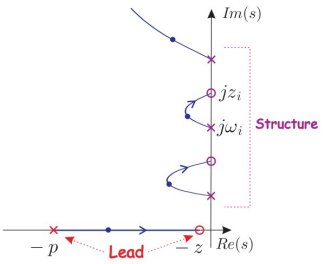

Figure 2.19: Root Locus of closed-loop Lead Control as g $\rightarrow \infty$ [2]

It is to be noted that under a condition when $z << \omega_i < z_i << p$, the characteristic equation and the maximum achievable modal damping turns out to be the same as that of IRC/IFF. The Lead filter suffers from stability issues due to actuator dynamics, It has been found that the LP filter behavior of actuator and sensor dynamics shifts the root locus to the RHP [2]. This is due to the fact that in a lead system, the root locus starts from an open-loop pole to a zero of higher frequency (as shown in figure 2.20).

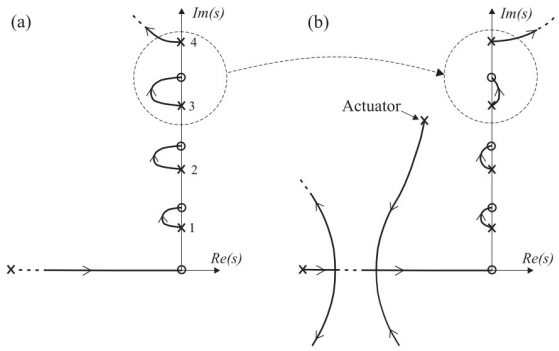

Figure 2.20: Root Locus of closed-loop Lead Control with (a) perfect actuator dynamics and (b) including actuator dynamics ($\omega_2 < \omega_a < \omega_3$) [2]

Controller	Structure	Features
DVF	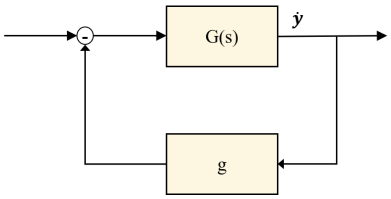	• Direct feedback of velocity signals • Unconditional stability • Subject to spillover effect • High Control effort at all frequencies • Requires an additional differentiator
PPF	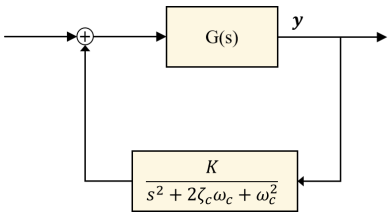	• 2nd order LP Filter • Parallel PPF for individual modes • Subject to Low Frequency spillover • Roll-off at High Frequencies • Lower closed loop stiffness
IRC	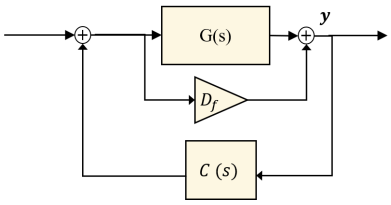	• Zero-pole systems (addition of feedthrough) • Similar to PPF but cannot be applied in parallel • Tuning requires Model of the Plant
Lead	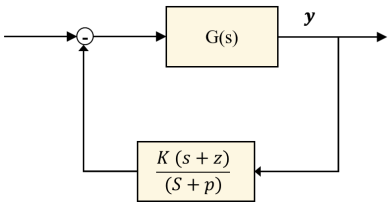	• Creates positive phase within a band • Noise Amplification • Suffers from stability issues due to actuator dynamics • No roll off at high frequencies

Table 2.1: Comparison of Control Structures

2.3 DISTRIBUTED ACTUATION

The word distributed actuation is used in the context to denote that the actuation is distributed along the area for the case of piezoelectric actuation. In general, a single actuator or sensor is not used over the entire length of the beam on account of poor observability and controllability for certain modes.

The concept of using additional actuators have been researched extensively in motion systems for disturbance rejection. Steinbuch et al [5] proved that using additional actuators in motion control improves the modal controllability in the

feedback path. The over-actuated design allows for additional actuators exclusively for controlling the resonances excited by the external disturbances while the other actuators are placed to get the desired motion.

The following plot shows the sensitivity plot for a flexible beam for various situations and it can be inferred that the bandwidth for the over-actuated case (dotted line in figure 2.21) is increased compared to nominal actuation.

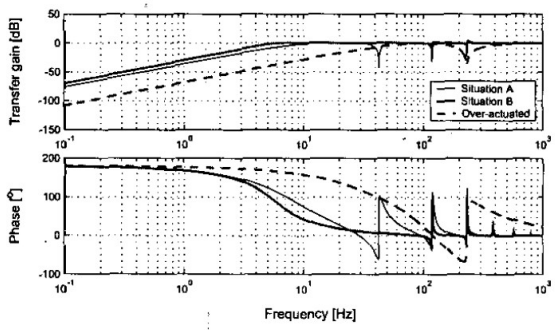

Figure 2.21: Disturbance attenuation of overactuated and traditional systems [5]

The tracking performance comparison for a third-order polynomial setpoint also shows a better tracking for the over-actuated case due to the fact that undesirable modes are not excited by the actuators responsible for movement.

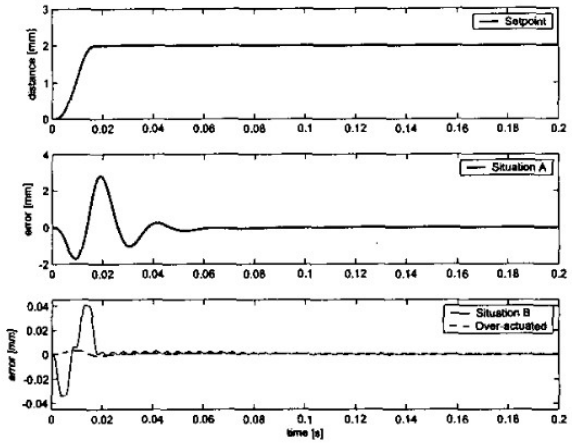

Figure 2.22: Tracking error for traditional and over-actuated systems [5]

Distributed actuation has also been studied in terms of cluster control, wherein eigenmodes of the structure are grouped based on a common characteristic and a modal force is applied on the grouped modes to achieve the desired performance. It can be seen that the control force is applied individually on each cluster to obtain a better performance in terms of energy efficiency for velocity control [40] .

2.4 PROBLEM DEFINITION

The above discussions in multimodal control and control algorithms point to the certain gap that can be summarised as

- The amount of damping is limited to actuator saturation and size, especially in higher-order modes. The amount of energy used is not optimal in under actuation.

- When a Parallel PPF is employed for damping multiple modes, it suffers from sub-optimal tuning for some modes as the closed-loop pole traverses at a different rate for each mode in the root-locus. (refer figure 2.23)

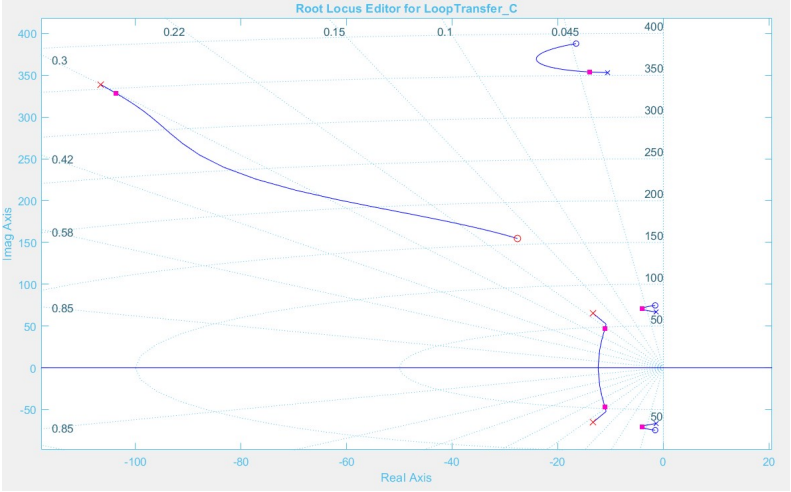

Figure 2.23: Sub-optimal tuning of mode 2

- There is also a limitation in the controllers being used. The well-known PPF suffers from spillover problems which change the location of lower-order modes during multi-mode suppression and require a tracking controller for lowering the steady-state error. (refer figure 2.24)

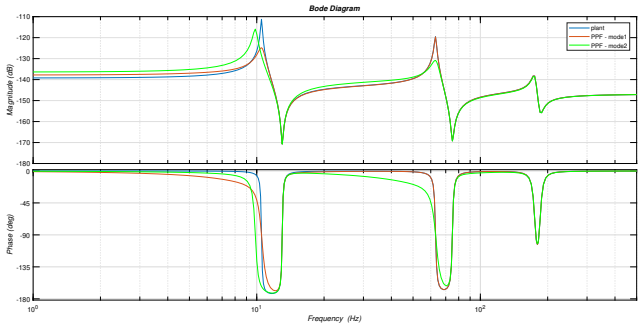

Figure 2.24: Low frequency spillover when tuning for mode 2

2.5 RESEARCH GOAL

To overcome the above-stated limitations, over-actuation is considered.

Thus, The goal of this thesis is to draw a comparative study between under-actuation and over-actuation, in a distributed way, in terms of the amount of damping, energy consumption.

This study also will provide an improvement of the PPF controller to mitigate the spillover problem and the restriction on tuning for stability which will be dealt with in chapter 4.

3 DYNAMICS OF CANTILEVER BEAM

Active vibration control requires the dynamic model of the structure and this can be achieved numerically by finite element approach or experimental approach. This section aims to provide the details of the experimental setup, placement of sensors, and actuators, and system identification.

3.1 PLACEMENT OF ACTUATORS AND SENSORS

Since most of the vibrations manifest themselves as bending modes or a combination of bending modes, a piezoelectric bending transducer or an extension mode of piezo-patch is usually used. Surface-mounted actuators are used rather than a completely distributed actuator filling the entire region [41]. This is due to the averaging property of piezoelectric transducers on the region of action. Thus, The performance of AVC not only depends on the control law but also on the placement of actuators and sensors. The emphasis is further strengthened by the comparative study made between a structure with unwise placement controlled by negative feedback and wise placement of non-collocated pairs. It was found that the former case could be unstable while the latter can be made stable [42].

The first four bending modes of a cantilever beam is shown in figure 3.1

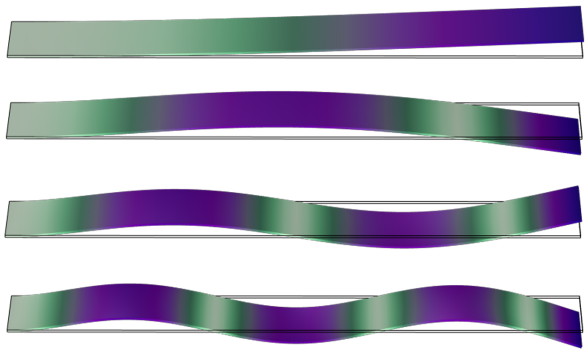

Figure 3.1: 4 Bending Mode of Cantilever beam

There are various objective functions which have been researched for optimal placements such as

1. **Maximising modal moments -** The objective of actuation in AVC is to provide strain in a direction opposite to the strains developed in the host structure. Thus, actuators can be placed such that modal force or moments are increased. The moment generated by a piezoelectric actuator on a cantilever beam is,

$$M = -2b_s Y_p d_{31} \int_{(h_s+h_p)/2}^{(h_s-h_p)/2} E_z y dy = -2b_s \int_0^d \sigma_x y dy \tag{3.1}$$

Y_p = Elastic Modulus of the piezo
y = distance from beam centerline
h_s = thickness of the structure
h_p = thickness of the piezoelectric patch
d = half thickness of the overall structure

In order to increase the moment which is a function of modulus ratio, the curvature ratio of piezoelectric and host structure can be optimized.

$$y'' = \frac{1}{d} \frac{d_{31} E_z (6\rho_a \rho_b)}{\rho_Y (1 - \rho_a \rho_c^2 - 2\rho_a^3) + (6\rho_a \rho_c^2 + 2\rho_a^3)} \tag{3.2}$$

$\rho_Y = Y_s / Y_p$
$\rho_a = h_p / 2d$
$\rho_c = h_s / 2d$

2. **Maximising deflection -** The transverse deflection of the host structure can also be used as a criterion for placement, which is a function of actuator placement. Transverse deflection (mode shapes method) is given by,

$$w(x,t) = \sum_{i=1}^{\infty} \psi_i(x) \eta_i(t) \tag{3.3}$$

The output sensor voltage is given by,

$$V_{sensor} = e_{31} b_p d \int_{x_1}^{x_2} w(x,t)'' dx \tag{3.4}$$

where x_1,x_2 are sensor co ordinates along x-axis.

The optimal locations of the actuator are where the system strains to a maximum. This corresponds to the position of the highest beam curvature. The optimal position is ascertained by the following equation as,

$$\frac{\partial^3 w(x,t)}{\partial x^3} = 0 \tag{3.5}$$

Thus, the maximum deflection of a host structure can be written as a sum of average angular displacement.

$$w_{max,j} = \frac{1}{\omega_j^2} \frac{a_0}{2\zeta_j m_j} (\theta_1 a_p + \theta_2 b_p)_j \tag{3.6}$$

where θ_1 and θ_2 are the average angular displacements of length and breadth vector about x and y axis, respectively.

3. **Minimising control effort -** AVC uses external energy to cause deflection in the structure. The dynamic equation of motion in modal domain is written as,

$$\ddot{\eta(t)} + D\dot{\eta(t)} + \Lambda \eta(t) = B_a V_{act} \tag{3.7}$$

Modal amplitude η is controlled by an external voltage.

In state space, it is written as,

$$\dot{X(t)} = AX(t) + BV_{act}(t) \tag{3.8}$$

$$Y(t) = CX(t) \tag{3.9}$$

where B = [o ; B_a] and C = [o B_v].

The active damping control law to increase energy dissipation through negative velocity feedback control law is,

$$V_{act} = -KY = -KB_v \dot{\eta} \tag{3.10}$$

Electrical energy spent in structural vibration suppression, which has to be minimized is

$$J_e = \int_0^\infty V_{act}^T R V_{act} dt \tag{3.11}$$

This optimization criterion results in the actuator placement at the root for first mode and at the areas of high strain for other modes.

4. **Maximising degree of controllability -** A system is controllable if every state can be affected in such a way that causes it to reach a particular value within a finite amount of time. It is a function of system dynamics and location and number of actuators. The essential condition is that the controllability matrix, R must have a full rank. It is possible when the actuator is placed at a location where energy consumption is less and modal forces are the largest. The optimization is constructed by the use of a controllability grammian matrix,

$$G_c(t) = \int_0^{t1} e^{At} B B^T e^{A^T t} dt \tag{3.12}$$

Criterion	Modes to be controlled	Location	Source
Maximizing modal forces/moments	First Second	Actuators placed near root One actuator at distance less than 0.216 times beam length driven 180° out of phase with second actuator at distance greater than 0.216 times beam length bonded to opposite side	(Crawley and de Luis, 1987) [43]
Maximizing deflection of structure	First Second and higher	Actuators placed near root Collocated pair where opposite edges of actuator correspond to equal curvature of beam mode (either side of anti nodes)	(Barboni et al.,2000) [44]
Minimizing control efforts/Maximizing energy dissipated	First four	DVF • Collocated pair placed at 0.153 times beam length (when one pair is used) • Collocated pair placed at 0.15 times beam length and second at 0.71 times beam length (when two pairs are used) • Collocated pair placed at 0.158 times beam length, second at 0.359 times beam length and third at 0.828 times beam length from root (when three pairs are used)	(Yang et al.,2005) [45]
Maximizing degree of controllability	First First two First three	Actuators placed at root Collocated pair placed at 0.56 times beam length from root Collocated pair placed at 0.7 times beam length from root	(Wang and Wang,2000) [46]

Table 3.1: Optimal Locations of surface bonded piezoelectric sensor and actuator patches on a cantilever beam structure

3.1.1 FEA Simulation for the placement of actuators and sensors

The optimal location for maximum control of modes is simulated in comsol by using the optimization module, which takes the minimization of tip displacement as the objective function.

Assumptions:

1. Piezoelectric patches are considered as moments with a spacing equal to the actuator length
2. Sensors are assumed to be placed at the same location as actuators
3. 1D approximation of beam is considered as only bending moments is of interest
4. Disturbance signal is applied at 50mm from the root of the beam as a point force at the resonance frequencies which was found from modal analysis of the beam (refer figure 3.1)

A 1-D comsol simulation was carried out with the location of counter moments as the design variable.

Figure 3.2 & 3.3 show the displacement of the beam tip for various locations of the counter-moment of mode-1 & mode-2 respectively. This inturn gives us the optimal locations of piezoelectric actuators.

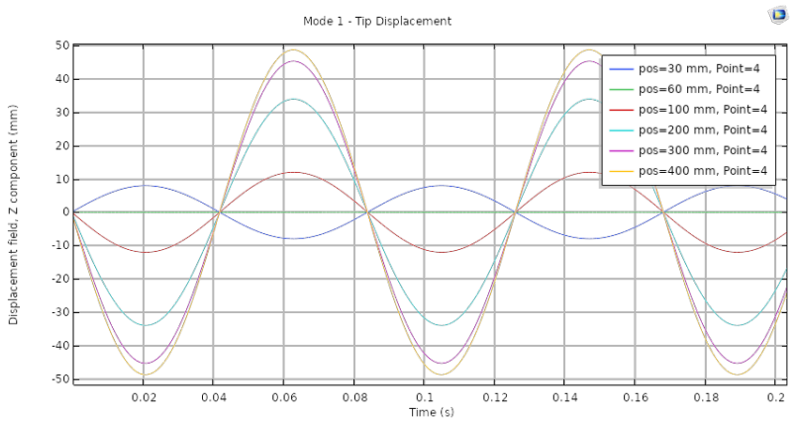

Figure 3.2: Optimal locations of Mode-1

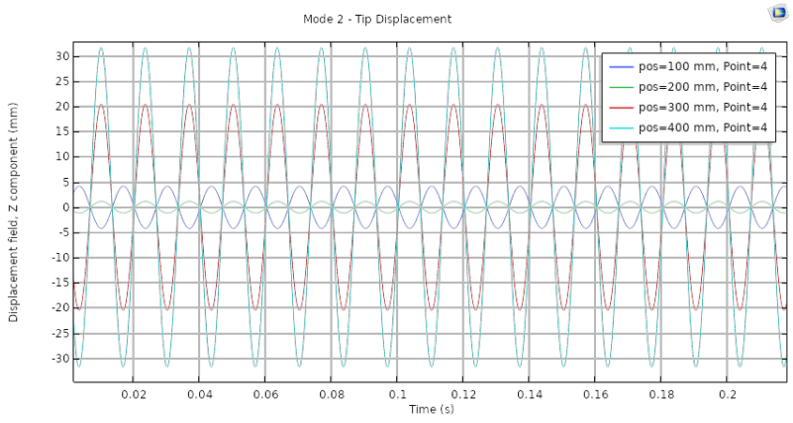

Figure 3.3: Optimal locations of Mode-2

It can be inferred that the tip displacement is the least at a location of around 60mm from the root for mode 1. Similarly, the tip displacement is the least at around 200 mm from the root for mode 2.

	FEM	Experiments
Mode 1 (Hz)	10.5	10.64
Mode 2 (Hz)	56.3	56.69
Mode 3 (Hz)	155	155.3
Mode 4 (Hz)	301	305

Further inspection of the maximum strain energy of a cantilever beam also reveals the location of actuators as found by the 1-D study to be feasible (refer figure 3.4).

Thus, the location of the center of actuators and sensors are

1. Mode 1 - 80 mm
2. Mode 2 - 237 mm
3. Mode 3 - 167 mm

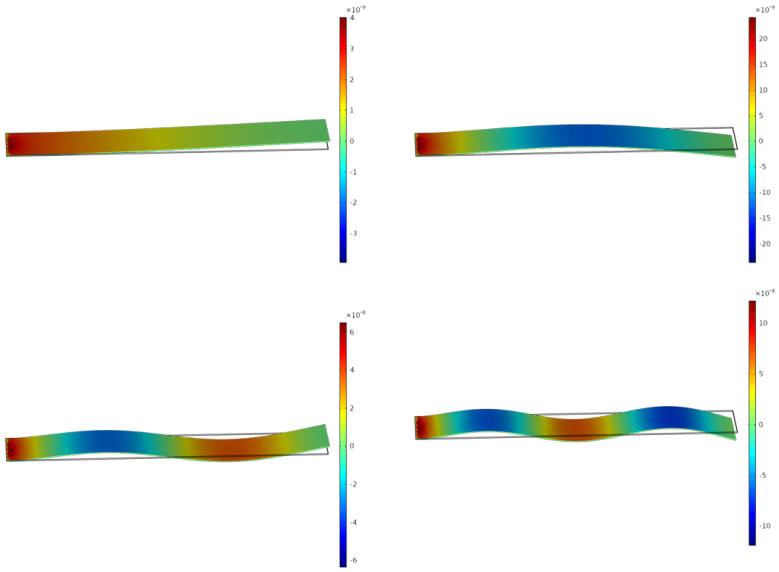

Figure 3.4: Location of Maximum strain energy (red or navy blue) - Mode 1 to Mode 4 (clockwise from top-left)

3.2 EXPERIMENTAL SETUP

A Cantilever beam, made of aluminum, representing a flexible resonant system is considered. The cantilever is clamped at one end and free at the other end. A disturbance signal applied to the system generates high amplitude vibrations at its resonant frequencies. For this work, there are two steps of the experiment. The parameter of the beam, type of sensor (P-876.A15), location of the sensor, and the number of sensors used remain the same for both the cases.

- Step-1 : 3 piezo-actuators (P-876.A12) (refer figure 3.5)
- Step-2 : 7 piezo-actuators (P-876.SP1) (refer figure 3.6)

.

The piezoelectric-stack near the root of the cantilever (refer 4 in figure 3.5) will be used to supply a disturbance to the beam through an electric signal (w). The tip deflection is measured by using a laser triangulation sensor (represented by 5 in figure 3.5)

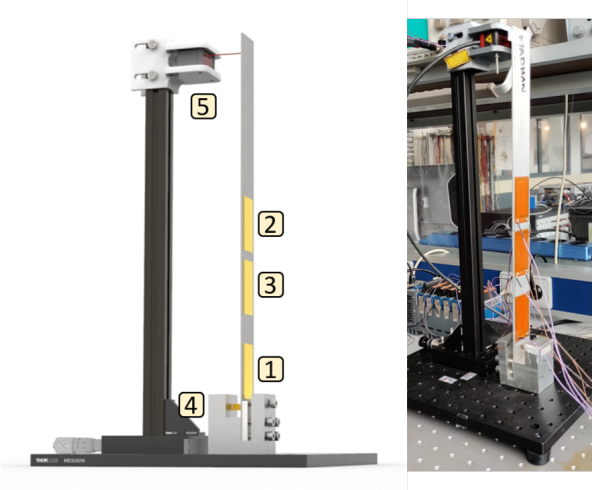

Figure 3.5: Case-1 Setup

Step 1 & 2 will be used to study the comparison for the under-actuated case and over-actuated case. The whole experiment is placed on a vibration isolation table. The Stack is also pre-tensioned sufficiently to prevent it from high tensile stress, which might lead to delamination and failure at high frequencies. Also, a spherical tip is used to apply a point load and to prevent the stack from uneven loading (shear) to prevent the dangerous bending and tensile stresses building up.

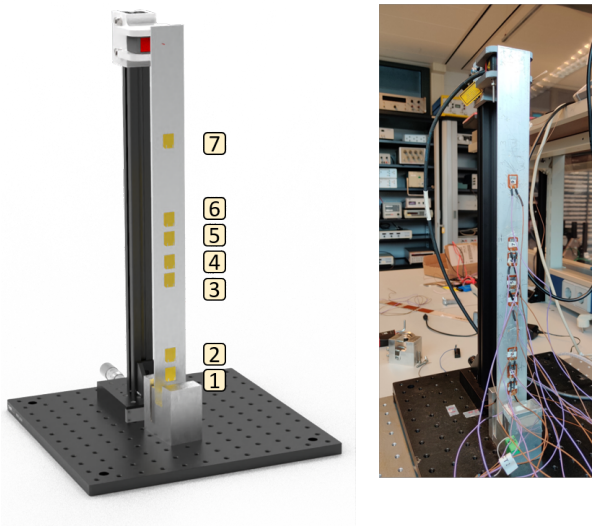

Figure 3.6: Case-2 Setup

The material properties of the beam and piezoelectric transducers are given in table 3.2 & 3.3.

length (mm)	450
width (mm)	40
thickness (mm)	2
Elastic Modulus (GPa)	69
Density (kg/m^3)	2700

Table 3.2: Parameters of beam

	P-876.A12	P-876.A15	P-876.SP1	P-887.31
Dimensions (mm x mm x mm)	61 x 35 x 0.5	61 x 35 x 0.8	16 x 13 x 0.5	7 x 7 x 16
Electrical Capacitance (nF)	90	45	8	2200
Active Thickness (mm)	0.2	0.5	0.2	13.5
Min Axial Deformation (um/m)	650	800	650	0.013
Blocking Force (N)	265	775	280	1700

Table 3.3: Transducer Properties

3.3 SYSTEM IDENTIFICATION

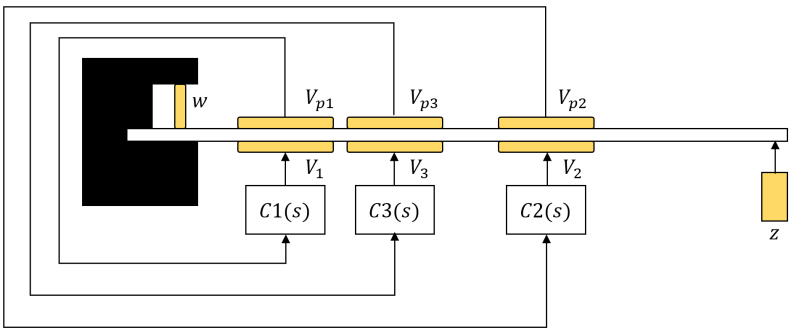

Figure 3.7: Case-2 Setup

The system is treated as a four-input-four-output system for step-1 and a seven-input-four-output system for step-2.

Case-1

The inputs (V_1,V_2,V_3) are the voltages applied to the actuators of the collocated piezoelectric patches and the outputs (V_{p1},V_{p2},V_{p3}) are the voltages induced at the corresponding sensors. Disturbance (w) is applied as the fourth input through a piezo-stack at the base of the beam and the tip displacement (z) as measured by the laser triangulation sensor, is considered as the fourth output.

The FRF $G(i\omega)$ is a 4x4 matrix with each element $G_{ij}(i\omega)$, i,j = 1,2,3,4.

$$G_{ij}(i\omega) = G_{y_i u_j} = \frac{Y_i(i\omega)}{U_j(i\omega)} \tag{3.13}$$

where $y_1 = v_{p1}$,$y_2 = v_{p2}$,$y_3 = v_{p3}$,$y_4 = z$,$u_1 = v_1$,$u_2 = v_2$,$u_3 = v_3$,$u_4 = w$.

The respective FRF are determined by applying a chirp signal (0.1 to 250 Hz) to the corresponding actuators and measuring the output signals from the corresponding sensors. The chosen frequency range captures the first three resonant modes of the beam.

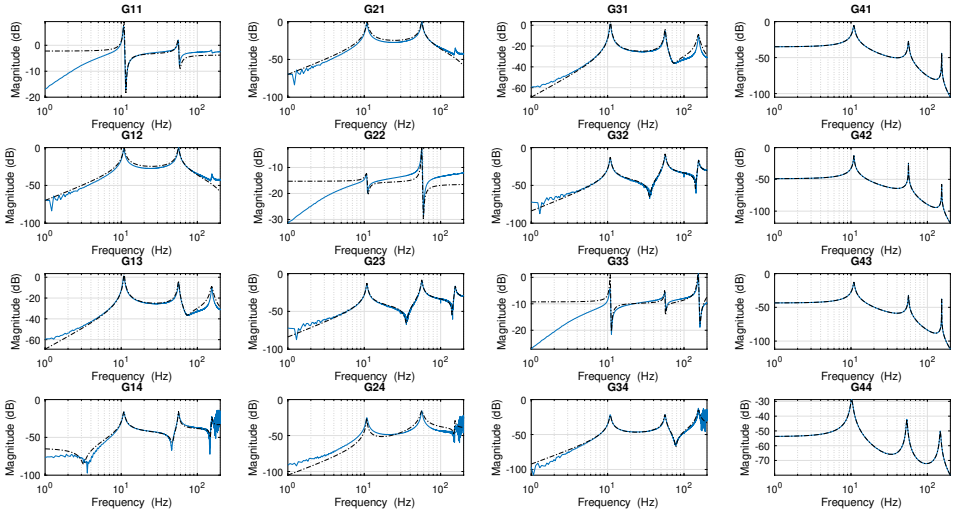

Figure 3.8: 4x4 FRF of Case-1

Case-2

The inputs (V_1,V_2,V_3, etc.,) are the voltages applied to the actuators of the collocated piezoelectric patches and the outputs (V_{p1},V_{p2},V_{p3}) are the voltages induced at the corresponding sensors. Disturbance (w) is applied as the eighth input through a piezo-stack at the base of the beam and the tip displacement (z) as measured by the laser triangulation sensor, is considered as the fourth output.

The FRF $G(i\omega)$ is a 8x4 matrix with each element $G_{ij}(i\omega)$, i = 1,2,3,4 j = 1,2,...,8.

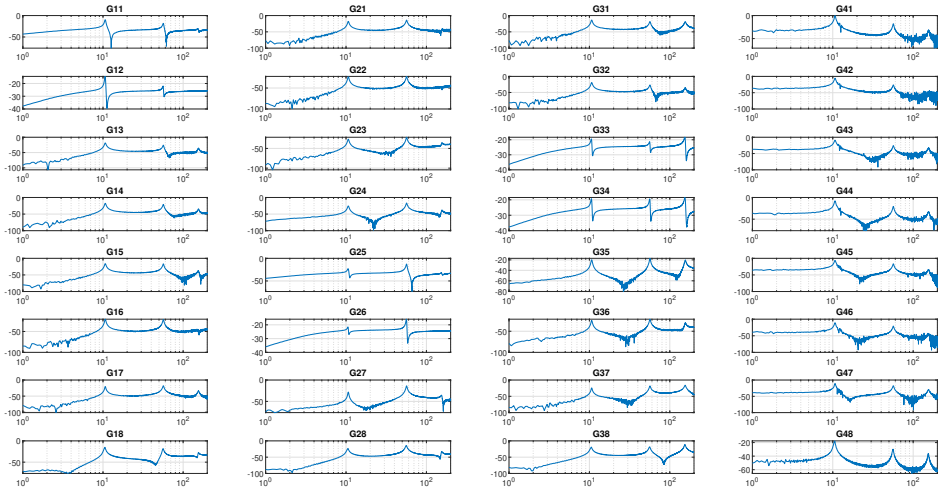

Figure 3.9: 8x4 FRF of Case-2

3.3.1 Reason for +2 Slope in FRF's with Piezoelectric Sensing

In section 2.1.1, it was concluded that

- Piezoelectric sensors act as a parallel plate capacitor

- The average strain measured along its length is related by.

$$\epsilon_1 = V_s C_p / E_p d_{31} \tag{3.14}$$

The piezoelectric sensor has a very high output impedance compared to the measuring device (NI 9201) that has an impedance on the order of MΩ. This reduces the sensor sensitivity at low frequencies[7].

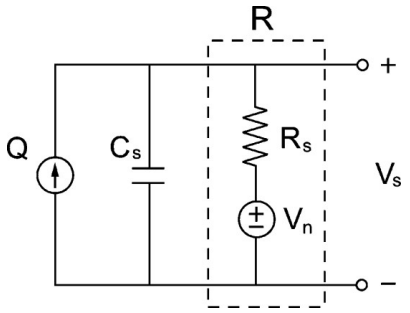

Figure 3.10: High pass nature of piezoelectric sensor [6]

Thus, The capacitive nature of the piezoelectric sensor and the finite input impedance create a high pass characteristic which has a [6] cut-off frequency, given by,

$$\omega_s = 1/R_s C_s \tag{3.15}$$

R_s = input impedance of measurement system ; 1MΩ
C_s = Capacitance of sensor ; 45nF

This high pass characteristic limits the use of a tracking controller as it could destabilize a tracking control. [47]. Also, at low frequencies, the charge tends to leak through the sensor.

The above problems are usually solved by some signal conditioning steps such as a charge amplifier, also called charge to voltage converter. This converts the high impedance signal to a low impedance signal for the measurement system to record (refer figure 3.11).

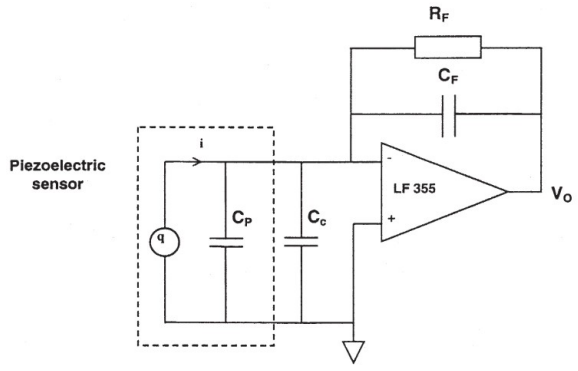

Figure 3.11: Piezoelectric sensor with charge amplifier [7]

The usage of the high pass is to provide a capacitance (C_f) in feedback such that the voltage signal is developed across the feedback capacitor which usually has a very low cut-off frequency. However, piezoelectric sensors with signal conditioning still suffer from poor static measurements. It is also worth noting that by using a charge amplifier, we negate the influence of cable capacitance which creeps up as a disturbance otherwise.

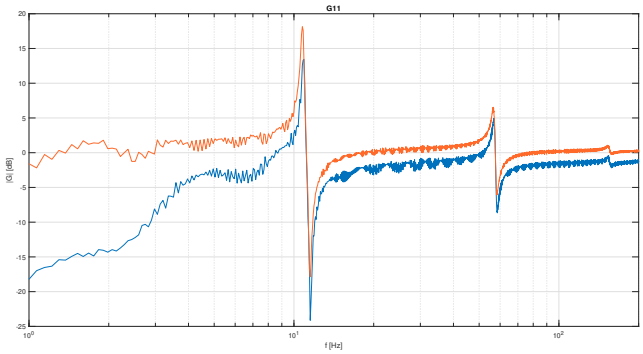

Figure 3.12: G11 comparison without (Blue) vs with charge amplifier (Orange)

The following plot (refer figure 3.12) shows the effect of charge amplifier on low frequency. It compares the G11 transfer function without a charge amplifier(blue) to G11 with a charge amplifier (orange).

However, in this study, we would be neglecting the usage of charge amplifier due to the fact that for active damping, the high pass nature does not affect a lot (This is due to the resonances being well above the cutoff of the high pass cutoff frequency. Only mode1 will be affected to a small extent).

4 TUNING OF CONTROLLER

This chapter deals with the detailed description of the novel band-pass PPF and its tuning methodology. Furthermore, the tuning of SISO PPF and bandpass PPF is discussed. This is followed by a discussion of 2-DOF controller namely the parallel PPF.

4.1 NOVEL BAND-PASS PPF

We have previously seen that PPF suffers from limitations such as low-frequency spillover and steady-state error.

Let us analyse it systematically with the closed loop sensitivity,

$$S = \frac{n}{y} = \frac{1}{1 + GC} \tag{4.1}$$

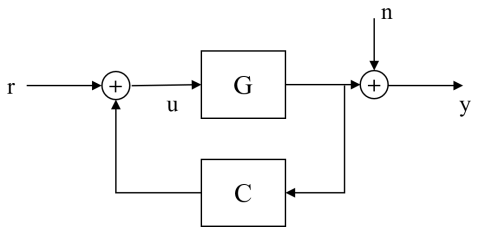

Figure 4.1: Closed loop of a system

We need to reduce the effect of the controller at low frequencies for the limitation of the PPF to disappear.

Thus our requirements are,

At low frequency,

$$|S| = |G| \tag{4.2a}$$

$$\angle S = \angle G \tag{4.2b}$$

At high Frequency,

$$|S| = |C| \tag{4.3a}$$

$$\angle S = \angle C \tag{4.3b}$$

At resonance frequency,

$$|S| = |\frac{1}{1 + GC}| \tag{4.4a}$$

$$\angle S = 90^\circ \tag{4.4b}$$

Thus, we require very low gain of C in equation 4.1 and this can be achieved by a band-pass filter. The bode plot of the 1st order Band pass (BP) (Red), 2nd order BP (yellow) is compared with the PPF (blue) in figure 4.2.

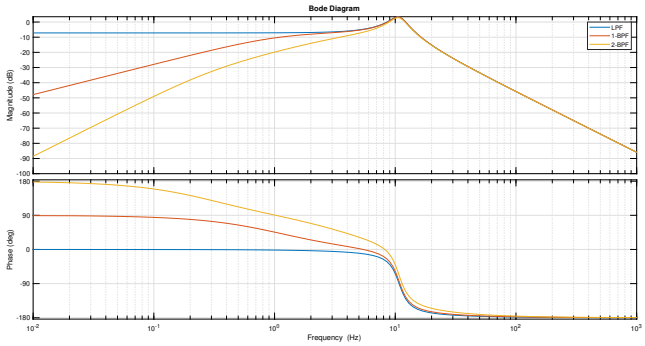

Figure 4.2: Low-pass filter and Band-pass filter

The transfer function of a first-order and second-order band pass filter is,

$$C(s) = \frac{Ks}{(s+\omega_z)(s^2+2\zeta_f\omega_f s+\omega_f^2)} \tag{4.5}$$

$$C(s) = \frac{Ks^2}{(s^2+2\zeta_z\omega_z s+\omega_z^2)(s^2+2\zeta_f\omega_f s+\omega_f^2)} \tag{4.6}$$

where

ω_z = cutoff frequency for lead filter
ω_f = Filter frequency
K = gain
ζ_f & ζ_z = filter and lead damping ratios

As seen in the figure 4.2, the Bandpass filter can be used to reduce the spillover effect or the flexibility being added to the lower resonance modes due to the low gain of the filter at low frequencies.

It is also to be noted that the band-pass filter needs to be tuned based on the phase. The cutoff frequency of the filter has to be tuned to a frequency a tad lower than the mode to be controlled. This is because the phase added by the lead part affects the region of interest. It can also be seen in figure 4.1, where the frequency of 90 ° phase shift occurs at a later frequency than the cut-off frequency.

The closed loop bodeplot for the controllers shown in figure 4.2 is shown in figure 4.3.

The corresponding transfer functions of LPF, 1-BPF and 2-BPF are

$$C(s) = \frac{2000}{s^2+40s+4630} \tag{4.7}$$

$$C(s) = \frac{2000s}{(s+6.805)(s^2+40s+4630)} \tag{4.8}$$

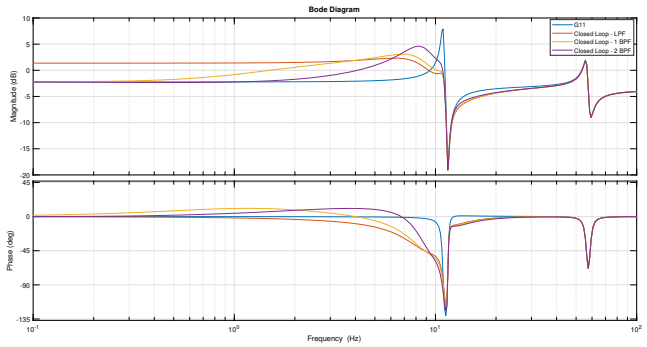

Figure 4.3: Plant tuned for same gain of LPF,1st order BPF and 2nd order BPF

$$C(s) = \frac{2000s^2}{(s+25.4)(s+1.823)(s^2+40s+4630)} \tag{4.9}$$

It can be seen that the same tuning does not work for the band-pass filter. This is due to the following reasons,

1. The additional zero and pole change the controller characteristic in root locus. The pole due to LPF is now coupled to the zero placed at $s = 0$ and there is a new pole placed at ω_z and the same gain does not hold anymore.

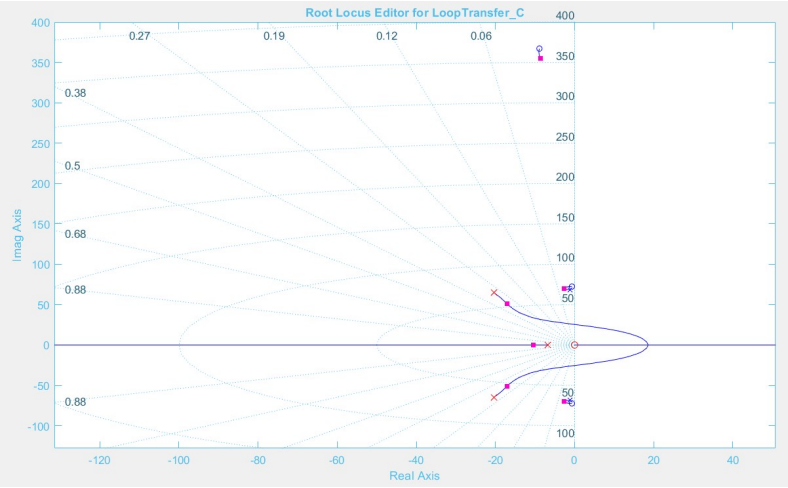

Figure 4.4: Root-locus for 1-BPF tuned for first mode

2. The frequency where the controller crosses 90 ° is shifted and hence needs re-tuning of the corner frequency (ω_f)

The correctly tuned Band-pass are shown below,

$$C(s) = \frac{1800s}{(s+6.805)(s^2+40s+4410)} \tag{4.10}$$

$$C(s) = \frac{1600s^2}{(s+25.4)(s+1.823)(s^2+40s+3500)} \tag{4.11}$$

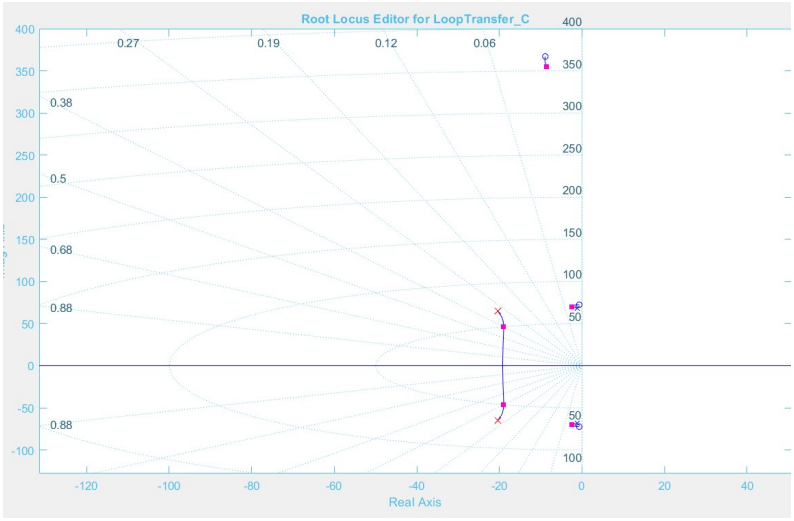

Figure 4.5: Root-locus for LPF tuned for first mode

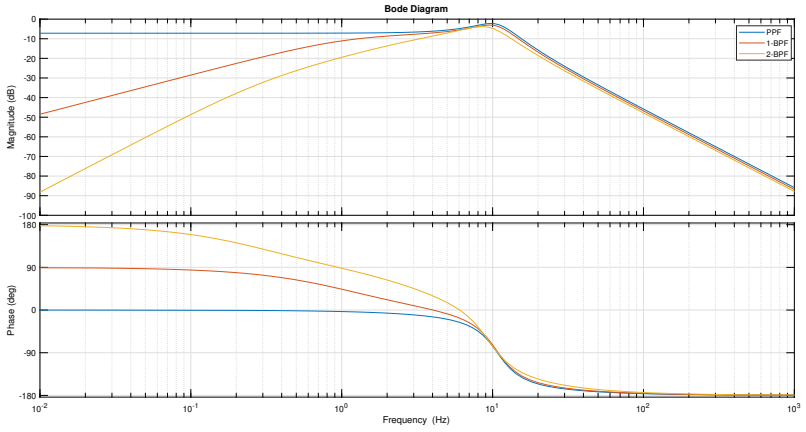

Figure 4.6: controller bode with PPF,1-BPF,2-BPF

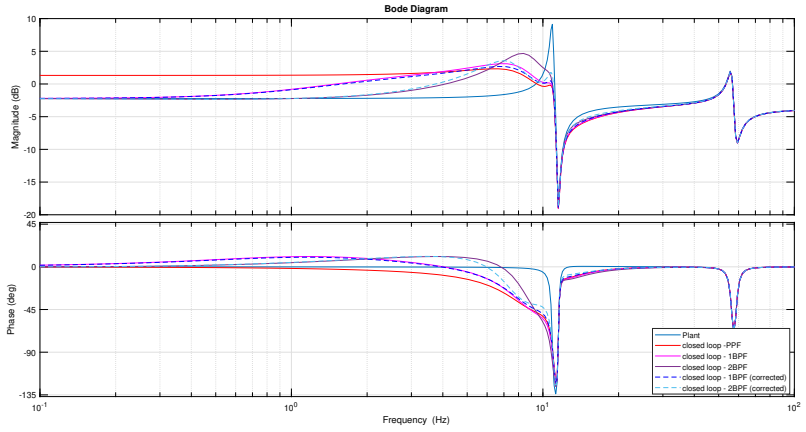

Figure 4.7: closed loop bode with PPF,1-BPF,2-BPF; Blue - Plant, Orange - Closed loop with PPF,Violet - Closed loop with 1-BPF, baby pink - Closed loop with 2-BPF, Dotted Blue - Closed loop with corrected 1-BPF, Dotted cyan - Closed loop with corrected 2-BPF

Thus, the characteristic of tuning are

- When tuning for the phase of the controller, the corner frequency is tuned for a lower frequency. Hence, the gain is at a different frequency which leads to less damping than the PPF case, which is shown in figures 4.3 & 4.7
- Steady-state error is reduced drastically at the expense of increased flexibility near the region of interest.
- Low-frequency spillover will be reduced if the two modes are separated by a sufficient margin
- The cutoff frequency for a lead component is maintained at 0.1 times the corner frequency to reduce the effect of phase spillover of lead component

4.2 EXPERIMENTAL TUNING OF SISO PPF AND PARALLEL PPF

In this section, we will implore the idea of experimental tuning based on the collocated transfer function and compare it to the simulated model for two cases

- SISO, G11 for mode-1
- Parallel PPF, G11 for mode-1 & mode-2

4.2.1 SISO PPF

The following figure 4.8 show the experimental bode of Plant (blue) and closed loop bode of the system (red). The third subsection of figure 4.14 indicates the coherence of the measurement.

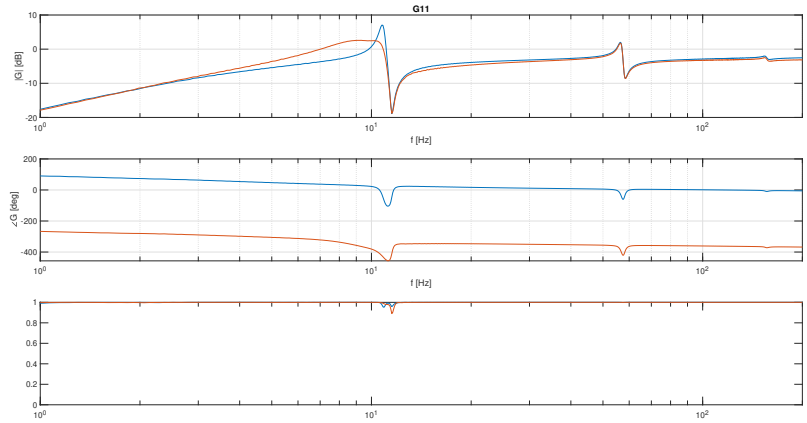

Figure 4.8: Bode plot of G11 - without (blue) and with control (red) - SISO PPF

It is also nice to note that the simulation agrees well with the simulations provided in the appendix (B). Further plots of G21, G31, G24, G34 are provided in the appendix along with time-domain plots.

The following figure 4.9 shows disturbance attenuation which is the main objective of vibration control. The disturbance is provided by a stack actuator as discussed earlier.

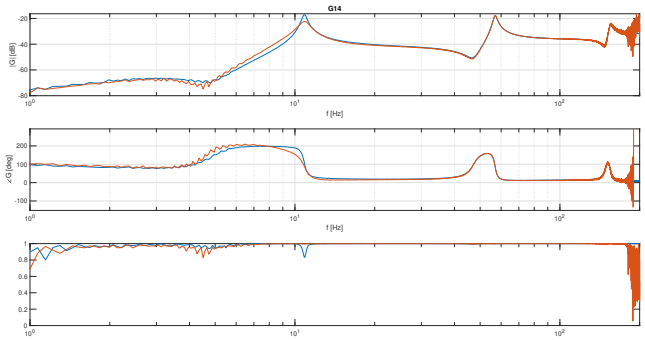

Figure 4.9: Bode plot of G14 - without (blue) and with control (red) - SISO PPF

Observation

The tuning of PPF can be based on two objectives,

- Tuning based on open-loop stability, in which the gain is selected such that steady-state gain is less than zero. We have two transfer functions G11 & G14. Tuning based on the optimal gain of G11 for particular damping leads to certain damping in G14 as well. This is not the sub-optimal damping for G14 i.e disturbance attenuation. But this ensures that all the actuators are not saturated and are stable. This type of tuning is called optimal damping.
- G14 has a lower damping ratio and when the root-locus of -G14C is analyzed, it is seen that the first pole is more attracted more to the LHP and the gain can be substantially increased to impart damping. However, for these values of gain, the actuator 1 will be saturated in the G11 case. This type of tuning is called maximum damping.

We will henceforth tune the controller for optimal damping and consider the amount of damping in disturbance attenuation as a performance indicator.

4.2.2 Parallel PPF

The idea of parallel PPF is the introduction of extra degree of freedom (2 DOF) in which two modes can be controlled. we have seen that the tuning based on one DOF attracts a particular mode. Thus, when tuning for the optimal gain, the other modes are not attracted to the LHP, This is evident in figure 4.5. To create an attraction we can add another controller pole, to create an attraction. Parallel PPF is a type of the SISO case and uses actuator-1 for controlling mode-1 and mode-2.

The equation of the controller will be,

$$C = \frac{K_1}{s^2 + 2\zeta_{f1}\omega_{f1}s + \omega_{f1}^2} + \frac{K_2}{s^2 + 2\zeta_{f2}\omega_{f2}s + \omega_{f2}^2} \tag{4.12}$$

The subscripts 1 and 2 denote mode-1 & mode-2 parameters.This leads to the creation of a zero, which is dependent on the relative gain of the two modes.

$$C = \frac{(K_1 + K_2)s^2 + (2\zeta_{f2}\omega_f 2K_1 + 2\zeta_{f1}\omega_{f1}K_2)s + K_1\omega_{f2}^2 + K_2\omega_{f1}^2}{(s^2 + 2\zeta_{f1}\omega_{f1}s + \omega_{f1}^2)(s^2 + 2\zeta_{f2}\omega_{f2}s + \omega_{f2}^2)} \tag{4.13}$$

The location of zero is,

$$\omega_z = \pm\sqrt{\frac{K_1\omega_{f2}^2 + K_2\omega_{f1}^2}{K_1 + K_2}} \tag{4.14}$$

Thus, the location of zero of the controller has an effect on the tuning.

Effect of controller zero on tuning

1. **Frequency of zero** - A constant damping factor for all zeros and poles of the controller is considered. Now, Placing the zero close to the second resonance results in optimal damping of mode-1 with a little degree of freedom for mode-2, while placing the controller zero below the first resonance causes a Pole-zero flip and causes instability. Placing the controller zero a tad higher than the first resonance attracts both the modes equally.

2. **Damping ratio of zero** - The gain and location of zero are kept constant and the damping ratio is changed. It is noticed that change of damping ratio influences the rate of attraction of modes, in simpler terms the loop of mode 1 changes. Increasing the damping ratio, increased the loop of mode-1, and decreased the loop of mode-2. A sweet spot is found out for the parallel PPF and is found to be 0.3.

For Brevity, the plots of root-locus are shown in the appendix (C). Thus, we fix the controller on the above discussion. Also, It is imperative to tune the controller from high frequency to low-frequency keeping in mind the low-frequency spillover phenomenon. The simulated plant and control are also shown in the appendix for brevity.

The tuning of the controller is based on two modes rather than one mode and It can be seen in figure 4.10 that both modes are damped for maximum possible damping.

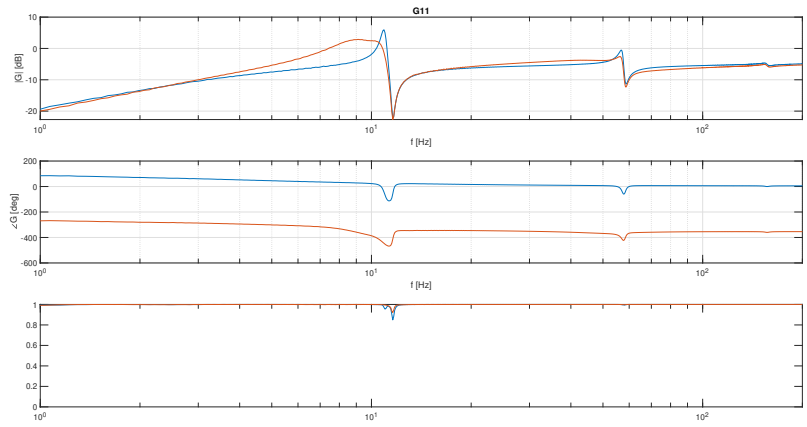

Figure 4.10: Bode plot of G11 - without (blue) and with control (red) - Parallel PPF

Also, the Bode plot of the disturbance attenuation (refer figure 4.11) shows that both the modes are attenuated is shown below. Other experimental transfer functions and time-domain signals are presented in the appendix (C) .

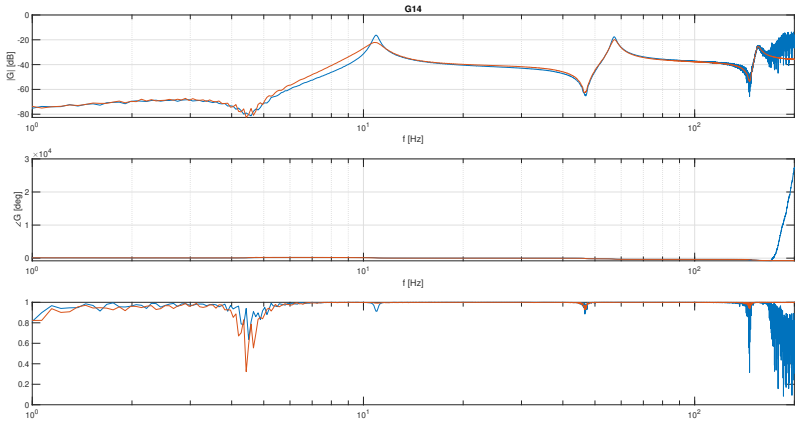

Figure 4.11: Bode plot of G14 - without (blue) and with control (red)- Parallel PPF

4.3 EXPERIMENTAL TUNING OF SISO 1-BPF AND PARALLEL 1-BPF

In this section, Bandpass is implemented to achieve the same damping with a reduction in steady-state error and to get over the problem of spillover. The First-order Bandpass filter is considered for the validation of the advantage provided by this filter and can be enhanced by a second-order filter.

4.3.1 SISO 1-BPF

Band-pass filter as given in equation 4.5 is employed and simulated for optimal gain. The characteristic as discussed in the previous section is used for tuning and the simulated results based on the tuning are shown in the appendix (B).

The optimally tuned closed loop systems is shown in comparison with the uncontrolled plant in figures 4.12 & 4.13 respectively.

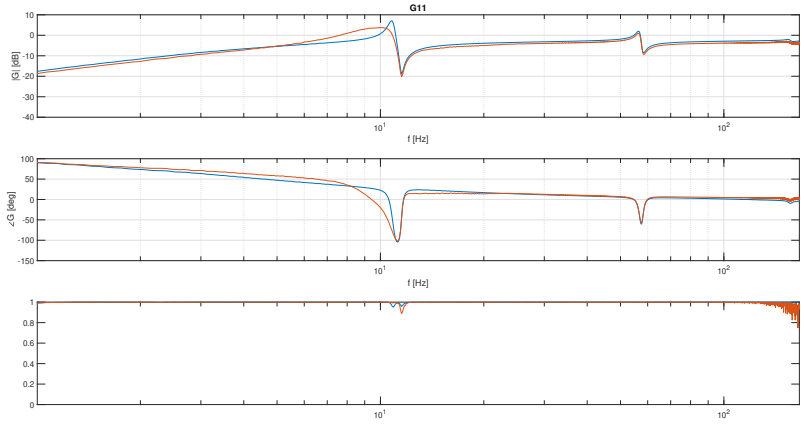

Figure 4.12: Bode plot of G11 - without (blue) and with control (red) - SISO BPF

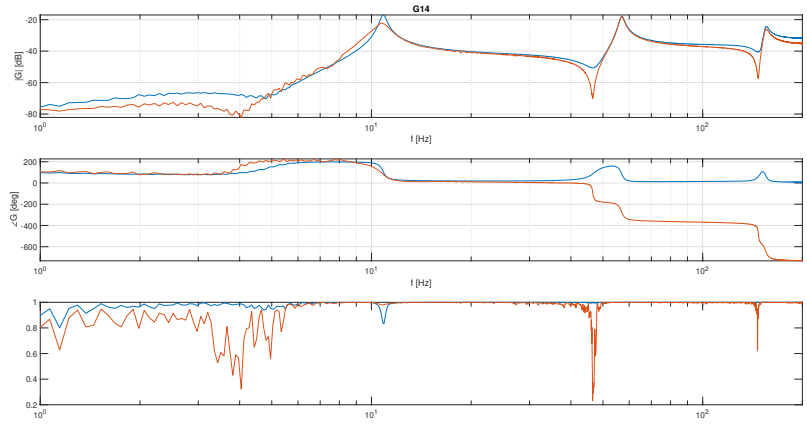

Figure 4.13: Bode plot of G14 - without (blue) and with control (red) - SISO BPF

The important difference to note from PPF is the low-frequency line of the transfer function. Thus, the steady-state error is effectively reduced. This eliminates the need for external control in PPF for steady-state error.

4.3.2 Parallel 1-BPF

Usage of Parallel PPF was limited by the performance of the low-frequency region and hence the introduction of the band-pass filter will aim to address the problem. However, we are limited in damping performance due to the phase shift of the lead component. Since they are linear filters and are limited by the bode sensitivity integral (water bed effect).

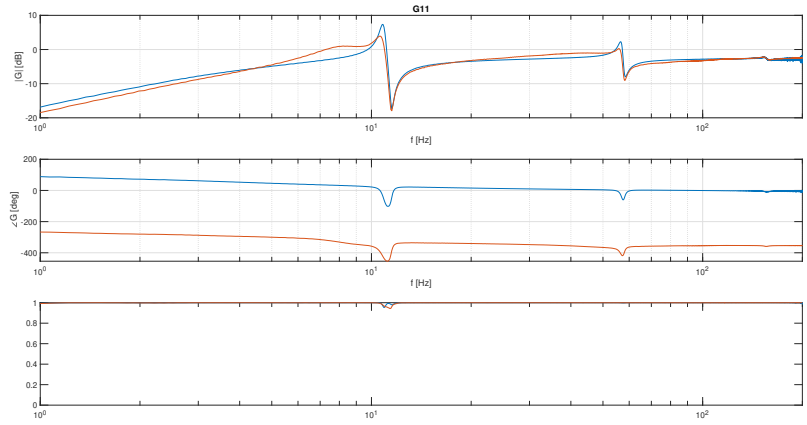

Figure 4.14: Bode plot of G11 - without (blue) and with control (red)- Parallel BPF

Figure 4.14 shows optimal tuning and on comparison with figure 4.12, the amount of damping achieved is nearly the same. It also shows that mode-1's location is not changed as well, which is nothing but the reduction of low-frequency spillover.

Also, the discussion on root-locus based tuning applies to band-pass filters as well since the behavior is similar around the damping region. The tuning based on maximum limits of G14 instead of G11 shows that band-pass PPF provides better disturbance attenuation than PPF due to low gain at low frequency and can be further improved by the introduction of a second-order band-pass filter.

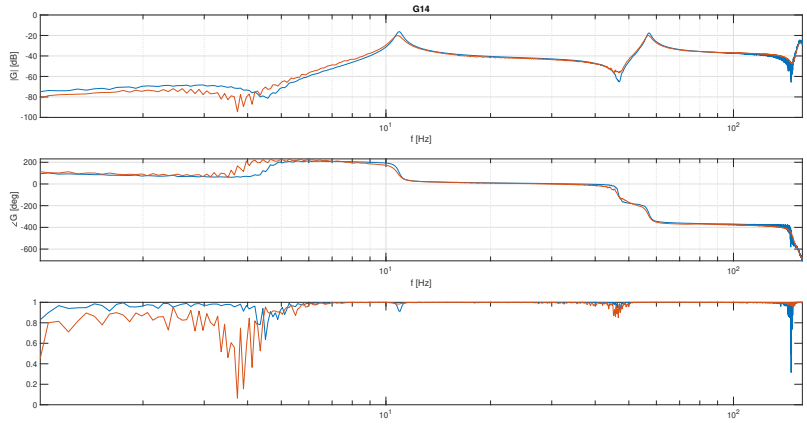

Figure 4.15: Bode plot of G14 - without (blue) and with control (red) - Parallel BPF

4.4 SUMMARY

Table 4.1 summarises the reduction of peaks for the the four tuning and it can be seen that, employment of parallel PPF reduces the damping of 1st mode due to spillover. Also, on comparing the SISO cases of PPF and BPF, there is a marginal reduction. The case of Parallel BPF offsets the problem of low frequency spillover but suffers from marginal reduction in damping due to lead pass nature at low frequency.

Magnitude (dB)		Reduction of Resonance (dB)			
Plant		SISO-PPF	Parallel PPF	SISO-BPF	Parallel BPF
Mode1	-17.66	5.31	4.51	4.49	4.2
Mode2	-19.96	0	2.28	0	1.82

Table 4.1: Reduction of resonance in SISO algorithms

The aim of this chapter was to provide the details of tuning and a new controller to mitigate the shortcomings of PPF. The characteristics can be summarised as,

- Parallel PPF can be used to effectively push the limits of saturation of damping multiple modes. But the tuning of higher-order mode affects the amount of damping on lower-order modes.
- Controllers can be tuned with respect to different objectives such as stability limits and disturbance attenuation. The latter will produce a new peak at a different location due to saturation in G11 but can effectively dampen the disturbance.
- Band-pass filter is tuned for the phase of the controller and hence is tuned to a lower frequency and hence offers a marginal reduction in damping performance with an added advantage in low-frequency behavior.

5 RESULTS AND DISCUSSION

This chapter is aimed to discuss the performance of the controller in terms of under-actuation, perfect-actuation, and over-actuation. The last chapter provided us with a band-pass controller for SISO. We will also consider the band-pass tuning for the decentralized Multi-Input Multi-Output (MIMO) system. The issue of active flexibility (loss of stiffness) and their suppression by the use of bandpass is also discussed in detail.

There are two cases of the experimental setup (refer figure 3.5 & 3.6) which is used for comparison

- Case-1 : 4x4 FRF Plant with three control actuators for three modes. With the discussion of parallel PPF and 1bpf, there are three sub cases possible
  1. Under-actuated case: Actuator 1 is used to control mode-1 & mode-2 while actuator 3 is used to control mode-3.
  2. Perfect-actuated case: Each actuator is deployed to control the mode of highest influence. Actuator-1 for mode-1, Actuator-2 for mode-2 and Actuator-3 for mode-3.
  3. Over-actuated case: Actuator 1 is used to control mode-1 & mode-2; Actuator-2 is used to dampen mode-2 ; Actuator-3 for mode1 mode-3. Thus mode-1 mode-3 are over-actuated.
- Case-2 : 7x4 FRF Plant with six control actuators for three modes with two cases of controller PPF and 1-BPF. This case is aimed at achieving localised control in terms of over actuation.

For brevity, the simulation is not shown and only the experimental results are shown and only the bode magnitude plot is shown. some desertions are made from the observations with reasoning and it is to be noted that the tuning is optimal. The considered system is linear and decentralized in terms of control.

5.1 CASE-1 : UNDER-ACTUATION

As discussed, under-actuation is achieved by a similar process of the parallel PPF tuning discussed in the previous section with the addition of actuator 3 for tuning mode-3, which is done by the same process of selection of controller parameters based on G33.

5.1.1 PPF

The plant with optimal controller parameters is shown in figure 5.1,

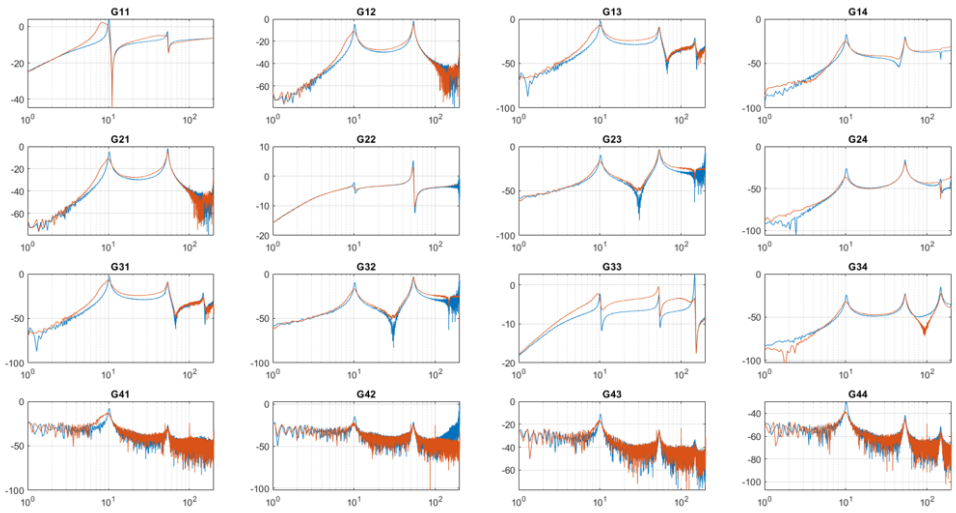

Figure 5.1: Uncontrolled plant (blue) and controlled plant (red) - Under actuation

observations

The tuning of mode-1 & mode-2 is done on G11 and hence there is no active flexibility introduced in G22. The cross-coupling transfer functions also show damping imparted without any instability according to the bode stability criterion. The abnormal behavior of mode 1 mode 2 in G33 can be explained by figure 5.2 which shows the time domain control signal for the disturbance attenuation and on zooming onto mode2 and mode1 as shown in figure 5.3. The control signal of actuator 3 has a control signal which a phase of 90 ° which translates to a control signal 180 ° with respect to the strain, thus contributing to the flexibility region.

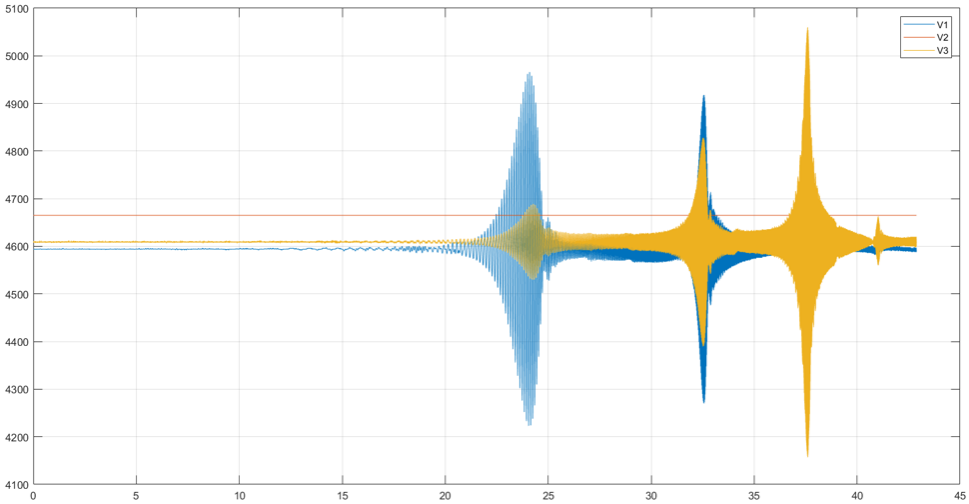

Figure 5.2: Corresponding control signal for disturbance attenuation - Under actuation

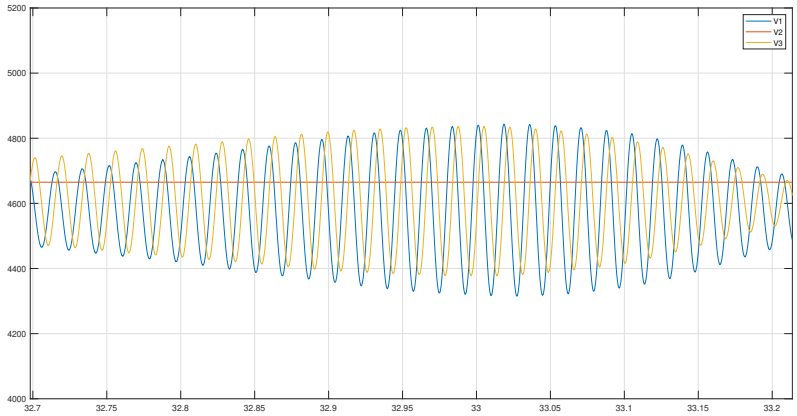

Figure 5.3: control signal spillover zoomed on mode 2

5.1.2 1-BPF

The improvement of spillover by referencing the amount of damping obtained in the PPF is achieved by optimal tuning based on the previous chapter.

During the tuning for the same damping, it was noticed that the performance of damping that can be achieved for mode 1 mode 2 was marginally better which is due to the low spillover. Parallel PPF has a limitation that tuning for a particular mode restricts the attenuation at lower mode while bandpass allows some decoupling to improve the performance better and hence the control signal is marginally efficient.

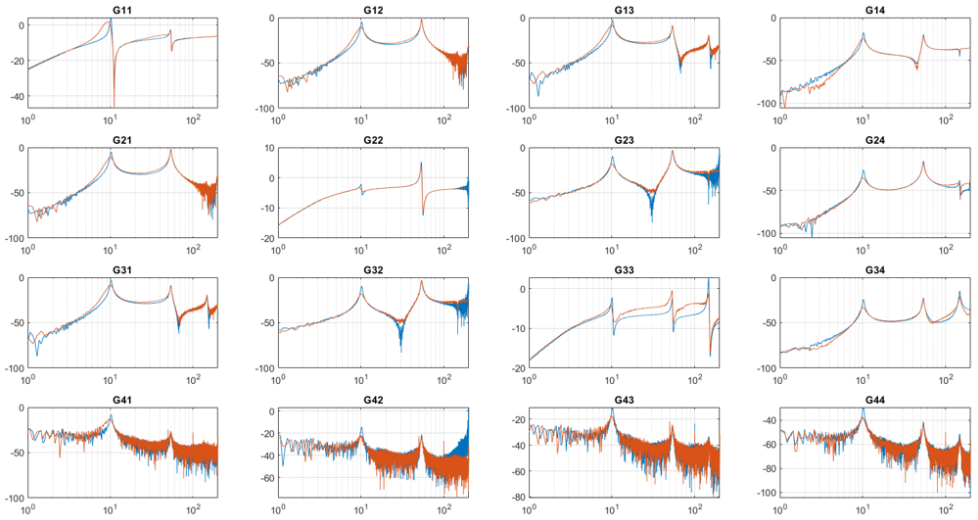

Figure 5.4: Uncontrolled plant (blue) and controlled plant (red) - Under actuation (bandpass PPF)

observations

With respect to disturbance attenuation, it can be seen that nearly the same amount of damping can be achieved. The gain used for the band-pass is lesser and due to the roll-off nature, the spillover control voltage is conserved as well. Comparing the damped G33 with the G33 in the case of PPF there is an improvement in the active flexibility due to the low gain of the controller at lower frequencies. Mode-2 still suffers from active flexibility because the location of mode-3 and mode-2 is closer than the slope of the lead functionality. This can be further strengthened

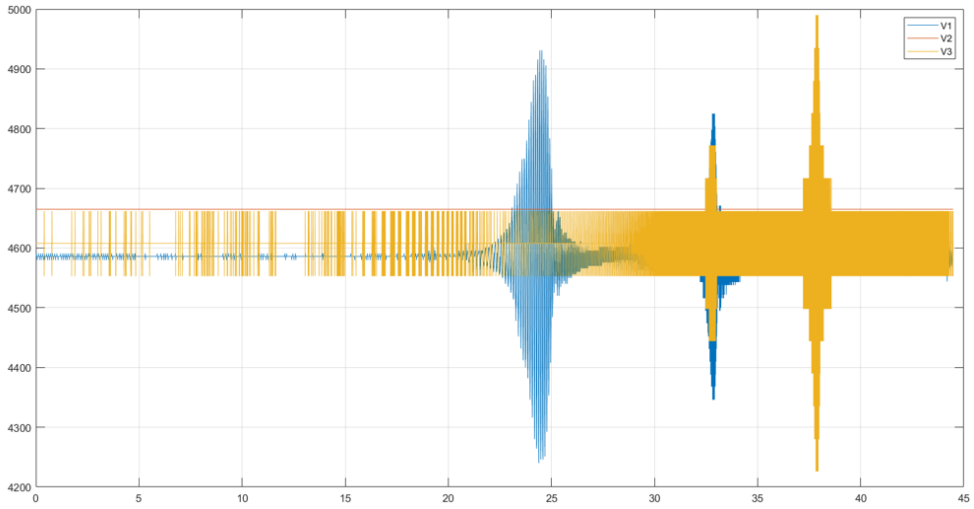

Figure 5.5: Corresponding control signal for disturbance attenuation - Under actuation (bandpass PPF)

by the control signal plot (refer figure 5.5). The constant lines present at the low-frequency region is a digital noise present due to the lead action in programming the controller.

5.2 CASE-1 : PERFECT-ACTUATION

Perfect actuation refers to the control with the number of actuators equal to the number of modes to be tamed. Since the interconnection in parallel PPF cannot be compensated completely by a band-pass. Perfect-actuation is expected to dampen the modes in an effective manner.

The tuning involves the optimal selection of gain of mode-1 based on G11, mode-2 based on G22, and mode-3 based on G33. Two cases of tunings are provided, the first one tuned referencing the underactuated case while the second one is tuned for maximum damping.

5.2.1 PPF

Here, the tuning of the controller based on the amount of damping as same as the under actuated case is discussed.

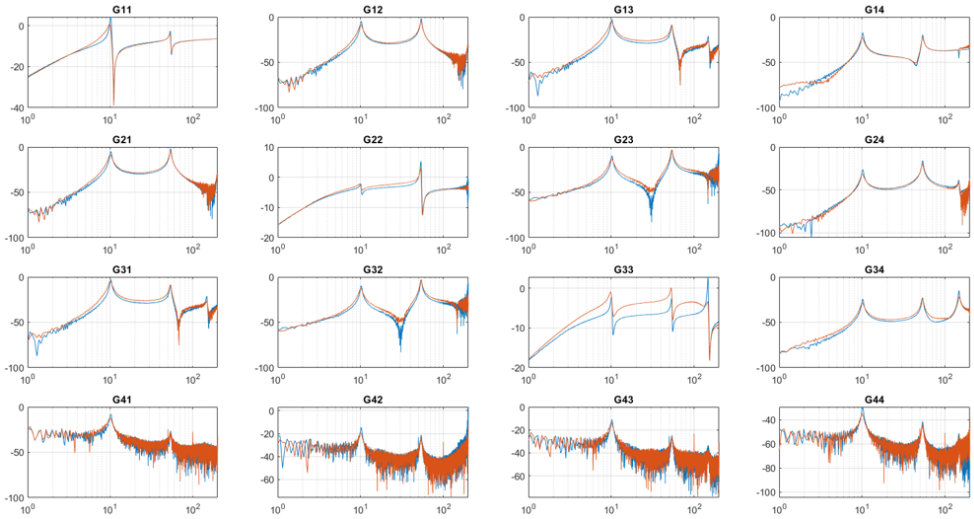

Figure 5.6: Uncontrolled plant (blue) and controlled plant (red) - Tuning referencing Under-actuation (Perfect actuation)

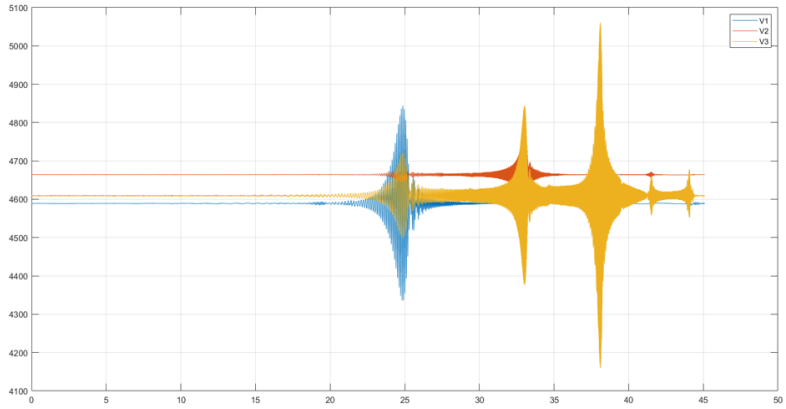

Figure 5.7: Corresponding control signal for disturbance attenuation - Tuning referencing Under-actuation (Perfect actuation)

observations

Since there is no parallel PPF case, the active flexibility is evident in G22. The degree of flexibility is quite less. This is not attributed to the location of the modes but rather the slight amount of damping imparted to mode 2 to match it to the former case. As can be seen in figure 5.8 for tuning based on maximum damping, the active flexibility of mode 1 in G22 becomes quite noticeable. G33 also suffers from the same phenomenon.

It is also interesting to note the control signal between the under-actuated case and perfectly actuated case. Earlier, mode-2 was controlled by actuator-1 which was not at the optimal location whereas the current situation uses actuator-2, placed at the optimal location of mode-2, to control. Hence, to achieve the same damping as the under-actuated case, the control signal is less (shown in red in figure 5.7).

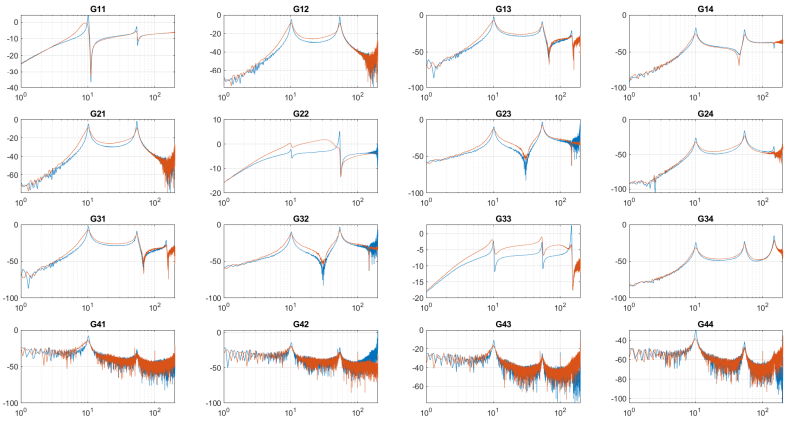

Figure 5.8: Uncontrolled plant (blue) and controlled plant (red) - Tuning based on optimal damping (Perfect actuation)

Figure 5.8 shows that the damping achieved is substantially higher compared to the under-actuation case.

5.2.2 1-BPF

Now, the same procedure of tuning a band-pass is carried on respective transfer functions for mode 1,2 & 3. This is mainly to reduce active flexibility and does not provide any energy advantage that existed in the parallel case.

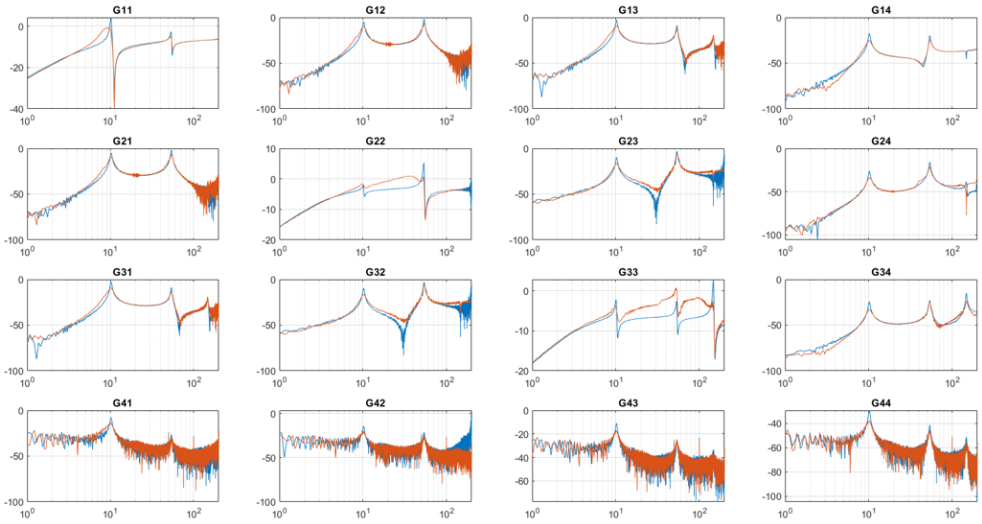

Figure 5.9: Uncontrolled plant (blue) and controlled plant (red) - Tuning for optimal damping (Perfect actuation - band pass)

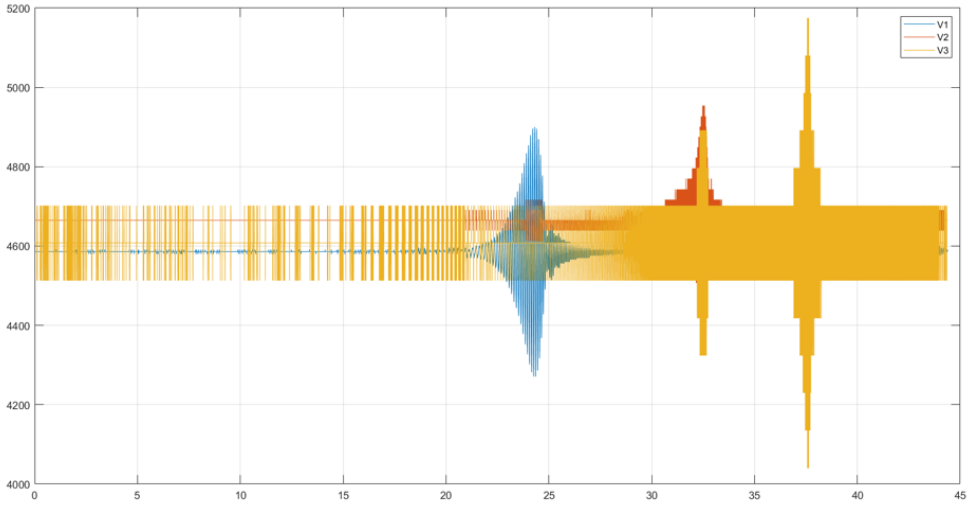

Figure 5.10: Corresponding control signal for disturbance attenuation - Tuning for maximum damping (Perfect actuation - band pass)

observations

The immediate observation on comparison with the under-actuated case is that there is no shift in the resonance peak of lower modes as the tuning is completely decoupled. Also, there is less active flexibility of mode 1 in G22, mode 1, and mode 2 in G33. An important observation to note is that the reduction of active flexibility of mode 1 in G22 is better than the active flexibility of mode 2 in G33. This reaffirms the assertion made in the previous section that the location of modes plays a huge difference in reduction. The gap between the modes required for the reduction of active flexibility reduces for a second-order band-pass filter. Also, there is no marginal improvement of the control signal because of the lack of parallel control.

5.3 CASE-1 : OVER-ACTUATION WITH PARALLEL PPF

Over-actuation is achieved when damping of a particular mode is achieved with more than one actuator. In this case, we employ parallel PPF to provide actuation. Actuator 1 is used to dampen mode 1 and mode 2. Actuator 2 is used to control only mode 2, while actuator 3 acts upon both mode 1 and mode 3. Hence, Mode 1 and Mode 2 becomes over actuated.

5.3.1 PPF

The tuning is nothing but two parallel ppfs for G11 and G33. The same tuned controller for the underactuated case can be reused with a similar process repeated for G33, while G22 has the tuning of perfect actuation as it is used to control only mode 2. Thus, this case is nothing but the *'best of both cases'*.

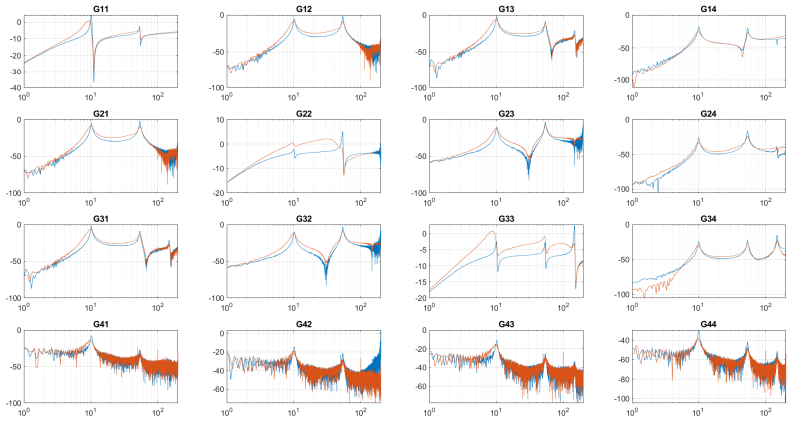

Figure 5.11: Uncontrolled plant (blue) and controlled plant (red) - tuned for optimal damping (over-actuation)

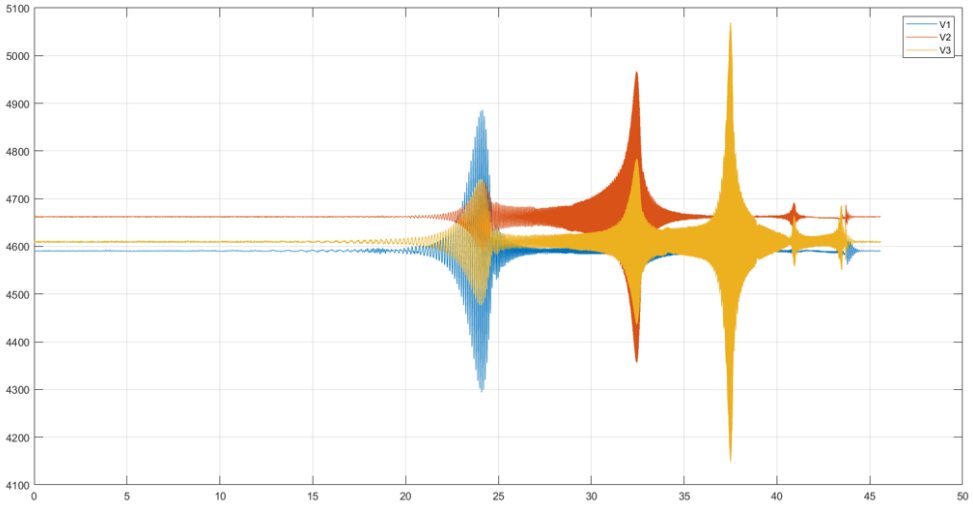

Figure 5.12: Corresponding control signal for disturbance attenuation (over-actuation)

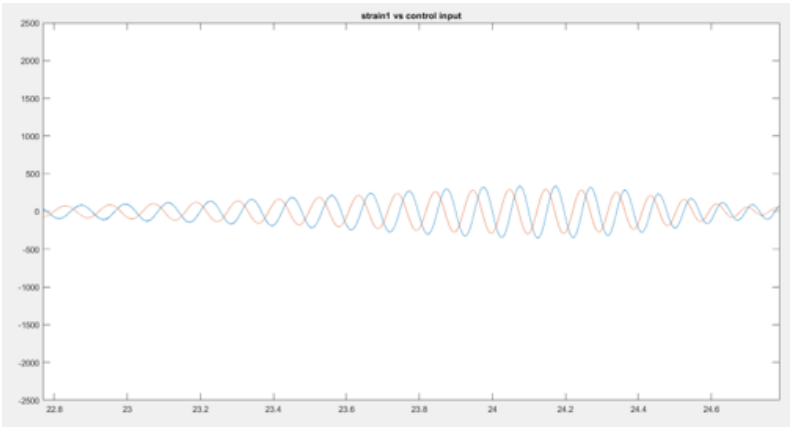

Figure 5.13: Strain1 vs Control input

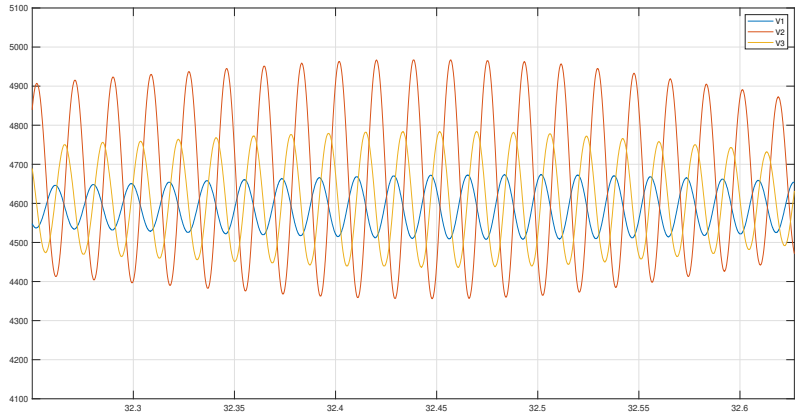

Figure 5.14: Control signal in time domain zoomed in on mode 2

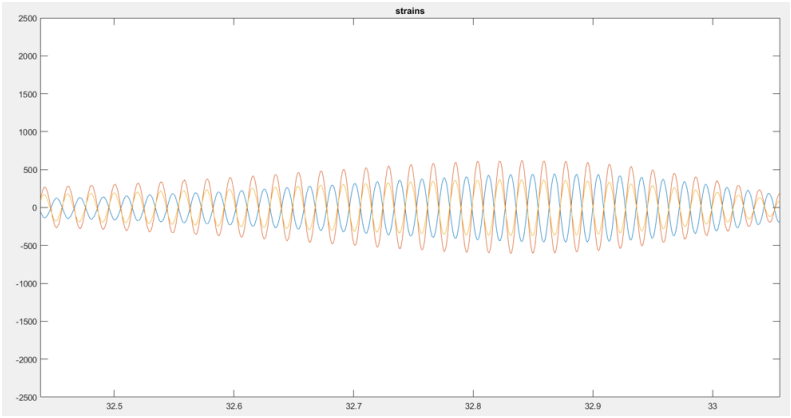

Figure 5.15: Strain signal recorded by sensor 1 (blue), sensor 2 (red), sensor 3 (yellow)

observations

Figure 5.13 shows the time domain signal of strain 1 (blue) along with the control input (red). There is a phase shift of 90 ° which provides a damping action. Also, from figure 5.15, there is a change in the sign of mode2 by 180 °. This is due to the location of sensor and by referring to figure 3.1, it can be seen that the the mode deflects in an opposite direction for mode2 compared to mode1. This is also evident in figure 5.14 which indicates the control action for mode 2 by three actuators. It shows that the control action of actuator 1 is opposite to that of the control action provided by actuator 2, when both the actuators are controlling the same mode. The active flexibility of actuator 3 is also seen in the figure as it is still PPF.

A stark difference to note is the change in lower resonance frequency in G11 and G33 due to the use of parallel PPF. Upon examination, it is seen that the control input by actuator 3 and actuator 1 is slightly off, because of the fact that in parallel PPF higher-order modes give a different spillover to lower order modes which creates an offset. Though the effect is not extensive, this phenomenon has a slight effect on the performance of lower-order modes. Since Parallel PPF is used, the energy consumption is not optimal and higher than the perfect actuation case.

5.3.2 1-BPF

Band-pass is used to offset the effects of spillover and active flexibility. Hence, the same tuning as discussed earlier is preferred.

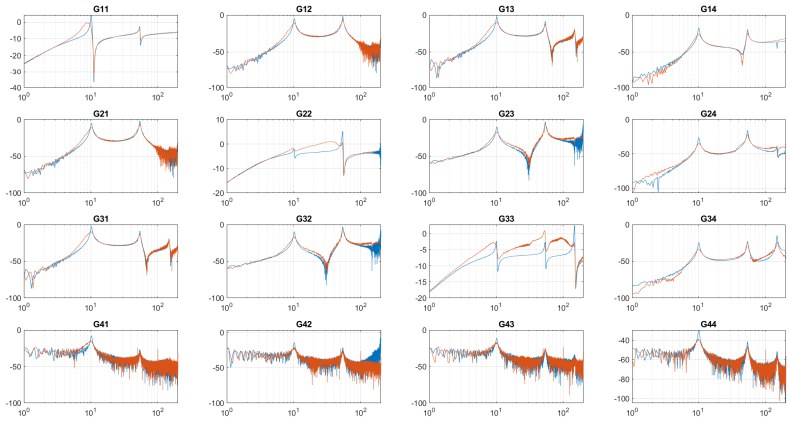

Figure 5.16: Uncontrolled plant (blue) and controlled plant (red) - Tuned for maximum damping (over-actuation band pass)

The band-pass in the over-actuated case may not be ideal as the tuning based on phase may vary at different frequencies. For example, the tuning frequency of mode 1 in G33 will be a different frequency compared to the frequency of mode 1 in tuning for G11. It should also be noted that for mode1 during simultaneous control a certain amount of damping provided by G11 will reduce the amount of freedom in G33 and might not be energy efficient.

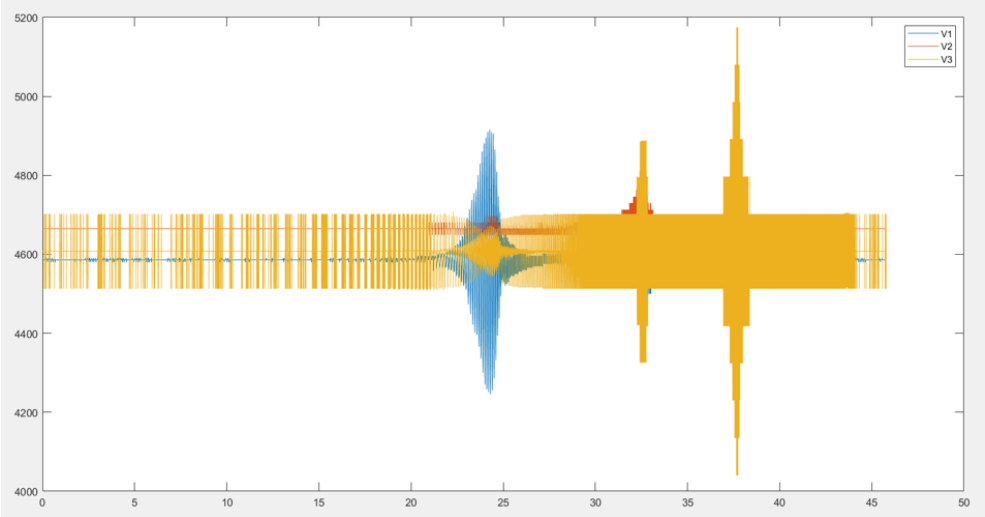

Figure 5.17: Corresponding control signal for disturbance attenuation - Tuned for maximum damping (over-actuation band pass)

5.4 CASE-2 : OVER-ACTUATION

Case-2 consists of a different beam with the same parameters and different actuators. The idea is to utilize perfect actuation with a higher number of smaller actuators (segmented for localized control) rather than parallel PPF. This involves the usage of seven actuators for control of 3 modes, with two actuators optimally placed for mode-1, two actuators placed for mode3, and three actuators placed for mode 3. The sensor is kept at the same location. In the sense, strictly over actuation is explored.

The FRF of the beam is represented in figure 3.9. The FRF reveals that actuator 7 cannot be used to control mode 3 as the non-collocation of the first two modes make it difficult to control mode 3. Hence, a possible solution is given as a recommendation for future work.

Hence, this work concentrates on the use of six actuators (2 for each mode). Since each actuator has a saturation limit and by placing it in an optimal location, we would be provided with a higher degree of freedom for control.

5.4.1 PPF

A similar approach is used to tune each mode based on achieving maximum damping. The disturbance attenuation of G18 is expanded to show the effectiveness of damping mode 1 and mode 2.

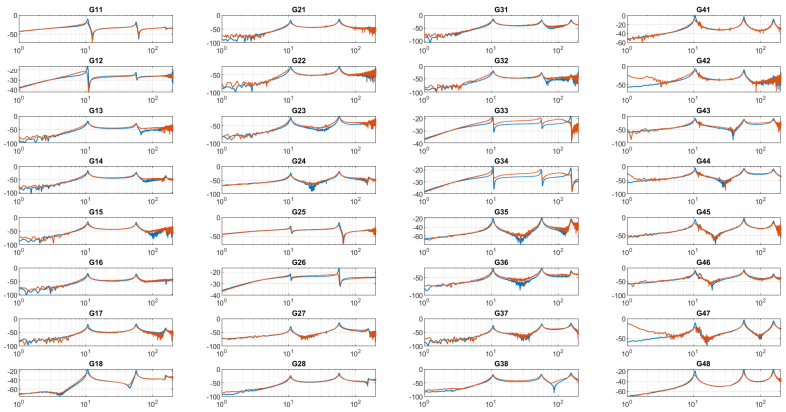

Figure 5.18: Case2 : Bode plot of plant (blue) and damped system (over actuated - red)

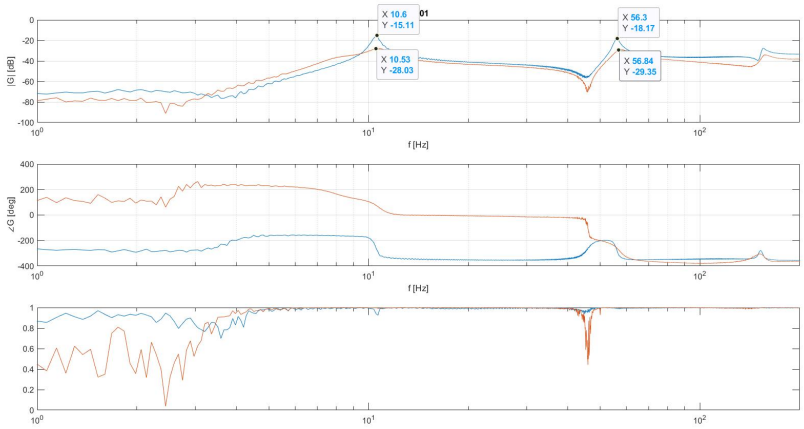

Figure 5.19: Case 2 : Corresponding control signal for disturbance attenuation

		Under-actuation		Perfect		Over-actuated		Case - 2
		PPF (dB)	BPF (dB)	PPF (dB)	BPF (dB)	PPF (dB)	BPF (dB)	PPF (dB)
G_{1w}	Mode1	7.36	5.99	8.06	6.94	8.16	8.75	14.06
G_{2w}	Mode2	3.54	3.22	7.28	6.29	7.05	6	10.77
G_{3w}	Mode1	7.93	8.88	7.29	8.43	7.95	8.96	11.41
G_{4w}	Mode1	8.61	8.5	8.96	8.44	9.68	9.52	16.02
	Mode2	3.55	2.77	5.98	7.34	9.21	6.17	9.69
	Mode3	7.18	7.24	7.92	7.12	9.35	8.08	8.47

Table 5.1: Comparison of peak reduction between case-1 & case-2

Figure 5.19 shows that each control loop is tuned for maximum damping and the fact that there are two-actuators used explicitly for one mode. This provides us with a higher degree of freedom. Figure 5.19 shows a higher amount of damping to disturbance than the previous cases.

Table 5.1 shows a summary of the reduction of peaks for disturbance attenuation with respect to the above-discussed cases. Only certain modes are shown with respect to transfer function as they are more dominant. Green shows an improvement in damping compared to the under-actuated case, while yellow suggests the same performance, and red shows a decrease in damping. As we know, that Band-

pass imparts sub-optimal damping, the damping performance is lesser compared to the PPF of its corresponding case. For example, there is a reduction of 7.36 dB when under-actuation is employed for mode-1 while the reduction is 6dB when a band-pass is used in under-actuation. However, Band-pass is advantageous in applications where low-frequency behavior is important and when several modes are damped that is over-actuation. It can be seen that band-pass has a higher reduction for the over-actuated case because when actuator 3 is employed in parallel PPF for mode1 & mode3, they are completely decoupled by the band-pass action. It can be seen from the general trend that extensive over-actuation as employed in case-2 has a substantially higher damping performance. This is due to the additional degree of freedom and segmented distribution of actuators.

5.4.2 1-BPF

The Bandpass is employed to the over-actuated case to reduce the flexibility, steady-state error, and has no added benefit. There might be a slight advantage in lesser control signal when compared with the PPF case, but it cannot be compared to control signals of case-1. This is again preceded by a marginal decrease in performance.

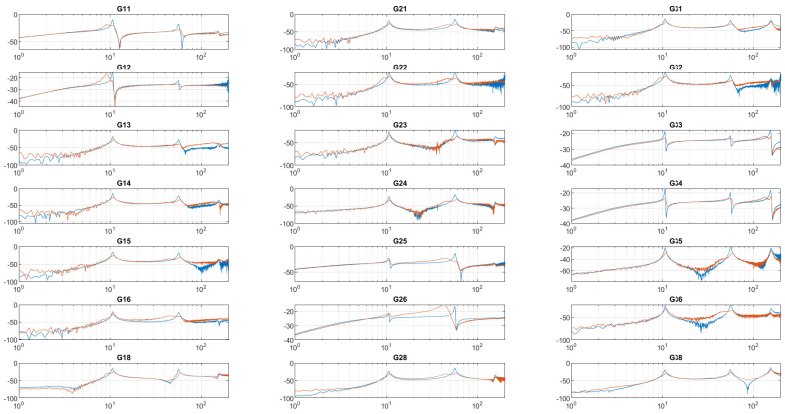

Figure 5.20: Corresponding control signal for disturbance attenuation

5.5 SUMMARY

The above comparison based on under actuation, perfect actuation, and over-actuation in beam-1 and beam-2 proves that perfect actuation or over-actuation is better in achieving damping than the currently used under-actuated case. Comparison based on energy consumption could not be carried out based on the control signal as the energy spent on damping requires the construction of a custom dynamometer due to the electro-mechanical behavior.Hence, sufficiently based on the amount of damping and settling time it can be concluded that over-actuation is beneficial and improve the bandwidth of the system to an extent as well.

6 CONCLUSION

6.1 GENERAL CONCLUSION

In this thesis, Different damping methods were analyzed and actuators, sensors were selected accordingly. A Finite Element Analysis (FEA) simulation was performed for the placement of actuators and identification was done experimentally using NI cRIO module. The identified system was modeled in Simulink for synthesis and also tuning was done experimentally by passing the reference on top of the control signal to tune the controller according to stability limits. Some drawbacks of PPF with respect to low-frequency spillover and active flexibility were identified and corrected by the introduction of a new band-pass filter and the tuning guidelines were introduced. The performance of the band-pass was compared to PPF.

An experimental study was set up to compare the damping performance of under-actuated, perfectly actuated and over-actuated systems using parallel PPF in case-1. It was concluded that perfect actuation provided the best result as the parallel ppf suffered from sub-optimal damping of other modes and was restricted by the saturation limit of the actuator. This was due to the fact that the root locus of different modes traversed at different rates and optimal tuning for a particular mode resulted in the sub-optimal performance of other modes. Though, the band-pass filter provided some flexibility in decentralization it was subject to the location of modes. Also, Band-pass provided some extra freedom while tuning for high disturbance attenuation due to the effect of a lead pass which offsets the low-frequency stability condition and provides some decoupling from other modes. Bandpass also prevented the translation of lower-order modes as a causal effect.

To study the benefits of over-actuation, a single-mode was controlled using two smaller actuators. This seemed to provide a damping close to 2x times the damping achieved in under-actuation (refer table 5.1) and it was due to the segmented distribution. The better sensitivity, damping results in higher bandwidth and precision. A fair comparison of energy consumption could not be made based on the electrical characteristic because of the electro-mechanical factor which is responsible for the damping force. It was also concluded that over damping system had the least settling time and rise time. In terms of mass, there is a significant advantage of over-actuation. While case-1 used 3 A-12 piezoelectric actuators for damping three modes, it weighed a total of 10.3g in mass while case-2, though employing six actuators, used up a mass of 1.6g to provide better disturbance attenuation and contributing a little amount in the reduction of moving mass which also translates to energy.

6.2 RECOMMENDATIONS

Chapter 3 of the thesis was focussed on bandpass filter and the performance was limited by the lead action which shifts the region of interest and the performance was decreasing for higher-order modes. A constant phase non-linear band-pass filters could be used to provide better performance in terms of the location of modes. The required gap for optimal performance can be reduced significantly by nonlinear controllers and can enable the modes to exist closer which happens usually at high frequencies.

In chapter 4, over-actuation was studied but as mentioned in the chapter, actuator 7 was placed in the optimal location of mode 3. But, it was not used to control due to the non-collocation of lower modes and this can be solved by over sensing on top of over-actuation. It has already been proved with this research that better damping characteristic is provided by the use of smaller actuators and hence over sensing can be used as well even with the advantage of reduced mass.

7 REFLECTION

The pace at which the world is running, we hardly take time to reflect on the decisions and experience we had. Looking back is as important as moving forward. Hence, I would like to talk about some challenges and leanings which I would be taking it throughout my life.

Concerning the whole process of the dissertation, it should be noted that overall it was very intriguing and exciting. It was a new domain and to be among the first to be involved excited me even more. This allowed me to talk to more experts to pick their brains and help me to obtain a system-level knowledge. There were a lot of mistakes in the selection of the sensor earlier, but it is where I learned the most. Towards, the end of my research the knowledge that I gained out of making these wrong selections enabled me to give suggestions and opinions to others as well.

The most challenging part of my thesis was the ordering and arrangement to get my experiment running. As soon as my literature study was done, there was a new norm caused by the CoVid situation. With my work being experimental, I lost a month's time without access although I was mentally and physically well. There was immediate action taken by my supervisors in creating alternate plans and setting up meetings. It required some time to get used to the new normal. The post-lockdown created a shortage of lab support and some order delays created uncertainties.

The next challenging part was the inherent property of experiments which is troubleshooting. Days passed by like minutes for several small problems and most of the time left me clueless. As they say, even mountains can be worn by running water. After a certain time, this helped me to think in a systematic way to troubleshoot, and some help from my peers it was up and running.

I had a regular meeting with my supervisor which added many new ideas into my project. Particularly, Monday meetings were informative and helped me connect to different people who helped me in various aspects of the project. From a person who was looking for reasons, I became a person who always looks for a solution no matter the situation I was in. This was a trait I developed from my supervisor who was always there to lend a hand and to give new dimensionality for every problem that I had.

I enjoyed discussion within the lab with my mates and pushed me to work diligently. Also, weekly meetings always pushed me to work hard before the day of the meeting to show progress. During the course of my thesis, I realized that **Discipline takes place where motivation cannot**. Experiments gave me long days and sleepless nights but in the end when the desired result was reached all was forgotten and gave me a sense of happiness which is second to none until now.

While reflecting on the experience of writing a thesis, I came to the realization that I truly enjoyed this process, at least most of it. I am the type of person who loves to learn and always seeks to obtain more knowledge in and out of the classroom. I am especially passionate about learning things that pertain not only to my major but also in other aspects as well, The environment I worked under gave me more dimensionality in developing myself academically and emotionally as well.

I spent many hours doing this project, but through it, I learned that, if I set goals, I can achieve anything. As I reflect upon what I learned, that was most valuable, I think it was truly seeing that persistence pays. I also learned that when I enjoy what I am doing, it is much easier for me to excel.

Additionally, working with my supervisor Dr. Niranjan Saikumar and Dr. Hassan HossienNia encouraged me to take up research and I appreciate the support they lent me in every step to make me feel comfortable. Overall, I feel that this has been both a valuable and enjoyable experience and I now feel prepared and excited for my upcoming academic and career years

BIBLIOGRAPHY

[1] S. R. Moheimani and A. J. Fleming, *Piezoelectric Transducers for Vibration Control and Damping*. Advances in Industrial Control, London: Springer-Verlag, 1 ed., 2006.

[2] A. Preumont, *Vibration Control of Active Structures, An Introduction 3 rd Edition*, vol. 246. Springer, 2018.

[3] A. J. den Hamer, G. Z. Angelis, and N. B. Roozen, "Broad-band active vibration suppression using PPF focused on industrial application," *IEEE/ASME Transactions on Mechatronics*, vol. 10, pp. 146–153, 4 2005.

[4] M. Namavar, A. J. Fleming, M. Aleyaasin, K. Nakkeeran, and S. S. Aphale, "An analytical approach to integral resonant control of second-order systems," *IEEE/ASME Transactions on Mechatronics*, vol. 19, no. 2, pp. 651–659, 2014.

[5] M. Schneiders MJG van de Molengraft and M. Steinbuch, "Benefits of over-actuation in motion systems," tech. rep., 2004.

[6] S. Kon and R. Horowitz, "A high-resolution mems piezoelectric strain sensor for structural vibration detection," *IEEE Sensors Journal*, vol. 8, no. 12, pp. 2027–2035, 2008.

[7] J. Sirohi and I. Chopra, "Fundamental understanding of piezoelectric strain sensors," *Journal of Intelligent Material Systems and Structures*, vol. 11, no. 4, pp. 246–257, 2000.

[8] Piezodrive, "Bd family of dual channel drivers for piezo bender actuators." Available at https://www.piezodrive.com/modules/bd300-dual-channel-drivers/.

[9] PI, "Material data." Available at https://www.piceramic.com/en/products/piezoelectric-materials/.

[10] B. Yan, K. Wang, Z. Hu, C. Wu, and X. Zhang, "Shunt Damping Vibration Control Technology: A Review," *Applied Sciences (Switzerland)*, vol. 7, no. 5, 2017.

[11] C. J. GOH and T. K. CAUGHEY, "On the stability problem caused by finite actuator dynamics in the collocated control of large space structures," *International Journal of Control*, vol. 41, no. 3, pp. 787–802, 1985.

[12] E. Pereira, S. S. Aphale, V. Feliu, and S. O. R. Moheimani, "Integral resonant control for vibration damping and precise tip-positioning of a single-link flexible manipulator," *IEEE/ASME Transactions on Mechatronics*, vol. 16, no. 2, pp. 232–240, 2011.

[13] F. Yang, R. Sedaghati, D. Younesian, and E. Esmailzadeh, "Optimal placement of active bars in smart structures," in *IEEE International Conference Mechatronics and Automation, 2005*, vol. 1, pp. 1–6 Vol. 1, 2005.

[14] B. N. Agrawal, J. L. Meyer, G. Song, and W. B. Harrington, "Application of piezoceramics to vibration suppression of a spacecraft flexible," 1996.

[15] J.-H. Han, K.-H. Rew, and I. H. Lee, "An experimental study of active vibration control of composite structures with a piezo-ceramic actuator and a piezo-film sensor," *Smart Materials and Structures*, vol. 6, pp. 549–558, 1997.

[16] D. Halim and S. O. R. Moheimani, "Spatial /spl hscr//sub 2/ control of a piezoelectric laminate beam: experimental implementation," *IEEE Transactions on Control Systems Technology*, vol. 10, no. 4, pp. 533–546, 2002.

[17] D. Halim and S. O. R. Moheimani, "Experimental implementation of spatial h/-sub /spl infin// control on a piezoelectric-laminate beam," *IEEE/ASME Transactions on Mechatronics*, vol. 7, no. 3, pp. 346–356, 2002.

[18] C. W. D. Silva, *Vibration: Fundamentals and Practice, Second Edition*, vol. 2. CRC Press, 2006.

[19] S. S. Aphale, A. J. Fleming, and S. O. R. Moheimani, "Integral resonant control of collocated smart structures," *Smart Materials and Structures*, vol. 16, 2007.

[20] L. Li, C.-X. Li, G. Gu, and L.-M. Zhu, "Positive acceleration, velocity and position feedback based damping control approach for piezo-actuated nanopositioning stages," *Mechatronics*, vol. 47, pp. 97 – 104, 2017.

[21] F. Lüleci, "ACTIVE VIBRATION CONTROL OF BEAM AND PLATES BY USING PIEZOELECTRIC PATCH ACTUATORS A THESIS SUBMITTED TO THE GRADUATE SCHOOL OF NATURAL AND APPLIED SCIENCES OF MIDDLE EAST TECHNICAL UNIVERSITY," tech. rep., 2013.

[22] M. I. Friswell and D. J. Inman, "The relationship between positive position feedback and output feedback controllers," tech. rep., 1999.

[23] Y. Wang and D. J. Inman, "Comparison of control laws for vibration suppression based on energy consumption," *Journal of Intelligent Material Systems and Structures*, vol. 22, no. 8, pp. 795–809, 2011.

[24] G. F. Franklin and J. D. Powell, *Feedback control of dynamic systems*. Addison-Wesley, 1994.

[25] J. FANSON and T. CAUGHEY, "Positive position feedback control for large space structures," 1987.

[26] Jeongho Hong and D. S. Bernstein, "Bode integral constraints, collocation, and spillover in active noise and vibration control," *IEEE Transactions on Control Systems Technology*, vol. 6, no. 1, pp. 111–120, 1998.

[27] G. Song, S. P. Schmidt, and B. N. Agrawal, "Experimental study of active vibration suppression of flexible structure using modular control patch," *IEEE Aerospace Conference Proceedings*, vol. 1, pp. 189–201, 1998.

[28] J. A. Bell and A. R. Kashani, "Structure-Borne Noise Reduction by Active Damping of a Radiating Panel," 5 1995.

[29] G. Song, S. P. Schmidt, and B. N. Agrawal, "Experimental robustness study of positive position feedback control for active vibration suppression," *Journal of Guidance, Control, and Dynamics*, vol. 25, no. 1, pp. 179–182, 2002.

[30] H. H. Syed, "Comparative study between positive position feedback and negative derivative feedback for vibration control of a flexible arm featuring piezoelectric actuator," *International Journal of Advanced Robotic Systems*, vol. 14, no. 4, pp. 1–9, 2017.

[31] L. Marinangeli, F. Alijani, and S. H. HosseinNia, "A Fractional-order Positive Position Feedback Compensator for Active Vibration Control," *IFAC-PapersOnLine*, vol. 50, no. 1, pp. 12809–12816, 2017.

[32] M. Ratnam, B. Bhikkaji, A. J. Fleming, and S. O. Moheimani, "PPF control of a piezoelectric tube scanner," in *Proceedings of the 44th IEEE Conference on Decision and Control, and the European Control Conference, CDC-ECC '05*, vol. 2005, pp. 1168–1173, 2005.

[33] S. M. Kim, S. Wang, and M. J. Brennan, "Comparison of negative and positive position feedback control of a flexible structure," *Smart Materials and Structures*, vol. 20, no. 1, 2011.

[34] L. Li, C. X. Li, G. Gu, and L. M. Zhu, "Positive acceleration, velocity and position feedback based damping control approach for piezo-actuated nanopositioning stages," *Mechatronics*, vol. 47, pp. 97–104, 2017.

[35] D. Halim and S. O. R. Moheimani, "Spatial resonant control of flexible structures-application to a piezoelectric laminate beam," *IEEE Transactions on Control Systems Technology*, vol. 9, no. 1, pp. 37–53, 2001.

[36] H. R. Pota, S. O. R. Moheimani, and M. Smith, "Resonant controllers for smart structures," *Smart Materials and Structures*, vol. 11, pp. 1–8, feb 2002.

[37] S.-M. Kim, S. Wang, and M. J. Brennan, "Comparison of negative and positive position feedback control of a flexible structure," *Smart Materials and Structures*, vol. 20, p. 015011, dec 2010.

[38] B. Bhikkaji and S. O. R. Moheimani, "Integral resonant control of a piezoelectric tube actuator for fast nanoscale positioning," *IEEE/ASME Transactions on Mechatronics*, vol. 13, no. 5, pp. 530–537, 2008.

[39] S. S. Aphale, M. Namavar, and A. J. Fleming, "Resonance-shifting integral resonant control for high-speed nanopositioning," in *2018 Annual American Control Conference (ACC)*, pp. 6006–6011, June 2018.

[40] N. Tanaka and S. D. Snyder, "Cluster control of a distributed-parameter planar structure—Middle authority control," *The Journal of the Acoustical Society of America*, vol. 112, pp. 2798–2807, 12 2002.

[41] H. S. Tzou and H. Q. Fu, "A study of segmentation of distributed piezoelectric sensors and actuators, part i: Theoretical analysis," *Journal of Sound Vibration*, vol. 172, pp. 247–259, Apr. 1994.

[42] S. Yang, G. Sheu, and C. Yang, "Optimal design of sensor/actuator location and feedback gain by taguchi method," *IFAC Proceedings Volumes*, vol. 29, no. 1, pp. 1032 – 1037, 1996. 13th World Congress of IFAC, 1996, San Francisco USA, 30 June - 5 July.

[43] E. F. Crawley and J. de Luis, "Use of piezoelectric actuators as elements of intelligent structures," *AIAA Journal*, vol. 25, pp. 1373–1385, 10 1987.

[44] R. Barboni, A. Mannini, E. Fantini, and P. Gaudenzi, "Optimal placement of PZT actuators for the control of beam dynamics," *Smart Materials and Structures*, vol. 9, no. 1, pp. 110–120, 2000.

[45] F. Yang, R. Sedaghati, and A. V. Model, "Optimal Placement of Active Bars in Smart Structures," *IEEE International Conference Mechatronics and Automation, 2005*, vol. 1, no. July, pp. 1–6, 2005.

[46] Q. Wang and C. M. Wang, "Optimal placement and size of piezoelectric patches on beams from the controllability perspective," *Smart Materials and Structures*, vol. 9, no. 4, pp. 558–567, 2000.

[47] Y. K. Yong, A. J. Fleming, and S. O. Moheimani, "A novel piezoelectric strain sensor for simultaneous damping and tracking control of a high-speed nanopositioner," *IEEE/ASME Transactions on Mechatronics*, vol. 18, no. 3, pp. 1113–1121, 2013.

A APPENDIX A

A.0.1 Data Sheet - Amplifier

Variant	Output Voltage	Differential Output	Gain	Peak Current	RMS Current	Buy Now
BD300	300 V	+/- 300 V	101	50 mA	11 mA	Buy Now
BD250	250 V	+/- 250 V	83.6	59 mA	13 mA	Buy Now
BD200	200 V	+/- 200 V	67.7	73 mA	16 mA	Buy Now
BD150	150 V	+/- 150 V	51.0	95 mA	21 mA	Buy Now

Figure A.1: Amplifier Specifications [8]

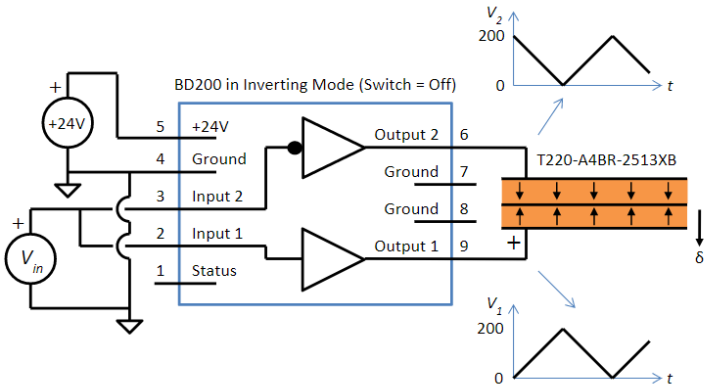

Figure A.2: Implementation - Differential Output [8]

$$V_{Load} = V_1 - V_2 = 2K(V_{in} - 1.5) \tag{A.1}$$

Where, K = 101 and hence an input of 0 V produces -300 V and 3 V produces +300 V.

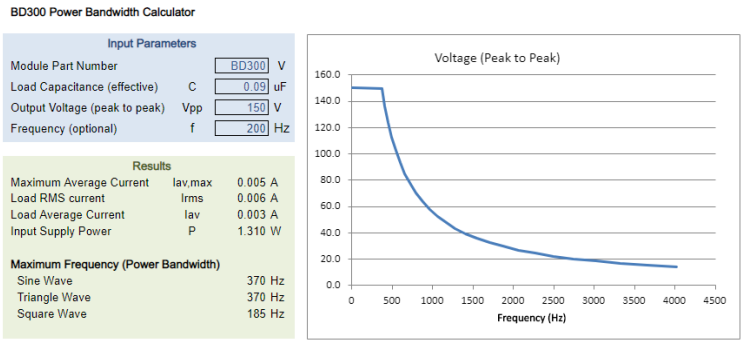

Figure A.3: Power Bandwidth of BD300 [8]

A.1 CHARACTERISATION OF AMPLIFIER

A.1.1 Input to amplifier vs Channel 1 of BD300

At 5 Hz,

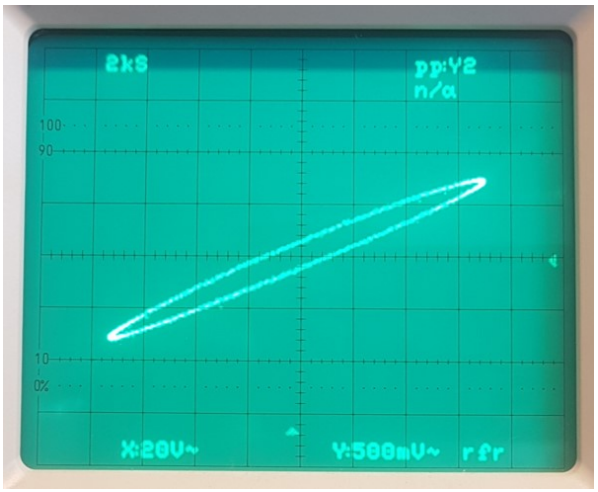

Figure A.4: Lissajous figure of Input vs CH1 at 5Hz

At 10 Hz,

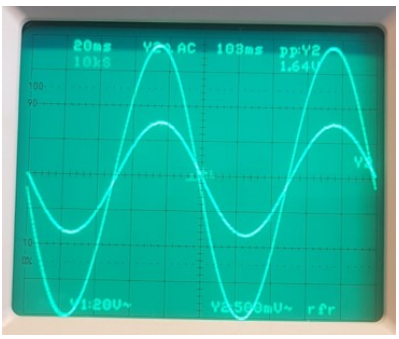

Figure A.5: Input vs CH1 output

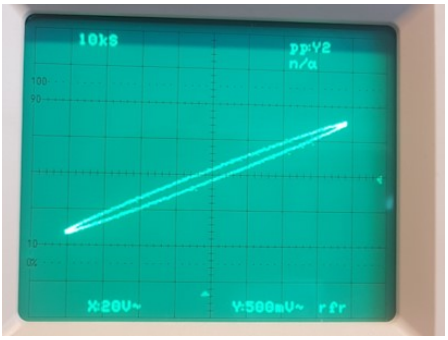

Figure A.6: Lissajous figure at 10 Hz

At 100 Hz,

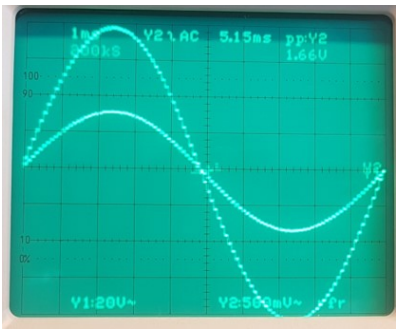

Figure A.7: Input vs CH1 output (100 Hz)

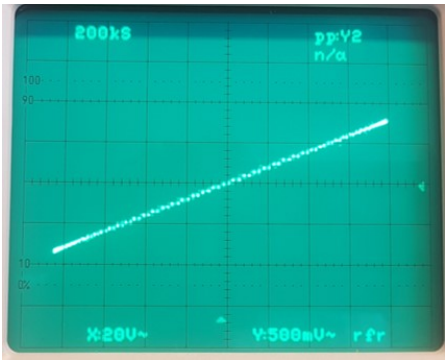

Figure A.8: Lissajous figure at 100 Hz

A.1.2 Channel 1 vs Channel 2 of BD300

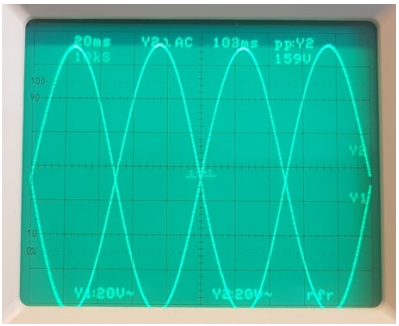

Figure A.9: CH1 vs CH2 output (10 Hz)

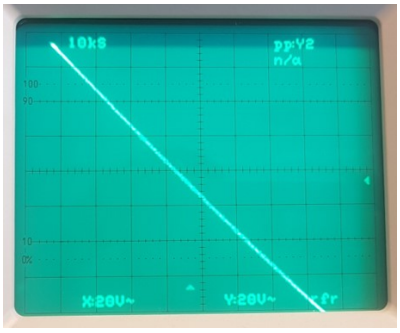

Figure A.10: Lissajous figure at 10 Hz

A.2 PIEZOELECTRIC MATERIAL DATA

SPECIFIC PARAMETERS OF THE STANDARD MATERIALS

			Soft PZT materials				
		Unit	PIC151	PIC255	PIC155	PIC153	PIC152
Physical and dielectric properties							
Density	ρ	g/cm³	7.80	7.80	7.75	7.60	7.75
Curie temperature	T_c	°C	250	350	340	160	340
Relative permittivity in the polarization direction	$\varepsilon_{33}^T/\varepsilon_0$		2400	1850	1550	4500	1350
Relative permittivity ⊥ to polarity	$\varepsilon_{11}^T/\varepsilon_0$		1980	1750	1400	3500	1100
Dielectric loss factor	$\tan\delta$	10^{-3}	20	20	25	30	15
Electro-mechanical properties							
Coupling factor	k_p		0.62	0.62	0.62	0.62	0.48
	k_t		0.53	0.47	0.48	0.49	0.41
	k_{31}		0.38	0.35	0.35	0.33	0.25
	k_{33}		0.69	0.69	0.69	0.72	0.58
	k_{15}		0.65	0.66	0.65	0.66	0.46
Piezoelectric charge coefficient	d_{31}	10^{-12} C/N	-210	-180	-165	-295	-90
	d_{33}		500	400	360	600	240
	d_{15}		610	550	540	780	235
Piezoelectric voltage coefficient	g_{31}	10^{-3} Vm/N	-11.5	-11.3	-12.9	-8.1	-8.7
	g_{33}		22	25	27	17	23
Acousto-mechanical properties							
Frequency coefficient	N_p	Hz·m	1950	2000	1960	1990	2250
	N_1		1500	1420	1500	1380	1570
	N_3^*		1750	1370	1780	1345	1530
	N_t^*		1950	2000	1990	2020	2100
	N_5^*		830	870	820	890	1130
Elastic compliance coefficient	S_{11}^E	10^{-12} m²/N	15.0	16.1	15.6	17.2	13.1
	S_{33}^E		19.0	20.7	19.7	20.0	14.8
Elastic stiffness coefficient	C_{33}^D	10^{10} N/m²	10.0	15.6	11.1	15.3	16.6
Mechanical quality factor	Q_m		100	80	80	50	100
Temperature stability							
Temperature coefficient of ε^T_{33} (in the range of -20 °C bis +125 °C)	$TK\,\varepsilon_{33}$	10^{-3}/K	4	3	4	15	2
Time stability (relative change of the parameter per decade of time in %)							
Relative permittivity	C_ε	%		-1.0	-2.0		
Coupling factor	C_K	%		-1.0	-2.0		

Figure A.11: PIC255 - Specification Sheet [9]

B APPENDIX B

B.1 SIMULATION OF PPF

As obtained in the system identification for case-1 and case-2, a combination of curve fitting algorithm (fmincon) and pole placement procedure is used to predict the transfer functions. The plant is modeled as shown below,

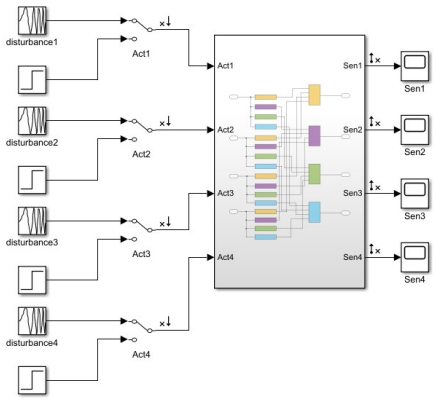

Figure B.1: Plant in Simulink

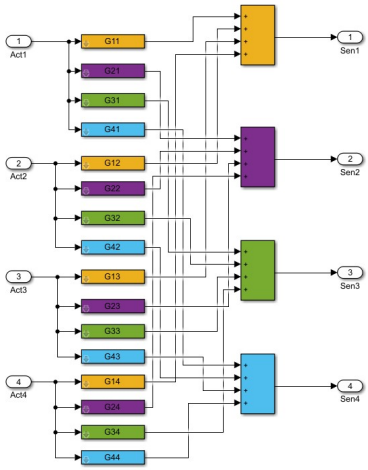

Figure B.2: closed loop bode with PPF,1-BPF,2-BPF

The 4x4 FRF of the plant is shown in blue and the plant with mode-1 damped is shown in red. Thus, the simulations are done on the modelled plant and then verified on the experimental setup.

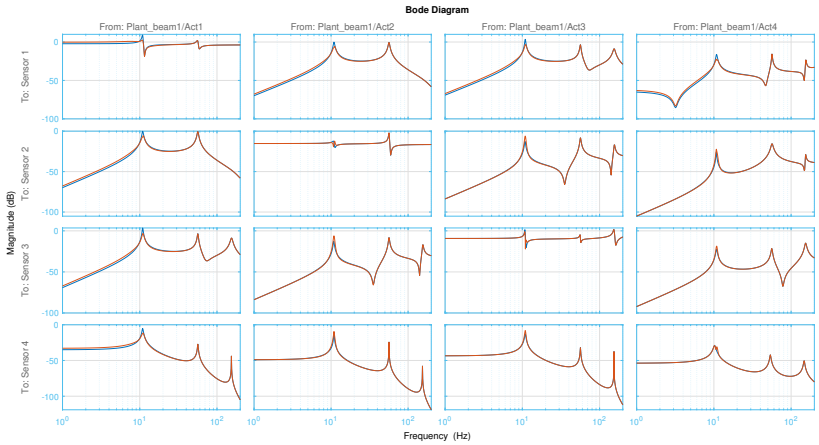

Figure B.3: 4x4 FRF of Plant in simulink with SISO PPF Tuning (figure 4.8)

B.2 EXPERIMENTAL RESULTS OF SISO PPF

B.2.1 Bodeplot

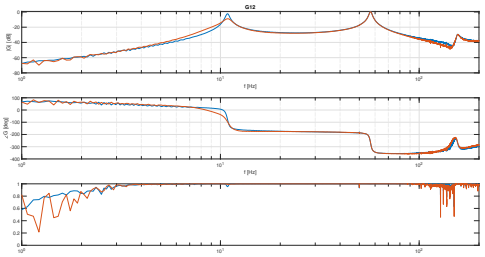

Figure B.4: G21

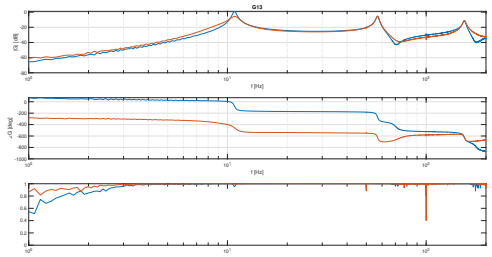

Figure B.5: G31 - SISO

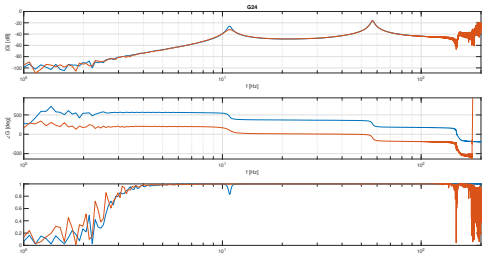

Figure B.6: G24 SISO

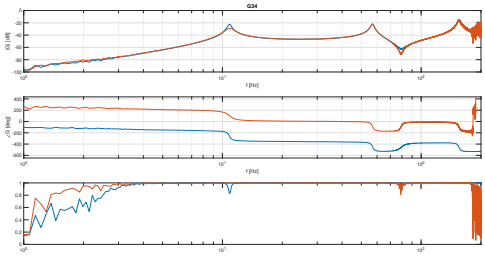

Figure B.7: G34-SISO

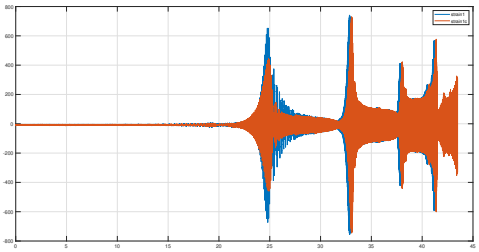

Figure B.8: G34-SISO

B.3 EXPERIMENTAL RESULTS OF SISO BPF

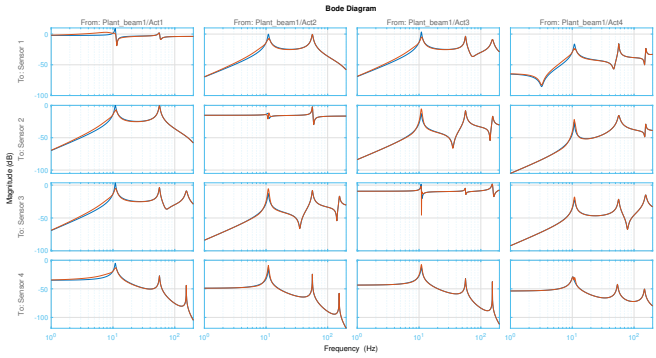

Figure B.9: Simulated Plant and tuning of controller of BPF (refer figure 4.12)

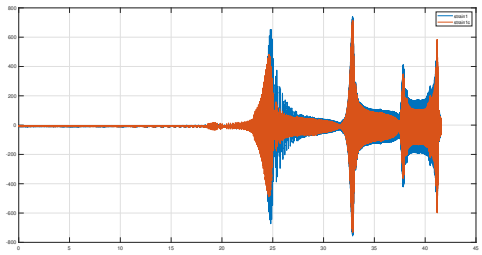

Figure B.10: Strain-1 uncontrolled(blue) & controlled (red)

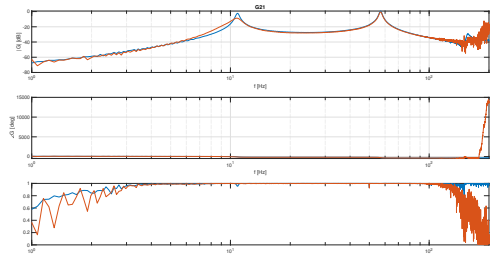

Figure B.11: G21-SISO - Bandpass

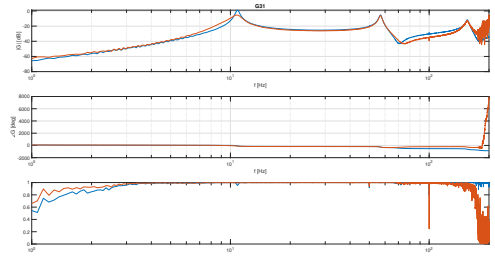

Figure B.12: G31-SISO - Bandpass

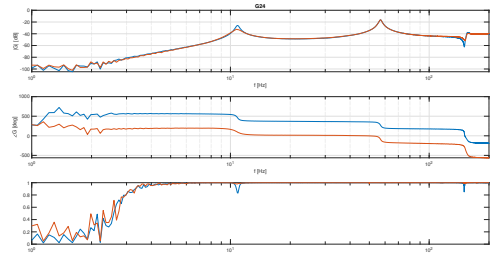

Figure B.13: G24-SISO - Bandpass

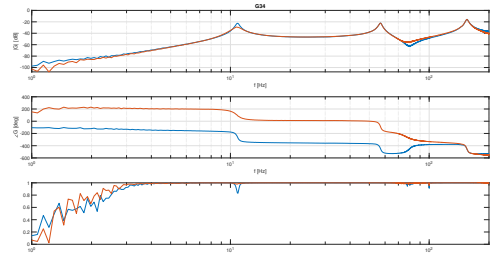

Figure B.14: G34-SISO - Bandpass

C APPENDIX C

C.1 PARALLEL PPF & PARALLEL BPF SIMULATION

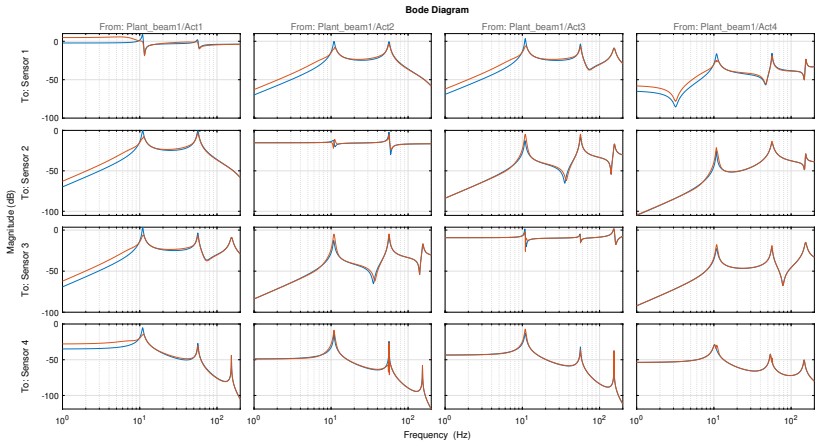

Figure C.1: Simulated Plant and tuning of controller - Parallel PPF (refer figure 4.10)

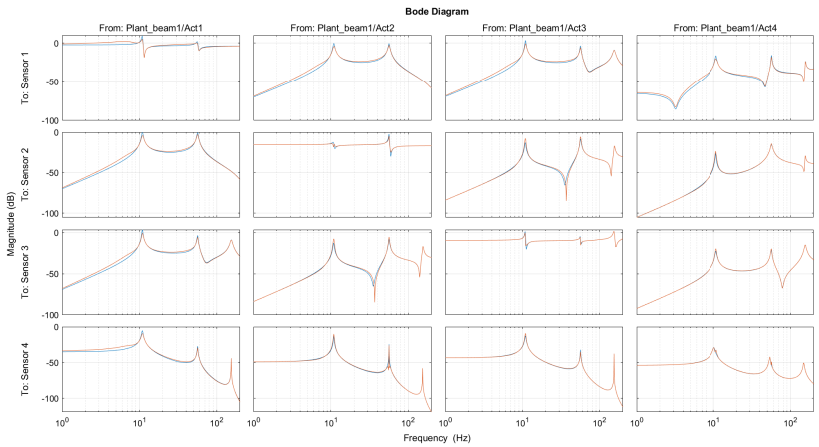

Figure C.2: Simulated Plant and tuning of controller - Parallel BPF (refer figure 4.14)

C.2 COMPARISON OF PARALLEL PPF AND PARALLEL BPF – TF'S

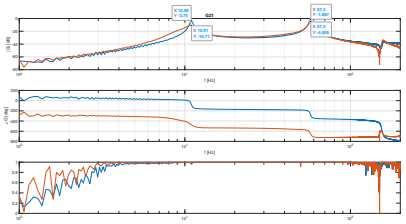

Figure C.3: G21 - Parallel PPF

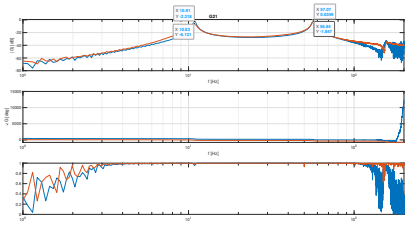

Figure C.4: G21 - Parallel Bandpass

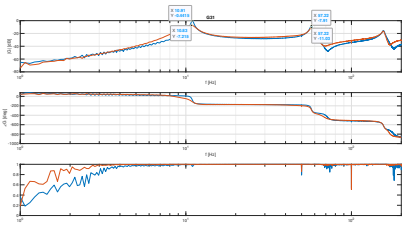

Figure C.5: G31 - Parallel PPF

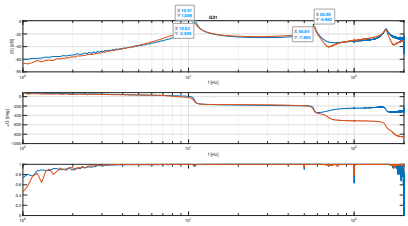

Figure C.6: G31 - Parallel Bandpass

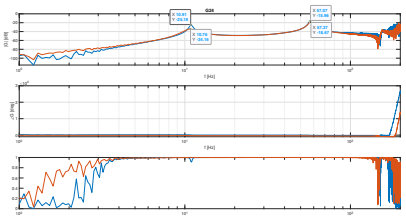

Figure C.7: G24 - Parallel PPF

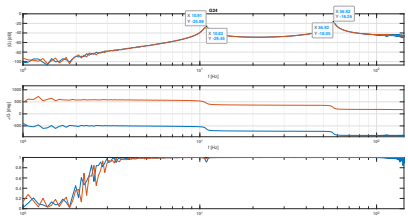

Figure C.8: G24 - Parallel Bandpass

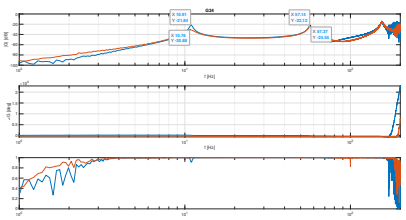

Figure C.9: G34 - Parallel PPF

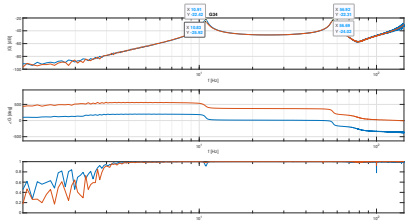

Figure C.10: G34 - Parallel Bandpass

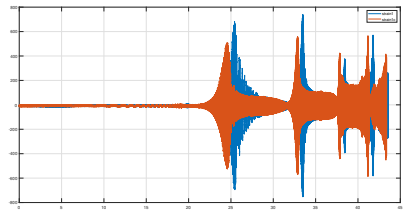

Figure C.11: Strain 1 - Parallel PPF

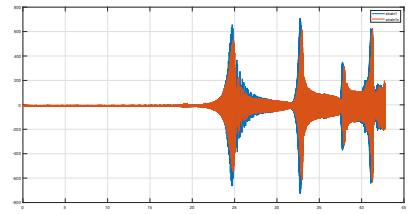

Figure C.12: Strain 1 - Parallel BPF

C.3 ROOT-LOCUS PLOTS FOR VARIOUS CONTROLLER ZEROS

C.3.1 Root-Locus for changing damping ratio of Controller Zero

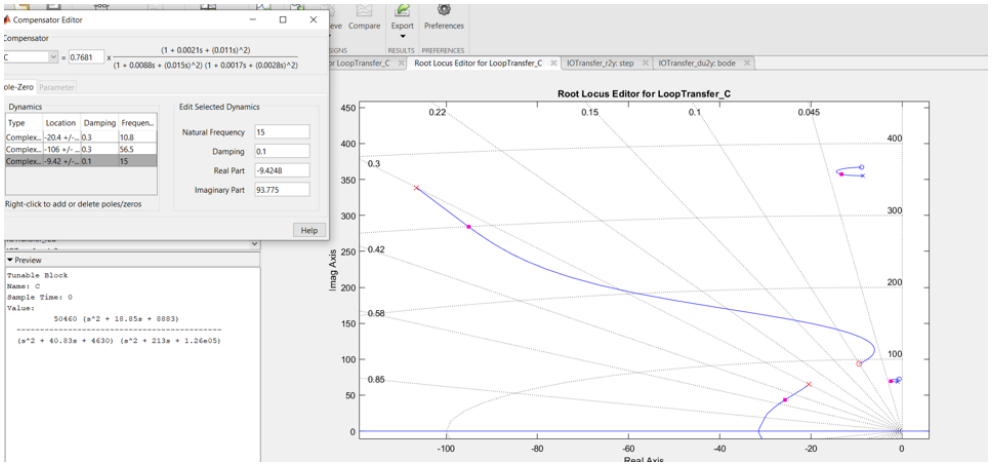

Figure C.13: Root-Locus of damping ratio 0.1 (refer figure 4.14)

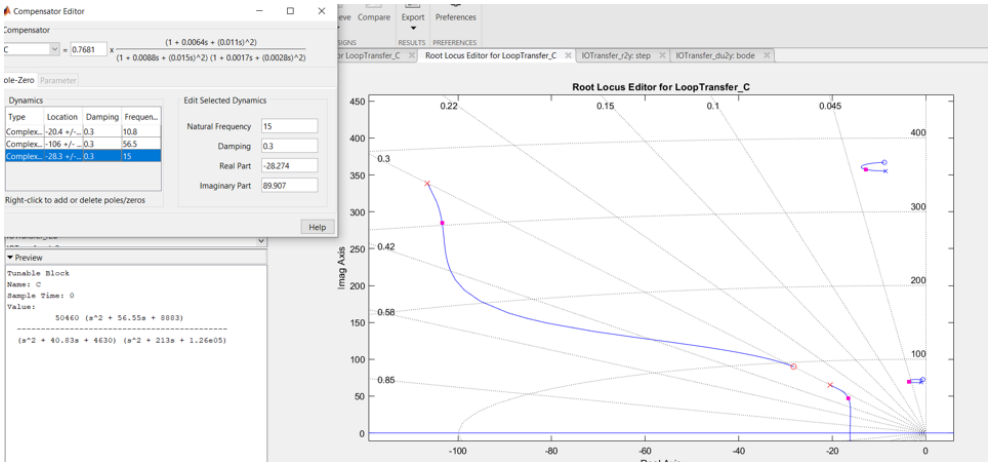

Figure C.14: Root-Locus of damping ratio 0.3 (refer figure 4.14)

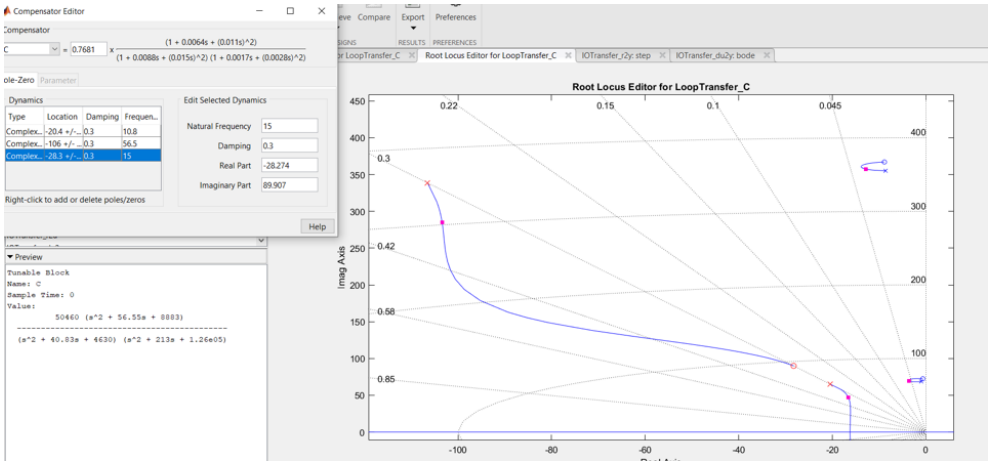

Figure C.15: Root-Locus of damping ratio 0.5 (refer figure 4.14)

C.3.2 Root-Locus for frequency of Controller Zero

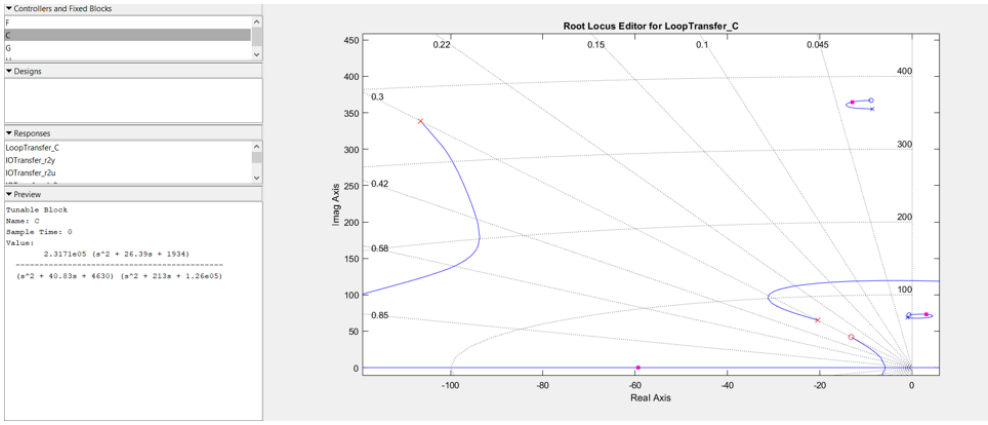

Figure C.16: Root-Locus of controller zero at 7 Hz

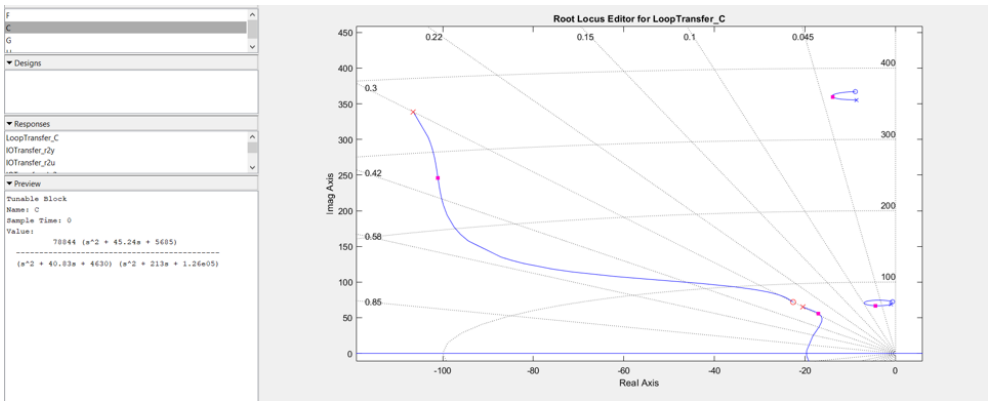

Figure C.17: Root-Locus of controller zero at 12 Hz

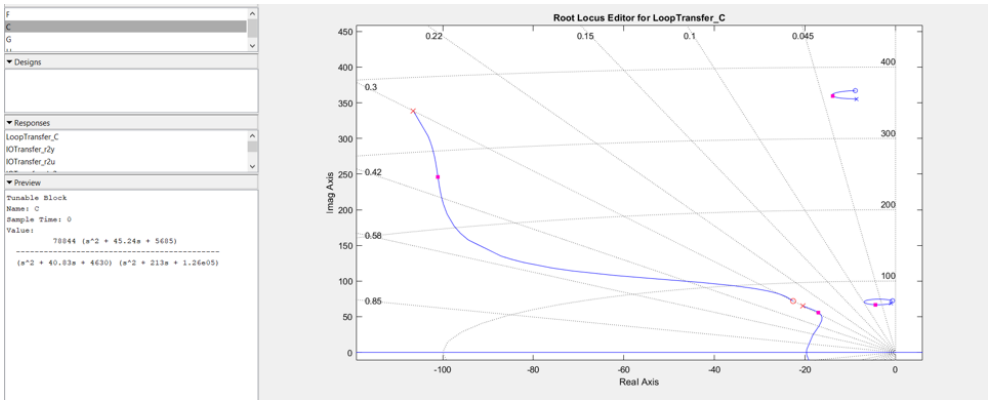

Figure C.18: Root-Locus of controller zero at 12 Hz

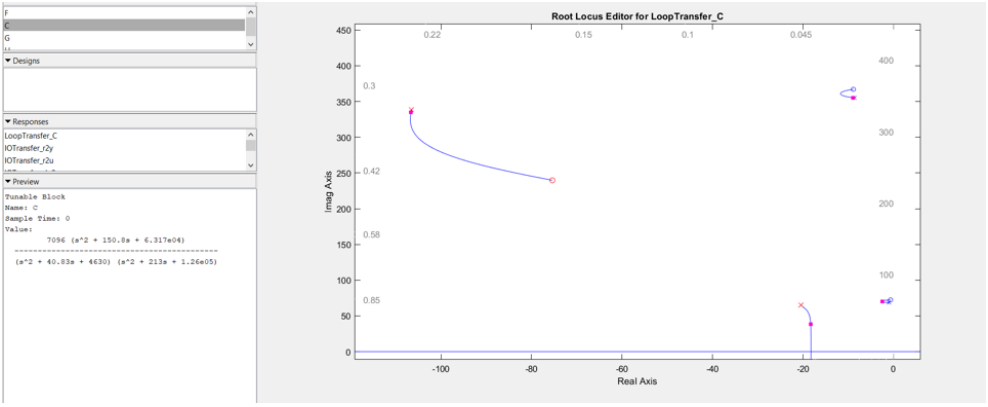

Figure C.19: Root-Locus of controller zero at 40 Hz

D APPENDIX D

D.1 CONTROL SENSITIVITY PLOTS

D.1.1 Case-1: Under actuation

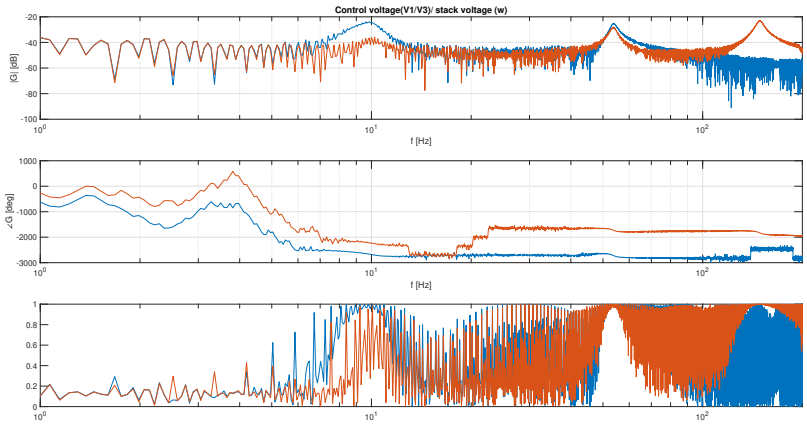

Figure D.1: Control Voltage / Reference Voltage: Blue(V1/w); Red(V3/w)

D.1.2 Case-1: Under actuation - Bandpass

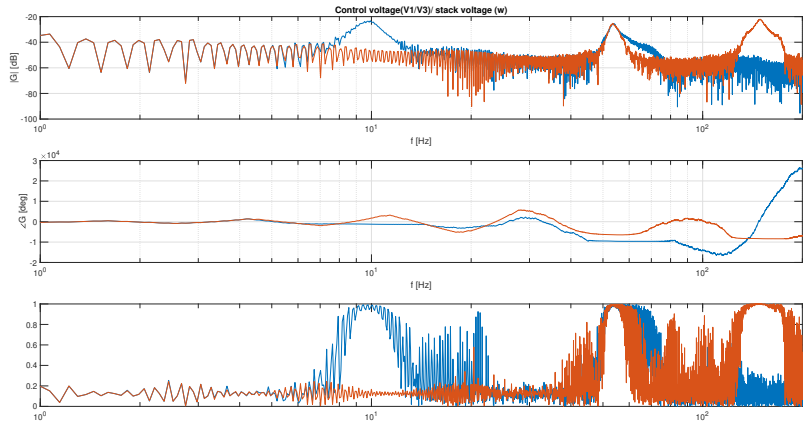

Figure D.2: Control Voltage / Reference Voltage : Blue(V1/w); Red(V3/w)

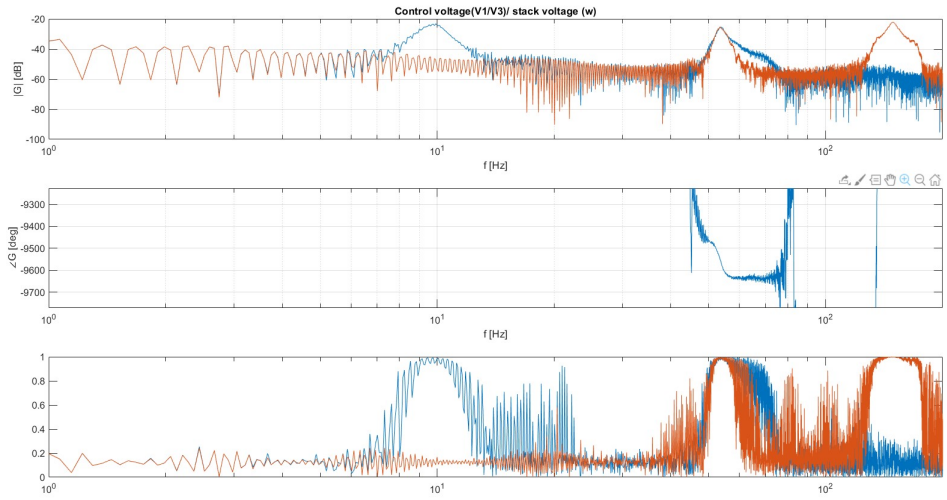

Figure D.3: Control Voltage / Reference Voltage: Blue(V1/w); Red(V3/w) zoomed to show phase drop

D.1.3 Case-1: Perfect actuation

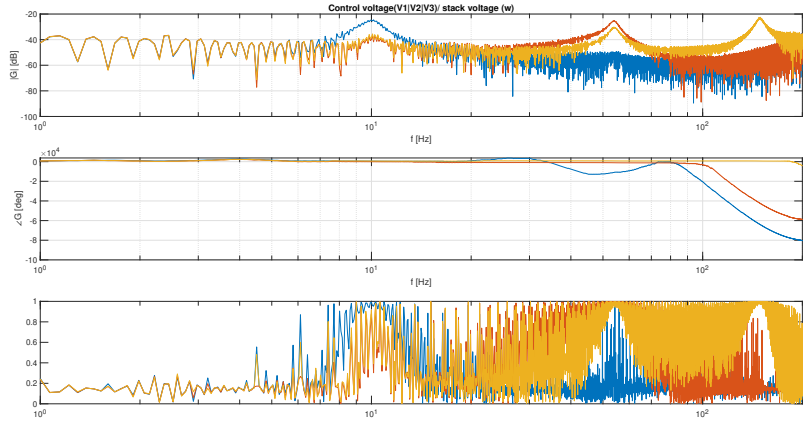

Figure D.4: Control Voltage / Reference Voltage: Blue(V1/w); Red(V2/w); yellow(V3/w)

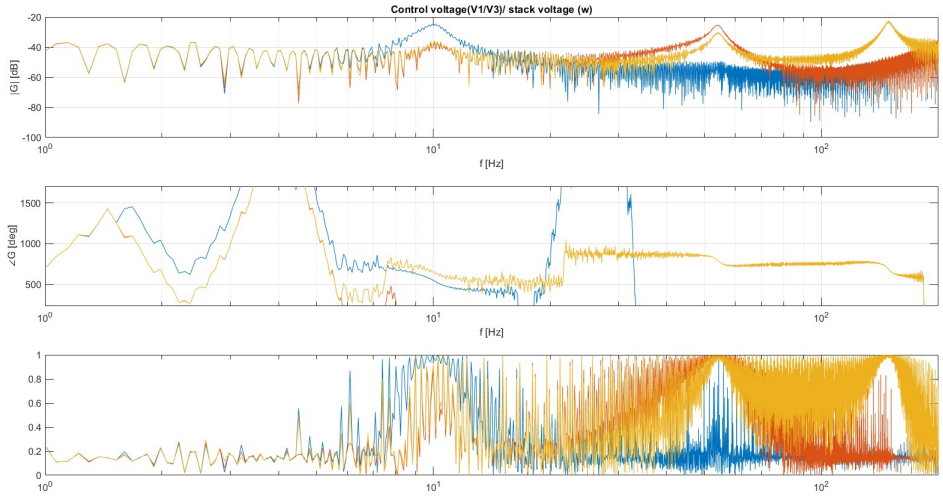

Figure D.5: Control Voltage / Reference Voltage: Blue(V1/w); Red(V2/w);yellow (V3/w) zoomed to show phase drop

D.1.4 Case-1: Perfect actuation - Bandpass

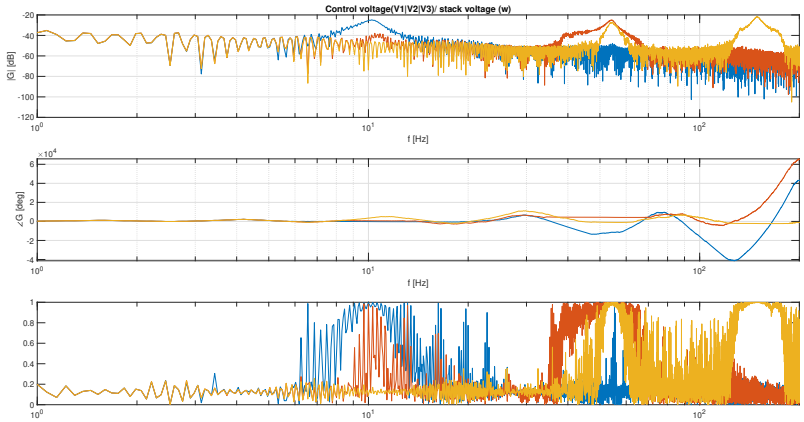

Figure D.6: Control Voltage / Reference Voltage: Blue(V1/w); Red(V2/w);yellow (V3/w)

D.1.5 Case-1: Over actuation

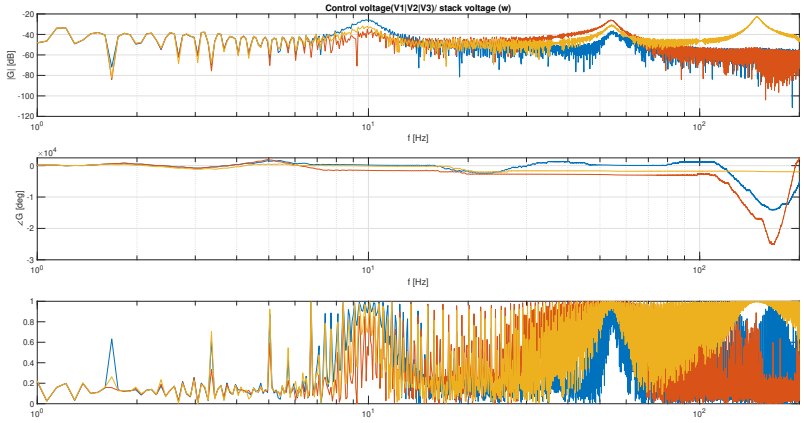

Figure D.7: Control Voltage / Reference Voltage: Blue(V1/w); Red(V3/w)

D.1.6 Case-1: Over actuation - Bandpass

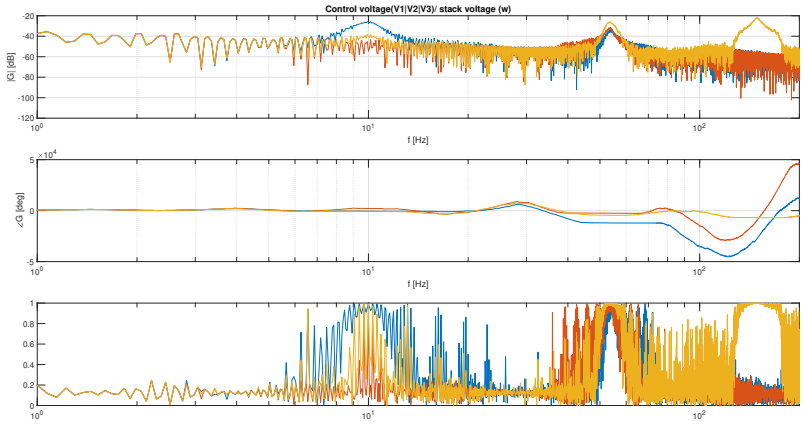

Figure D.8: Control Voltage / Reference Voltage: Blue(V1/w); Red(V3/w)

D.1.7 Case-2 : Over-actuated

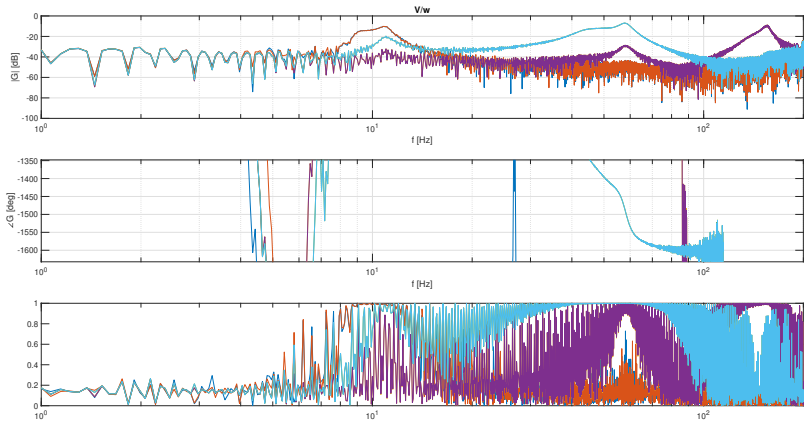

Figure D.9: Control Voltage / Reference Voltage

D.2 PEAK VALUES OF CASE-1

TF	Case - 1	Plant	Underactuated		Perfect		Overactuation	
		Mag	PPF (dB)	BPF (dB)	PPF (dB)	BPF (dB)	PPF (dB)	BPF (dB)
G14	Mode1	-17.66	-25.02	-23.65	-25.72	-24.6	-25.82	-26.41
	Mode2	-19.96	-22.49	-22.52	-26.27	-23.88	-26.56	-24.96
G24	Mode1	-26.38	-32.52	-35.19	-32.85	-33.09	-32.57	-34.95
	Mode2	-16	-19.54	-19.22	-23.28	-22.29	-23.05	-22
G34	Mode1	-24.41	-32.34	-33.29	-31.7	-32.84	-30.36	-33.37
	Mode2	-22.78	-24.11	-24	-26.08	-24.94	-27.42	-24.79
	Mode3	-15.04	-22.71	-22	-21.95	-23.39	-23.35	-24.2
G44	Mode1	-29.4	-38.01	-37.9	-38.36	-37.84	-39.08	-38.92
	Mode2	-41.29	-44.84	-44.06	-47.27	-48.63	-50.5	-47.46
	Mode3	-51.26	-58.44	-58.5	-59.18	-58.38	-60.61	-59.34

Table D.1: Peak values of case-1 trasnfer functions

E | APPENDIX E

E.1 STEP RESPONSES

E.1.1 Case-1 : Under-actuation

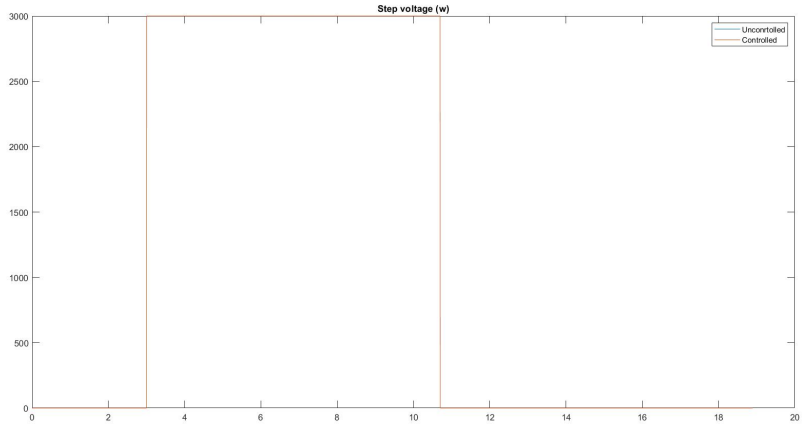

Figure E.1: Reference Voltage

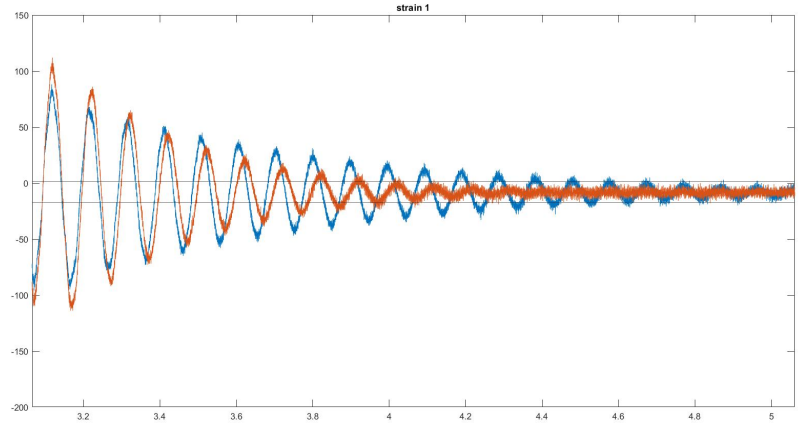

Figure E.2: Step response - G14

E.1.2 Case-2 : Perfect-actuation

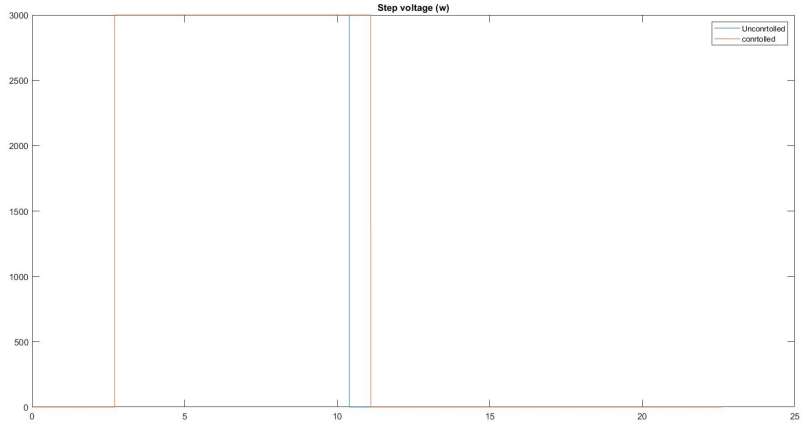

Figure E.3: Reference Voltage

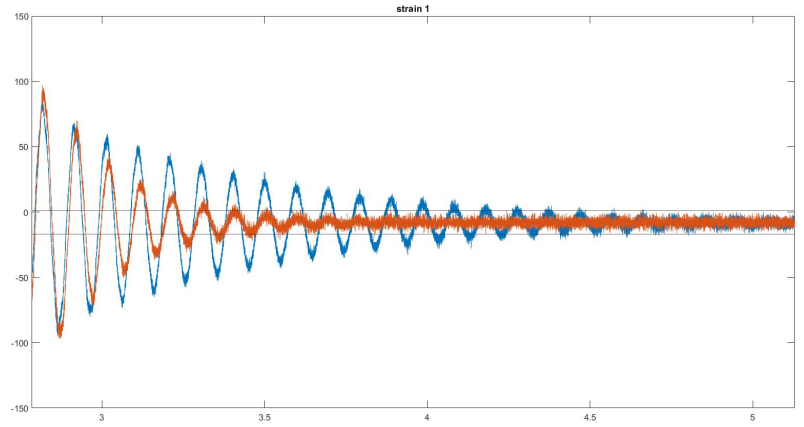

Figure E.4: Step response - G14

E.1.3 Case-1 : Over-actuation

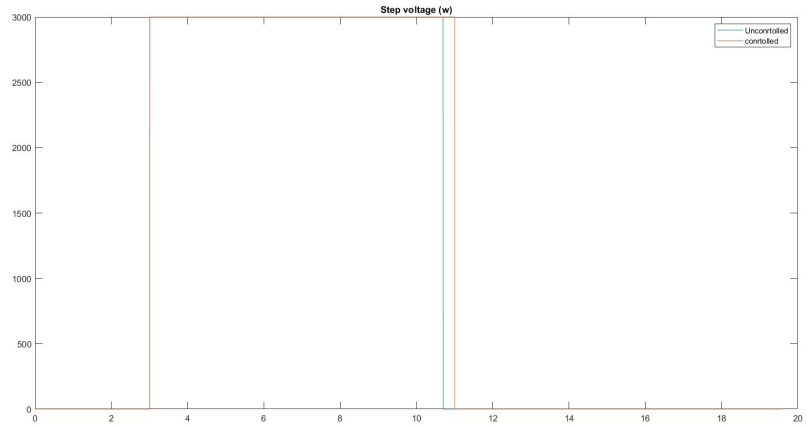

Figure E.5: Reference Voltage

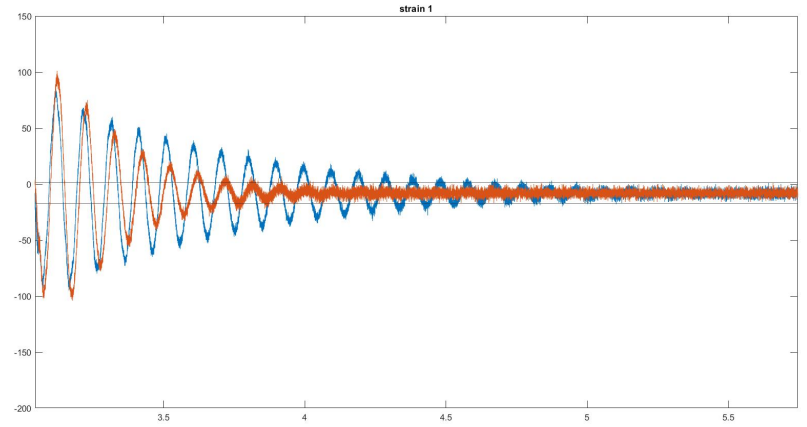

Figure E.6: Step response - G14